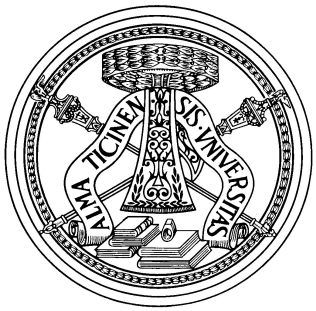

Università degli Studi di Pavia

Facoltà di Ingegneria

Dipartimento di Ingegneria Civile e Architettura

Master degree in Civil Engineering

FDM - 3D Printing: From Mesostructure to Equivalent Homogeneous Solid Through Sintering Process. Applications and Numerical Simulations

3D Printing: Dal Reticolo Cristallino al Solido Omogeneo Equivalente Attraverso il Processo di Sinterizzazione. Applicazioni e Simulazioni Numeriche.

Supervisor: Professor

Ferdinando Auricchio

Co - supervisor:

Gianluca Alaimo

Author:

Claudio Della Cagnoletta

UIN **423610**

Academic year 2014/2015

. . . a mia nonna Erminia

Parrebbe che lo stato delle scienze dovesse esser più costante che della letteratura, e la fama degli scienziati più durevole dei letterati. Pure accade tutto l'opposto. Un secolo distrugge la scienza del secolo passato: la letteratura resta immobile, o se si muta, si riconosce ben tosto per corrotta, e si torna indietro.

Giacomo Leopardi

Abstract

The earliest 3D printing technologies first became visible in the late 1980's. This technology, initially also called Rapid Prototyping (RP), was originally conceived as a quick and convenient method for creating prototypes aimed to improving a product.

Throughout the 1990's and early 2000's a host of new technologies continued to be introduced, still focused wholly on industrial applications and while they were still largely processes for prototyping applications. Nowadays, 3D printing is used in many different areas, such as the biomedical sector, mechanical, industrial and civil.

The present work is focused on a specific technique: Fused Deposition Modeling (FDM). This is an additive manufacturing technology commonly used for modeling applications, prototyping and manufacturing. The filament deposed, binds with the previous by high temperatures and by the physical-chemical properties of the polymer. Depending on how the printed material is deposited, we can give to the final product different characteristics and different mechanical properties.

The purpose of this thesis is to predict the mechanical behavior of the final product, according to the intrinsic characteristics of the polymer and the micro-mechanics approach, simulating the sintering process of two particles, in order to calculate, by the density of voids of the final solid obtained by the superimposition of the layers, the elastic parameters of the material. The world of 3D printing seems to be little inherent in structural engineering, however, one of the most important goals of this thesis is to predict the mechanical behavior in order to exploit its potential. In this way, the evolution of this technology, may also contribute to the improvement of structures, guaranteeing improved efficiency during the project and efficacy during exercise.

Sommario

Il primo concetto di stampa 3D si è diffuso negli anni '80. Questa tecnologia, inizialmente chiamata anche Rapid Prototyping (RP), è stata originariamente concepita come un metodo più rapido e conveniente per la creazione di prototipi volti al miglioramento di un prodotto. Successivamente, nel corso degli anni '90 e nei primi anni 2000, sono state introdotte, nel campo industriale, un numero sempre maggiore di tecniche; Al giorno d'oggi, la stampa 3D è utilizzata in molti ambiti differenti, ad esempio il settore biomedico, meccanico, industriale e civile. Il presente lavoro è focalizzato su una specifica tecnica: Fused Deposition Modeling, in breve FDM; questa è una tecnologia di produzione additiva usata comunemente per applicazioni di modellazione, prototipazione e produzione.

Il filamento deposto, si lega con i precedenti grazie alle alte temperature ed alle proprietà chimico-fisiche del polimero. In base alla modalità con cui il materiale stampato viene deposto, si conferiscono al prodotto finale differenti caratteristiche e diverse proprietà meccaniche. Lo scopo di questa tesi è di prevedere il comportamento meccanico del prodotto finale, in base alle caratteristiche intrinseche del polimero e alla micro-meccanica del reticolo cristallino, simulando il processo di fusione di due particelle, al fine di calcolare, in base alla densità dei vuoti del solido finale, ottenuto con la sovrapposizione degli strati, i parametri elastici del materiale. Il mondo della stampa 3D trova oggi poco spazio nell'ambito dell'ingegneria strutturale; tuttavia è proposito di questa tesi, prevederne il comportamento meccanico al fine di sfruttarne il potenziale. In tal modo, l'evoluzione di questa tecnologia, può contribuire al miglioramento anche delle strutture, garantendo maggiore efficienza durante la fase di progettazione ed efficacia durante l'esercizio.

Contents

List of Figures

List of Tables

Chapter 1

Introduction

1.1 3D Printing

Invented by Chuck Hull back in 1986, 3D printing is a process of taking a digital 3D model and turning such digital file into a physical object. While Hull went on to launch one of the world's largest 3D printer manufacturers, 3D Systems, his invention concentrated solely on a fabrication process called Stereolithography (SLA). Since that time numerous other 3D printing technologies have been developed, such as Fused Deposition Modeling (FDM)/Fused Filament Fabrication (FFF), Selective Laser Sintering (SLS), PolyJetting and others, all of which rely on layer-by-layer fabrication and are based on a computer code fed to the printer.

While there are numerous technologies which can be used in 3D printing phenomenon, the majority of 3D printers one will find within a home or an office setting are based on the FDM/FFF or SLA processes, as these technologies are currently cheaper and easier to implement within a machine. '3D printing' can also be referred to as 'additive manufacturing,' especially when referring to its use within a manufacturing setting, and many individuals will used both phrases interchangeably.

How Do 3D Printers Work? This is a broad question, which was partially explained in the section above. With that said, the best way to really understand how 3D printing works is to understand the various technologies involved. Similarly to the way that engines function based on some of the same principles as one another, but don't all use gasoline or solar power, all 3D printers don't use the same base technology, but still manage to accomplish the same basic tasks. Before we get into each of these individual technologies, however, one should

understand the basic principles of transferring a 3D model on a computer screen to a 3D printer.

Computers are not like humans. Lot's of 1s and 0s are involved, meaning lots and lots of computer code. Once a 3D model is designed, the file (these usually have extensions such as 3MF, STL, OBJ, PLY, etc.) must be converted into something called G-code. G-code is a numerical control computer language used mainly for computer aided manufacturing (both subtractive and additive manufacturing). It is a language which tells a machine how to move. Without G-code there would be no way for the computer to communicate where to deposit, cure or sinter a material during the fabrication process. Once the G-code is created it can be sent to the 3D printer, providing a blueprint as to what its next several thousand moves will consist of. These steps all add up to the complete fabrication of a physical object. There are other computer languages out there and perhaps many will eventually gain popularity, but for now G-code is by far the most important.

Now let's take a look at some of the more popular technologies behind 3D printing:

- Fused Deposition Modeling (FDM): was invented by a man named S. Scott Crump a few years after Chuck Hull initially invented 3D printing. Crump went on to commercialize the technology in 1990 via Stratasys, which actually has a trademark on the term.

  Basically the way in which this technology works is rather simple, and this is the reason why 95% of all desktop 3D printers found within homes and garages today utilize FDM/FFF. A thermoplastic polymer such as PLA or ABS is fed into an extruder and through a hotend. The hotend then melts the plastic, turning it into a gooey liquid. The printer then acquires its instructions from the computer via G-code and deposits the molten plastic layer by layer until an entire object is fabricated. The plastic melts rather rapidly, providing a solid surface for each additional layer's deposition. Depending on the maximum temperature of the hotend as well as other variables, numerous other materials besides ABS and PLA may be used, including composites of both materials, nylon, and more.

- Stereolithography (SLA): as we've mentioned above, this was the very first 3D printing technology to be invented in 1986. With 3D Systems holding many of the patents involving this technology, which are in the process of 33 expiring over the next few years, there has not been a tremendous amount of competition within the market. This means

that the technology has been overpriced and used less often than the FDM alternative has. Instead of extruding a material out of a hot end, the SLA process works with a laser or DLP projector combined with a photosensitive resin. Objects are printed in a vat of resin as a laser or other lighting source like a projector slowly cures (hardens) the resin layer-by-layer as the object is formed. Typically SLA machines are able to achieve minor layer height.

- Selective Laser Sintering (SLS)/Selective Laser Melting (SLM)/Direct Metal Laser Sintering (DMLS): all three of these technologies are very similar, yet have marked differences. We've found that many individuals use the terms interchangeably when, in fact, there are reasons to use one method over the others. Both Selective Laser Sintering (SLS) and Direct Metal Laser Sintering (DMLS) are in fact the same technology. The 34difference in terminology is based on the materials used. DMLS specifically refers to the layer-by-layer sintering of metal powders using a laser beam, while SLS is simply the same process but with non-metal materials such as plastics, ceramics, glass, etc. Both DMLS and SLS do not fully melt the materials, instead sintering them or fusing them together at the molecular level. When dealing with metals, DMLS is ideal for metal alloys, as the molecules have varying melting points, meaning a full melt can sometimes be difficult to achieve. On the other hand, when dealing with metals consisting of one material, for instance titanium, Selective Laser Melting (SLM) is the way to go as a laser is able to completely melt the molecules together. All three processes are currently expensive, and out of the budgets of most individuals and even small businesses because of the high powered laser beams that are required. Additionally safety precautions must be taken, meaning additional expenses on the part of the user.

- Others: Every week it seems as though new approaches are presented for 3D printing. There are new technologies which have recently been unveiled like that of HP's Multi Jet Fusion, as well as Carbon3D's CLIP technology or PolyJetting.

What Is 3D Printing Used for and by Whom?

While initially 3D printing was primarily a technology for prototyping, this is quickly changing. Now numerous manufacturers are producing end-use components and entire products via additive manufacturing. From the aerospace industry, to medical modeling and implantation,

to prototyping of all kinds, 3D printing is being used by virtually every major industry on the planet in one way or another.

- Medicine: 3D printed models of human organs have been a frequent tool for surgeons over the last two to three years, as they provide a more intricate view of the issues at hand. Instead of relying on 2D and 3D images on a computer screen or a printout, surgeons can actually touch and feel physical replicas of the patient's organs, bone structures, or whatever else they are about to work on. Additionally, there is research underway by companies like Organovo to 3D print partial human organs such as the liver and kidney. Organovo is already 3D printing live human liver tissue for pharmaceutical toxicology testing. They do so by using a process similar to an FDM desktop 3D printer that you might find in a home, but instead of thermoplastics and heat, they use hydrogels infused with living cells. Over the next decade, this research should really begin to pay dividends, and within 15 to 20 years it's very possible that we will be 3D printing entire human organs for transplantation.

  Organizations such as Enabling The Future are printing prosthetic hands on sub-$2,000$ 3D printers by the hundreds, offering those with upper limb amputations something to cheer about. Besides 3D printing hands and arms, as well as legs, we have also seen 3D printed prosthetics for animals of all kinds, including a titanium jaw for a turtle, a shell for a tortoise, and legs for ducks, geese and even canines.

- Aerospace: because of the unique geometries offered by additive manufacturing, militaries around the world, as well as agencies such as NASA and the ESA, along with numerous aircraft manufacturers are turning to 3D printing in order to reduce the overall weight of their aircraft. Complex geometries and new materials offer superior strength with less mass, potentially saving organizations like NASA boatloads of fuel, and thus money, during the launching of spacecraft and/or rockets out of our atmosphere. At the same time, companies like Boeing and Airbus are using 3D printing to reduce the weight of their aircraft, allowing them to cut fuel costs for each flight.

- Prototyping: manufacturing facilities across the globe are using 3D printing as a way to reduce costs, save time, and produce better products. By no longer needing to outsource the prototyping of parts, companies are able to quickly iterate upon designs on the fly, oftentimes saving weeks of waiting for third parties to return molds or prototypes. From

automobile manufacturers to electronics companies and anyone in between, 3D printing is an invaluable technology.

- Art/Education: 3D printing is able to bring the imagination to life. Artists are not only able to jot their ideas down on a computer screen, they are able to physically bring those ideas into reality via digital models. What this technology does is it unleashes a whole new medium for creativity, not only for artists but for children and young adults who are now able to better visualize concepts, create functional products, and learn via hands-on experience.37 Over the next several years we will see an incredible expansion of the number of elementary, middle and high schools incorporating 3D printing into their curricula. This will in effect set these students up for careers which will almost certainly require 3D printing in one way, shape or form over the next decade or two.

1.2 Fused Deposition Modeling

Fused Deposition Modeling (FDM) is a basic Rapid Prototyping (RP) technologies used in technical practice. It's a process that consists of extruding and depositing semi-molten filaments on to a platform. FDM is an additive manufacturing technology commonly used for modeling, prototyping, and production applications. It is one of the techniques used for 3D printing and it is often used to build complex geometries and functional parts, including low-volume production pieces, manufacturing aids, jigs and fixtures.

The fused deposition modeling (FDM) machine is a computer-numerical-controlled (CNC) gantry machine carrying one or more miniature extruders with headed nozzles. The machine fabricates prototypes by extruding a semi-molten filament through a heated nozzle in a prescribed pattern onto a platform. As the material is deposited, it cools, solidifies, and bonds with the surrounding material. The formation of the bonding in the FDM process is driven by the thermal energy of the semi-molten material. The FDM prototypes are non-isotropic composites of polymer filaments, partial bonding between filaments, and voids.

In figura 1.1 is shown a simplified scheme of Fused Deposition Modeling process.

With this technique is possible to fabricate prototypes with locally controlled properties. Changing the deposition density and deposition orientation, referring to the direction in which the force is applied, it's possible to ensure the material more resistance in a desired point and greater flexibility in another, as in 1 figure 1.2:

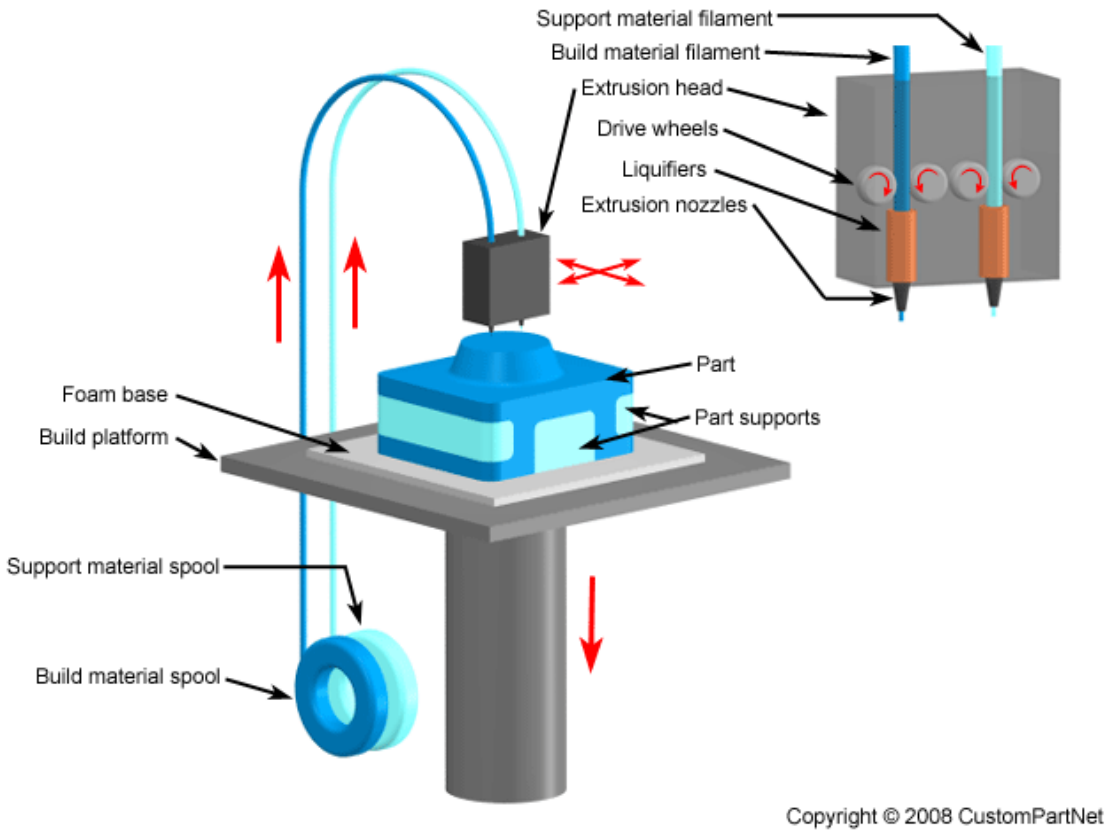

Figure 1.1: Schematic FDM process.

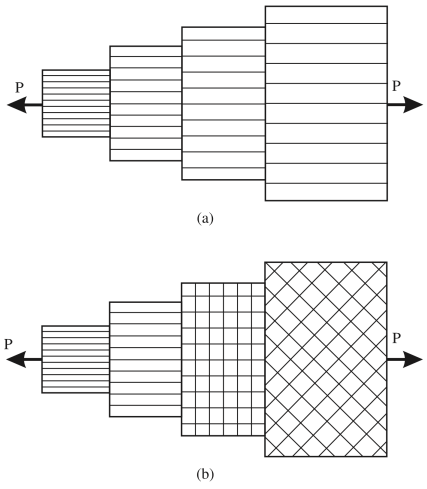

Figure 1.2: Parts with graded mechanical properties.

1.3 Rheology

Rheology is the science of the flow and deformation of matter (liquid or 'soft' solid) under the effect of an applied force.

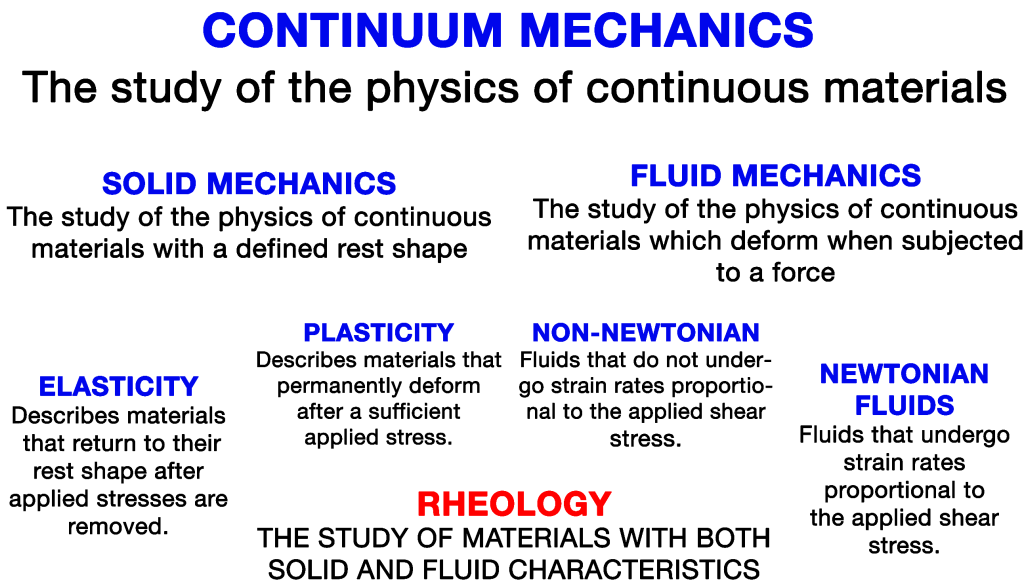

Figure 1.3: Rheology framing

It is the study of the flow of matter, primarily in a liquid state, but also as 'soft solids' or solids under conditions in which they respond with plastic flow rather than deforming elastically in response to an applied force. It applies to substances which have a complex microstructure, such as muds, sludges, suspensions, polymers and other glass formers (e.g., silicates), as well as many foods and additives, bodily fluids (e.g., blood) and other biological materials or other materials which belong to the class of soft matter.

Newtonian fluids can be characterized by a single coefficient of viscosity for a specific temperature. Although this viscosity will change with temperature, it does not change with the strain rate. Only a small group of fluids exhibit such constant viscosity. The large class of fluids whose viscosity changes with the strain rate (the relative flow velocity) are called non-Newtonian fluids.

Rheology generally accounts for the behavior of non-Newtonian fluids, by characterizing the minimum number of functions that are needed to relate stresses with rate of change of strain or strain rates. For example, ketchup can have its viscosity reduced by shaking (or other forms of mechanical agitation, where the relative movement of different layers in the material actually causes the reduction in viscosity) but water cannot. Ketchup is a shear thinning material, like yoghurt and emulsion paint (US terminology latex paint or acrylic paint), exhibiting thixotropy,

where an increase in relative flow velocity will cause a reduction in viscosity, for example, by stirring. Some other non-Newtonian materials show the opposite behavior, rheopecty: viscosity going up with relative deformation, and are called shear thickening or dilatant materials. Since Sir Isaac Newton originated the concept of viscosity, the study of liquids with strain rate dependent viscosity is also often called Non-Newtonian fluid mechanics.

The term rheology was coined by Eugene C. Bingham, a professor at Lafayette College, in 1920, from a suggestion by a colleague, Markus Reiner. The term was inspired by the aphorism of Simplicius (often attributed to Heraclitus), panta rhei, 'everything flows' [5].

The experimental characterization of a material's rheological behaviour is known as rheometry, although the term rheology is frequently used synonymously with rheometry, particularly by experimentalists. Theoretical aspects of rheology are the relation of the flow/deformation behaviour of material and its internal structure (e.g., the orientation and elongation of polymer molecules), and the flow/deformation behaviour of materials that cannot be described by classical fluid mechanics or elasticity.

What is the scope of Rheology?

In practice, rheology is principally concerned with extending continuum mechanics to characterize flow of materials, that exhibits a combination of elastic, viscous and plastic behavior by properly combining elasticity and (Newtonian) fluid mechanics. It is also concerned with establishing predictions for mechanical behavior (on the continuum mechanical scale) based on the micro- or nanostructure of the material, e.g. the molecular size and architecture of polymers in solution or the particle size distribution in a solid suspension. Materials with the characteristics of a fluid will flow when subjected to a stress which is defined as the force per area. There are different sorts of stress (e.g. shear, torsional, etc.) and materials can respond differently for different stresses. Much of theoretical rheology is concerned with associating external forces and torques with internal stresses and internal strain gradients and flow velocities. [68]

Rheology unites the seemingly unrelated fields of plasticity and non-Newtonian fluid dynamics by recognizing that materials undergoing these types of deformation are unable to support a stress (particularly a shear stress, since it is easier to analyze shear deformation) in static equilibrium. In this sense, a solid undergoing plastic deformation is a fluid, although no viscosity coefficient is associated with this flow. Granular rheology refers to the continuum mechanical description of granular materials.

One of the major tasks of rheology is to empirically establish the relationships between deformations (or rates of deformation) and stresses, by adequate measurements, although a number of theoretical developments (such as assuring frame invariants) are also required before using the empirical data. These experimental techniques are known as rheometry and are concerned with the determination with well-defined rheological material functions. Such relationships are then amenable to mathematical treatment by the established methods of continuum mechanics.

1.4 ABS Material

Acrylonitrile butadiene styrene (ABS) (chemical formula $(C_8H_8 \cdot C_4H_6 \cdot C_3H_3N)_n$) is a common thermoplastic polymer. Its glass transition temperature is approximately $178\ K$.ABS is amorphous and therefore has no true melting point. ABS is a terpolymer made by polymerizing styrene and acrylonitrile in the presence of polybutadiene. The proportions can vary from 15 to 35% acrylonitrile, 5 to 30% butadiene and 40 to 60% styrene. The result is a long chain of polybutadiene criss-crossed with shorter chains of poly(styrene-co-acrylonitrile). The nitrile groups from neighboring chains, being polar, attract each other and bind the chains together, making ABS stronger than pure polystyrene. The styrene gives the plastic a shiny, impervious surface. The polybutadiene, a rubbery substance, provides toughness even at low temperatures. For the majority of applications, ABS can be used between 253.15 K and 353.15 K as its mechanical properties vary with temperature. The properties are created by rubber toughening, where fine particles of elastomer are distributed throughout the rigid matrix.

1.5 ABS Material Properties

In the following table 1.1, are presented some of its characteristics, necessary to the following work:

ABS MATERIAL PROPERTIES			
Young Modulus	**Poisson Ratio**	**Bulk Modulus**	**Shear Modulus**
$E\ [Mpa]$	$\nu\ [-]$	$K\ [Mpa]$	$G\ [Mpa]$
2000 ÷ 2300	0.25	1333.33	800
Lame Constant	**Filament Radius**	**Extrusion Speed**	**Density**
$\lambda\ [Mpa]$	$R\ [mm]$	$v\ [mm/s]$	$\rho\ [Kg/m^3]$
800	0.2	20÷60	1050
T Critica	**t Critico**	**Viscosity**	**Melt Viscosity**
$T_{cr}\ [K]$	$t\ [s]$	$\eta_0\ [Pa \cdot s]$	$\eta\ [Pa \cdot s]$
573.15	1.7504	5100	300
Atomic Volume	**Diffusivity**	**Surface Tension**	**H. Trans. Coeff.**
$\Omega\ [m^3/mol]$	$D\ [mm^2/s]$	$\Gamma\ [N/mm]$	$h\ [W/m^2K]$
5.53024E-07	1.0E-12	2.90E-05	50
Thermal Conductivity	**Specific Heat**	**T Room**	
$k\ [W/mK]$	$c\ [J/kgK]$	$T_{inf}\ [K]$	
0.177	2080	343.15	

Table 1.1: ABS properties [43], [44], [45], [42], [36], [37], [38]

1.6 Levels of Analysis

The solidification process of a polymer layer on the others (layer-to-layer) is called Bonding formation.

This process is examined at *micro level*: analyzing the adhesion between the adjacent filaments and adhesion of a layer on the other, and at it macro level: analyzing the behavior of the layer forming the homogeneous solid as orthotropic plates.

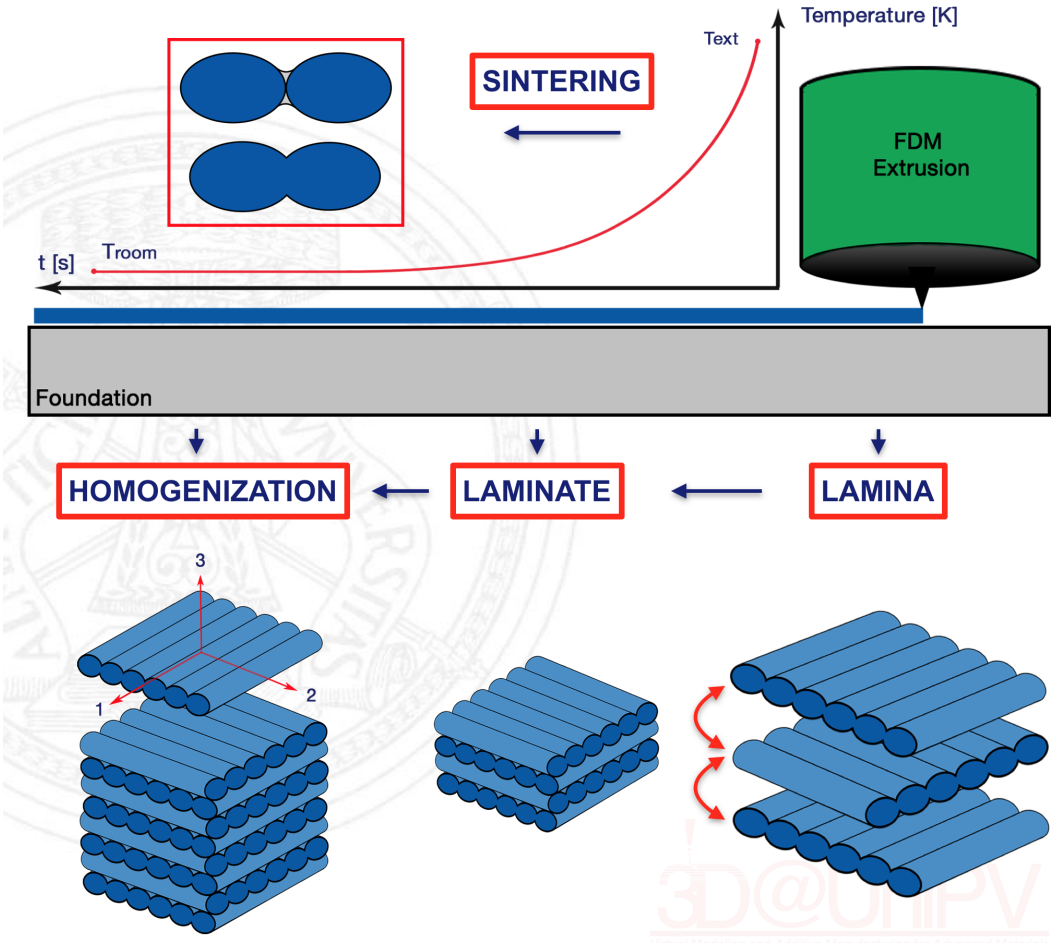

Figure 1.4: Levels of analysis

Thus, at macro level, the properties are referred to laminated sheets glued. On a micro level, the properties of each lamina are functions of the filaments properties, the bonds quality between the filaments, and the density of voids.

Io order to study the polymer layers deposited as a equivalent laminae, it's necessary to obtain parameters that characterize the material in a homogeneous manner, thus taking into

account of the voids generated by the failure of the complete fusion, and of the non-perfect adherence of one filament with each other.

The adhesion between filaments is controlled by the thermal energy exchange of the semi-molten material. The temperature evolution of interfaces plays an important role in determining the bonding quality and thus, the properties of final prototype.

As shown in figure 1.4, there are 3 big steps to analyze in this work:

1. Sintering Process;
2. Lamination Analysis;
3. Characterization of the Homogeneous Equivalent Material.

Part I

Thermal Analysis

Chapter 2

Thermal Analysis

The formation of the bonding in FDM process is driven by the thermal energy of the semi-molten material.

The required heat transfer is a function of the thermal properties of the liquefier, tip, and modeling materials, as well as the diameter of the filament and volumetric flow rate.

When the filament is deposited and is in contact with surrounding material, the interface's temperature is well above the material's glass transition temperature[1].

The heat transfer modeling of the FDM process can provide the temperature profile during the cooling process, which is useful for analyzing the bonding phenomenon.

It can provide thermal compatibility between the various layers.

The bonding quality, is assessed by the degree of wetting or the size of the neck formed between adjacent filaments. This chapter is aimed at modeling the dynamics of bond formation among polymer filaments during the FDM extrusion process and evaluating the effects of different manufacturing parameters on the bond formation.

2.1 Modelling the cooling process

To analyze the phenomenon, we use the global energy balance equation, by applying the appropriate boundary conditions [43] .

The assumptions made are the following:

[1] Usually indicated by the symbol T_g, it rapresents the temperature value below which an amorphous material behaves as a glassy solid

- uniform temperature distribution across the cross-sectional area of the filament;
- the cooling process of a single filament is thus simplified into a one-dimensional transient heat transfer model;
- lumped-capacity analysis applicable: it reduces a thermal system to a number of discrete "lumps" and assumes that the temperature difference inside each lump is negligible. This approximation is useful to simplify otherwise complex differential heat equations (Biot number Bi«1);
- the head moves at a constant speed of v along the x-axis when extruding;
- semi-infinite filament length (Length > Diameter);
- constant heat transfer/convection coefficients.

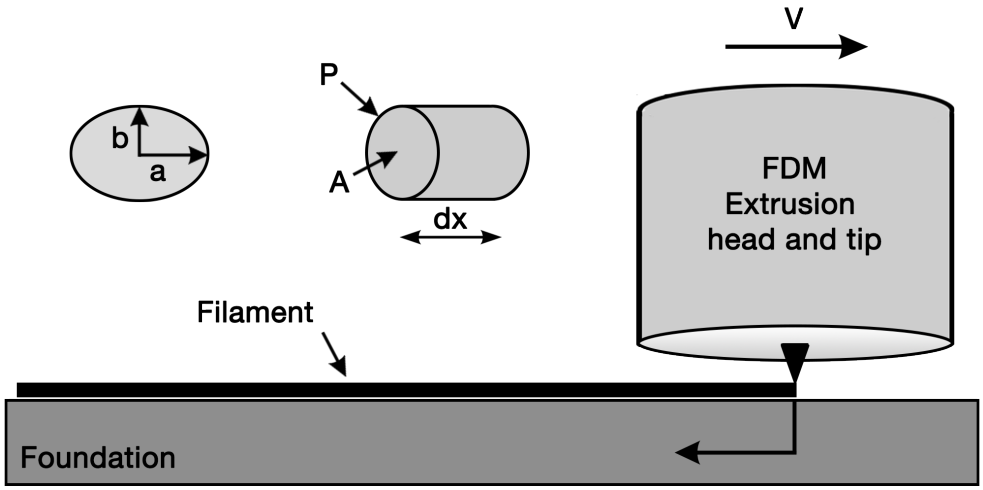

Figure 2.1: Schematic of Deposition and Cooling of A filament in the FDM process

In 2.1 a schematic diagram of FDM extrusion process is shown. A single deposition road is modeled as one-dimensional block. The head moves at a constant speed of v along the X axis when extruding. The origin of the reference coordinate is set at the beginning of the extruded filament. The cross-sectional shape of the filament is an ellipse with area A and perimeter P. At time t, the tip is at position $l = vt$.

$$P = \pi(a+b)\left(\frac{64-3\lambda^4}{64-16\lambda^2}\right) \quad with \quad \lambda = \frac{a-b}{a+b} \tag{2.1}$$

$$A = \pi ab \tag{2.2}$$

The thermal energy analysis for the differential element of thickness dx, is studied as follows:

- Energy out left face:

$$-kA\frac{\partial T}{\partial x}$$

- Change in the internal energy:

$$\rho CA\frac{\partial T}{\partial t}dx$$

- Energy in the right face:

$$-kA\frac{\partial T}{\partial x}\bigg|_{x+dx} = -A\left[k\frac{\partial T}{\partial x} + \frac{\partial\left(k\frac{\partial T}{\partial x}\right)}{\partial x}dx\right]$$

- Convection heat transfer with air:

$$h'(P - S)(T - T_\infty)dx$$

- Conduction heat transfer with foundation:

$$h'' S(T - T_\infty)dx$$

where:

- T_∞, T_0 and T are envelope, liquefier temperature and averaged cross-section temperature respectively;
- $k\ \left[\frac{W}{m^2 \cdot K}\right]$ is the thermal conductivity;
- $\rho\ \left[\frac{kg}{m^3}\right]$ is the density of material;
- $C\ \left[\frac{J}{kg \cdot K}\right]$ represent the specific heat;

- h' and h'' $\left[\frac{W}{m^2 \cdot K}\right]$ are convective coefficients of the system;
- S is the cross-sectional contact length between the filament and the foundation.

Since the mass of the foundation is much higher than that of the filament, the conduction at the interface would not appreciably change the temperature of foundation. The conduction heat transfer with the foundation can be considered in the form of convection, with a convection coefficient h''.

For an infinitesimal element, the energy balance is made:

$$\rho C A \frac{\partial T}{\partial t} = A \frac{\partial \left(k \frac{\partial T}{\partial x}\right)}{\partial x} - hP(T - T_\infty) \tag{2.3}$$

with

$$T = T_0 \ at \ x = 0, \ t \geq 0 \qquad T = T_\infty \ at \ x = \infty, \ t \geq 0 \tag{2.4}$$

The time-dependence term $\frac{\partial T}{\partial t}$ is transformed to $\frac{\partial T}{\partial x}\frac{\partial x}{\partial t} = \frac{\partial T}{\partial t}v$.

The governing equation is reduced to an ordinary differential equation:

$$\rho C A v \frac{\partial T}{\partial t} = A \frac{\partial \left(k \frac{\partial T}{\partial x}\right)}{\partial x} - hP(T - T_\infty) \tag{2.5}$$

The analytical solution of 2.5, with the boundary conditions defined by 2.4 is follows:

$$T = T_\infty + (T_0 - T_\infty)e^{-mx} \tag{2.6}$$

with

$$m = \frac{\sqrt{1 + 4\alpha\beta} - 1}{2\alpha} \qquad \alpha = \frac{k}{\rho C v} \qquad \beta = \frac{hP}{\rho C A v}$$

It's shown that, as expected, the temperature profile, depends mostly on materials characteristics. The parameters that can be modified are the temperature T_{inf}, T_0, v, a and b.

2.2 Temperature Profile

Setting parameters in Mathematica, based on experimental values in [43], the temperature profile is obtained. It's important to remember that the aforesaid profile is reported to a one-dimensional filament that is deposited along the x-direction. the parameter values are summarized in table 2.1:

Table 2.1: Parameters for the temperature profile

T_∞	T_0	a	b	v	C	h	ρ	k
$[K]$	$[K]$	$[mm]$	$[mm]$	$[m/s]$	$[J/kgK]$	$[W/m^2K]$	$[kg/m^3]$	$[W/mK]$
343.15	543.15	0.254	0.127	0.024	2080	50	1050	0.177

Through equations 2.1 and 2.2, it's possible to calculate perimeter and area of filaments. Once calcualted all parameters, the temperature profile, function of x, is as follows:

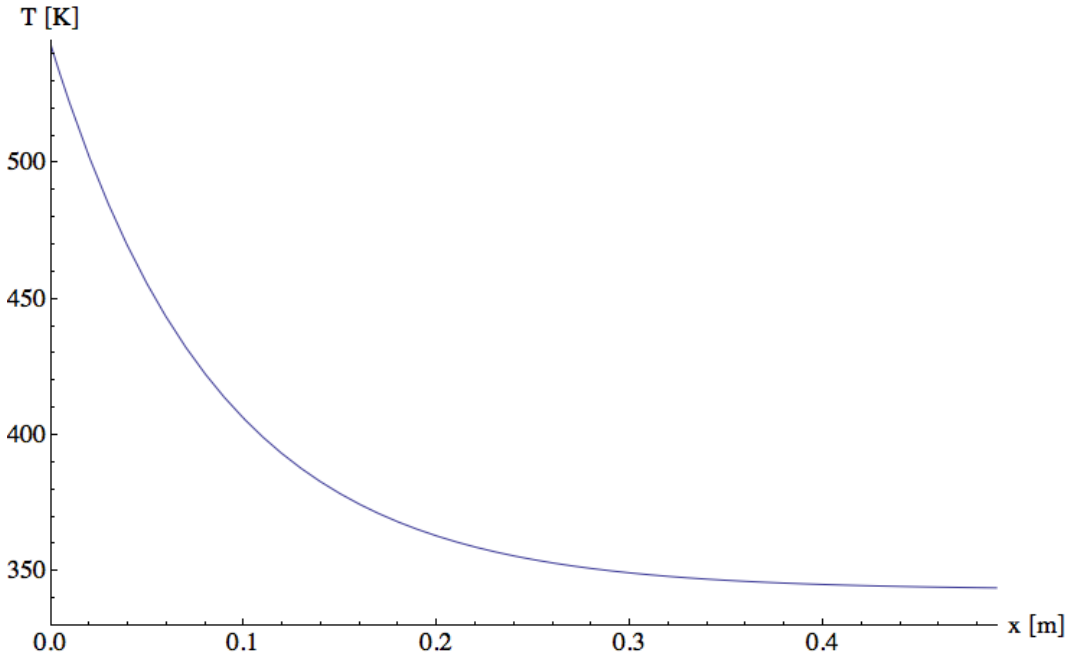

Figure 2.2: Temperature profile function of space

Making explicit the space as velocity v multiplied t, and substituting in equation 2.6, you

get the temperature profile function of time, as shown in figure 2.3.

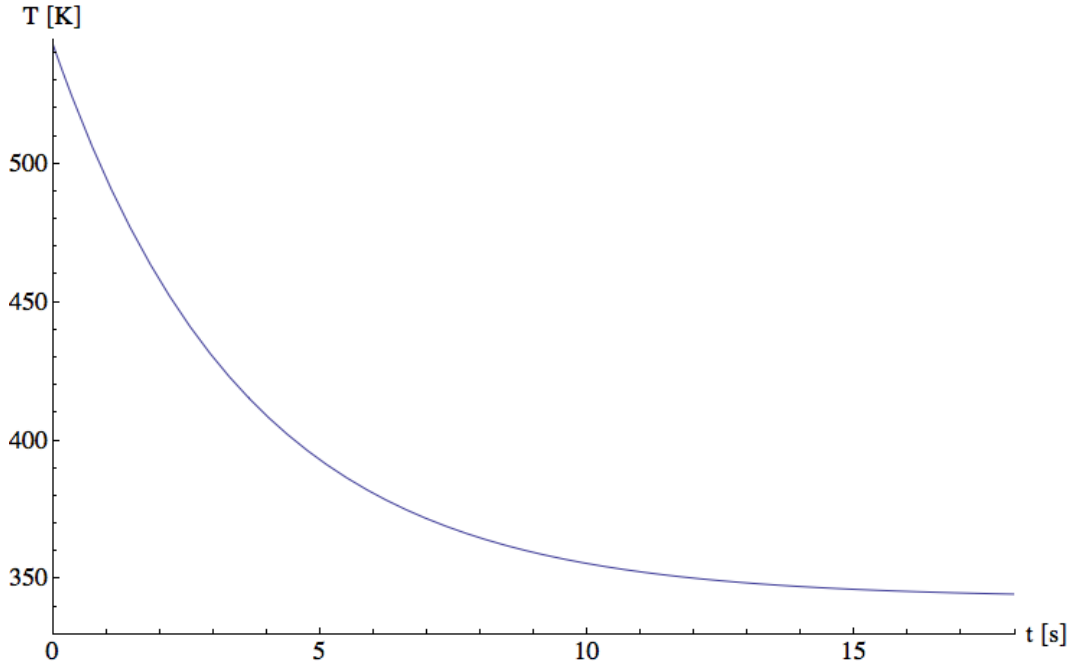

Figure 2.3: Temperature profile function of time

It's important to have an idea of temperature evolution over time because, as will be subsequently shown, the sintering process, is negligible below 473.15 K. For convenience, the aformentioned temperature, will be called T_{sint}. It can be seen that, the temperature window over T_{sint} in which sintering happens, is very small and this is the cause of the non-perfect bonding between filaments.

Part II

Sintering Process

Chapter 3

Continuum Approach to Sintering

3.1 Description of Sintering Process at Grain Scale

From a physical point of view, sintering is a thermally activated phenomenon driven by the excess of free energy of the system and which allows the passage from a consolidated particles to a coherent material. From a practical point of view, this process can be described as an operation where a lattice compact changes its structure to obtain a solid density-controlled body with some specific mechanical properties.

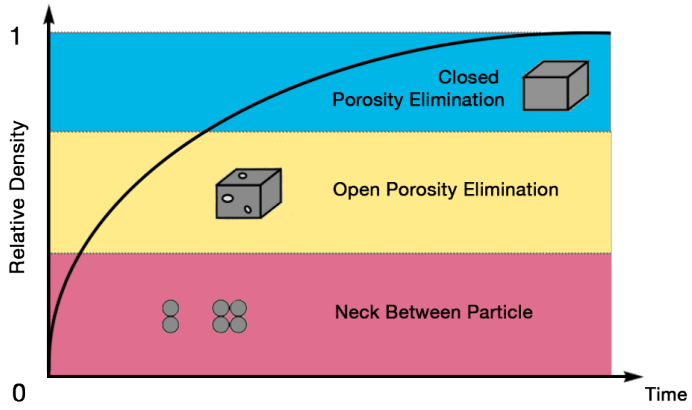

Figure 3.1: Sintering stages

Referring to figure 3.1, it can be possible to identify three sequential stages during sintering process:

1. In the first stafe, the neck bridging the particles is rapidly created and the particles of the system are still distinguishable. This stage is supposed to last until the radius of the

neck between the particles has reached a value about **0.4 – 0.5** of the particle radius. (equivalent to a packing density of about 0.65).

2. At the beginning of this intermediate stage, the porosity is still open, which means that pores are interconnected and their shape is roughly cylindrical. As the different diffusion paths take place, the porosity shrinks, some isolated pores appear and the packing density continues raising up to a value of about 0.92. It is important to highlight that this stage covers the major part of the sintering process.

3. This final stage leads to the final microstructure of the material. The pores, which are isolated and spherical, are supposed to continue shrinking to finally end up by almost disappearing. The final relative density of the material can raise up to **0.999**.

It is possible to distinguish at least six mechanisms leading to the neck growth and/or the densification of the solid, collected in the following table, and shown in figure 3.2:

Diffusion Path	**Source**	**Sink**	
1	Surface diffusion	Surface	Neck
2	Volume diffusion	Surface	Neck
3	Vapour transport	Surface	Neck
4	Grain boundary diffusion	Grain boundary	Neck
5	Volume diffusion	Grain boundary	Neck
6	Surface diffusion	Dislocation	Neck

Table 3.1: Diffusion routes

As the diffusion phenomena take place, the total free surface is reduced, but at the same time, the surface of the solid-solid interfaces (the grain boundary surface) increases. The grain boundary energies usually are lower than surface energies. However the mass transport can stop because of the establishment of local equilibrium between grain boundary and surface energy. Only some of above mentioned routes lead to a densification of structure, respectively the last three. At the particle scale, the densification is defined as the rate at which the particle centres approach each other.

Sintering is not considered as a chemical diffusion process studied in term of chemical potential. In this work, it's adopted a different point of view, that is more general. The

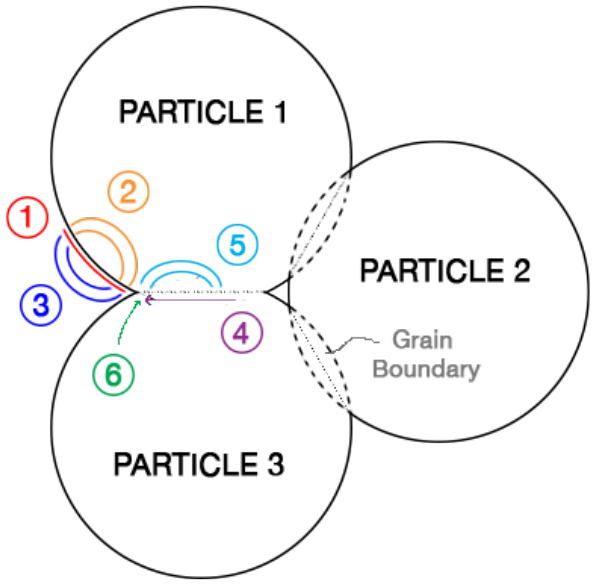

Figure 3.2: Diffusion routes

momentum and energy balances and the entropy imbalance are the starting point of the theory. Following this approach, chemical potentials are introduced at a basic level in the energy balance equation as characterizing the energy carried by chemical species transport. The advantage of this approach is that it leads to the automatic formulation ofterms of coupling between the continuum mechanics scale (described by a strain tensor or a stress tensor) and the diffusion phenomena (described by the chemical species densities and chemical potentials).

As shown in the next section (Figure 3.4), only a certain fraction of atoms will have sufficient energy to be able to move from one position to another.

It took note of this, the diffusion coefficient D is expected to depend on the temperature as follows:

$$D = D_0 \exp - \left(\frac{Q}{kT} \right) \tag{3.1}$$

where Q is the activation energy, k is the Boltzmann's constant and $T > 0$ is the absolute temperature. For further details about diffusion coefficient see A.4.

3.2 Mechanical Problem: Continuum Thermodynamics for Lattice Diffusion

The aim of this section is to find the set of equations that describes the phenomenon of sintering from a mechanical point of view.

3.2.1 Equilibrium Equations

Consider the equilibrium of a body of volume V and surface S subject to the following actions:

(a) Body force field f of components b_i in V;

(b) Acceleration field $\mathbf{a} = \frac{d^2\mathbf{u}}{dt^2}$ of components a_i in V;

(c) Stress vectors t of components t_i on S.

Dynamic equilibrium along any direction x_i requires

$$\int_S t_i dS + \int_V b_i dV = \int_V \rho a_i dV \tag{3.2}$$

where ρ is the body density. Substituting $t_i = \sigma_{ij} n_j$ in surface integral:

$$\int_S \sigma_{ij} n_j dS + \int_V b_i dV = \int_V \rho a_i dV \tag{3.3}$$

To transform the surface integral to a volume integral we use Divergence Theorem. For any vector field a:

$$\int_S a_j n_j dS = \int_V \frac{\partial a_j}{\partial x_j} dV \tag{3.4}$$

Consequently the equilibrium integral may be reduced to

$$\int_V \left[\sigma_{ij,j} + b_i - \rho a_i\right] dV = 0 \tag{3.5}$$

for an arbitrary volume. Because the volume is arbitrary we must have

$$\sigma_{ij,j} + b_i - \rho a_i = 0 \tag{3.6}$$

If the medium is at rest or moving uniformly with respect to an inertial frame, such as in sintering process, the accelerations vanish and we obtain the equations of static equilibrium:

$$\sigma_{ij,j} + b_i = 0 \tag{3.7}$$

3.2.2 Atom Population Balance Law

To have an idea of what "Atom Population" means, figure 3.3 show a simple example of the problem.

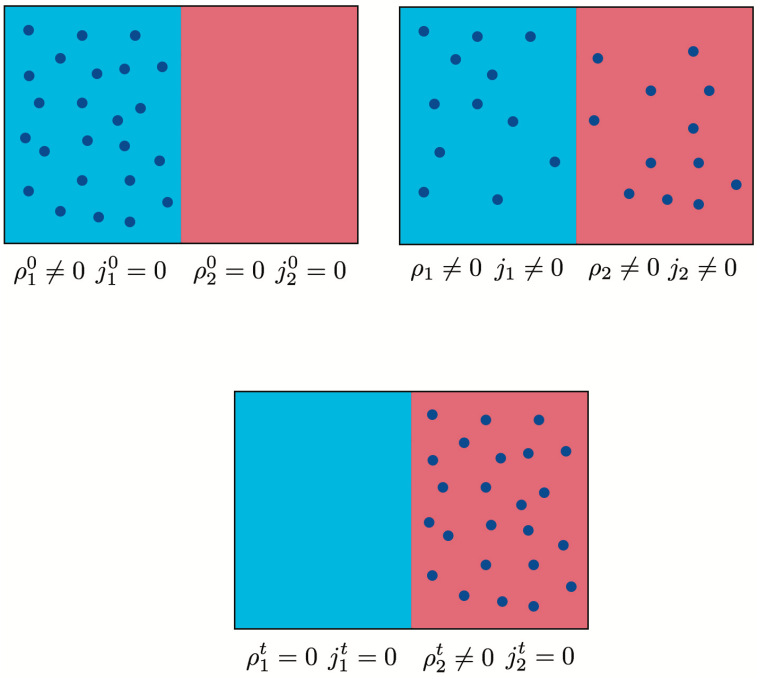

Figure 3.3: A simple example of atom population of two identical representative volumes. The three figures are, respectively, atom population at $t = 0$, at $t = t$ and $t = t_{end}$

Treatment of solids is, in this work, more complicated than descriptions usually encountered in continuum mechanics as the theory, although macroscopic, allows for microstructure by associating with each $x \in \mathcal{B}$ a lattice (or network) through which atoms diffuse.

N species of atoms are consided, labelled $\alpha = 1, 2, ..., N$ and let $\rho^\alpha(x, t)$ denote the atomic density of species α, which is the density measured in atoms per unit volume. If $\mathcal{P}$ is a part of $\mathcal{B}$, then $\int_{\mathcal{P}} \rho^\alpha dV$ represents the number of atoms of α in $\mathcal{P}$. Changes in the number of α-atoms in $\mathcal{P}$ are generally brought about by the diffusion of species α across the boundary $\partial\mathcal{P}$. This diffusion is characterized by an atomic flux (vector) $j^a(x, t)$, measured in atoms per unit area, per unit time, so that $-\int_{\partial\mathcal{P}} j^\alpha \cdot \nu dA$ the number of α-atoms entering $\mathcal{P}$ across $\partial\mathcal{P}$,

per unit time. The balance law for atoms therefore is:

$$\frac{d}{dt}\int_{\mathcal{P}} \rho^{\alpha} dV = -\int_{\partial\mathcal{P}} j^{\alpha} \cdot v dA \tag{3.8}$$

for all species α and every part of $\mathcal{P}$. Using divergence theorem in the integral over $\partial\mathcal{P}$, equation 3.8 become:

$$\int_{\mathcal{P}} (\dot{\rho}^{\alpha} + div j^{\alpha}) dV \tag{3.9}$$

Consequently, the local atom balance is:

$$\dot{\rho}^{\alpha} + \nabla \cdot j^{\alpha} = 0 \tag{3.10}$$

and, for notation simplicity, in the rest of present work, we'll use:

$$\dot{\rho} + \nabla \cdot j = 0 \tag{3.11}$$

3.2.3 Constitutive Equation

Let $\Theta(\boldsymbol{x}, t)$ denote the internal energy per unit of volume. The internal energy of any part of control volume ω is the same defined in Eq. B.1. The first law of thermodynamics implies that changes in the internal energy of ω are balanced by energy carried into ω by atomic transport, heat transferred through $\partial\omega$ and power expended by tractions on $\partial\omega$.

Chemical potentials is viewed as primitive quantities that enter the theory through the manner in which they appear in the basic law expressing balance of energy. As shown in [23], we use considers balance of energy as basic, and in a continuum theory that involves a flow of atoms through the material it is necessary to account for energy carried with the flowing atoms. To characterize the energy carried into ω by atomic transport, chemical potentials $\mu^{\alpha}(\boldsymbol{x}, t)$ of the individual species α it's introduced; specifically, the flow of atoms of species α, as represented by $\boldsymbol{j}^{\alpha}$ (number of atoms per unit area per unit time), is presumed to carry with it a flux of energy described by $\mu^{\alpha}\boldsymbol{j}^{\alpha}$. Assuming, for the moment, that $\boldsymbol{N}$ species are diffusing into the solid body, the net rate at which energy is carried into ω by the atom diffusive fluxes is expressed by

$$-\sum_{\alpha=1}^{N}\int_{\partial\omega}\mu^{\alpha}\boldsymbol{j}^{\alpha}\cdot\boldsymbol{n}dA \tag{3.12}$$

Finally, by expressing the heat transferred to ω with the heat flux $\boldsymbol{q}$, the energy can be written as:

$$\frac{d}{dt}\int_{\omega}\Theta dV=\int_{\partial\omega}(\boldsymbol{\sigma}\boldsymbol{n})\cdot\dot{\boldsymbol{u}}dA-\int_{\partial\omega}\boldsymbol{q}\cdot\boldsymbol{n}dA-\sum_{\alpha=1}^{N}\int_{\partial\omega}\mu^{\alpha}\boldsymbol{j}^{\alpha}\cdot\boldsymbol{n}dA \tag{3.13}$$

for any $\omega\subset\Omega$.

First thermodynamics law, expressed by Eq. 3.13, is completed with the second thermodynamics law which says that the entropy of any domain ω changes at a rate not less than the entropy flow into ω. Let recall Eq. B.13:

$$\frac{d}{dT}\int_{\omega}SdV\geq-\int_{\partial\omega}\frac{\boldsymbol{q}}{T}\cdot\boldsymbol{n}dA \tag{3.14}$$

to be satisfied any $\omega\subset\Omega$.

Isothermal conditions are now assumed prevailing in Ω, let recall Eq. B.18 (Helmotz free energy). Multiplying Eq. 3.14 by T, and subtracting the result to Eq. 3.13, leads to the Helmotz free energy imbalance:

$$\frac{d}{dt}\int_{\omega}\varphi dV\leq\int_{\partial\Omega}(\boldsymbol{\sigma}\boldsymbol{n})\cdot\dot{\boldsymbol{u}}dA-\sum_{\alpha=1}^{N}\int_{\partial\omega}\mu^{\alpha}\boldsymbol{j}^{\alpha}\cdot\boldsymbol{n}dA \tag{3.15}$$

By the Divergence theorem and Eq. 3.15, the imbalance can be rewritten as:

$$\int_{\omega}\left(\rho\frac{d\varphi}{dt}-\boldsymbol{\sigma}:\dot{\boldsymbol{\varepsilon}}+\sum_{\alpha=1}^{N}\nabla\cdot(\mu^{\alpha}\boldsymbol{j}^{\alpha})\right)dV\leq 0 \tag{3.16}$$

where $\dot{\boldsymbol{\varepsilon}}$ is the strain rate tensor.

We conclude to the dissipation inequality:

$$\delta\overset{def}{=}-\sum_{\alpha=1}^{N}(\mu^{\alpha}\nabla\cdot\boldsymbol{j}^{\alpha}+\nabla\mu^{\alpha}\cdot\boldsymbol{j}^{\alpha})+\boldsymbol{\sigma}:\boldsymbol{\varepsilon}-\rho\dot{\varphi} \tag{3.17}$$

where δ represents the dissipation per volume unit.

The theory exposed up to this point is pretty general. Next, this theory is used to obtain constitutive laws coupling stress and diffusion. However, developments will be restricted to the sintering framework, and consequently, will be made the following assumptions:

- Solid body is considered as a binary of mixture of atoms (one species) and vacancies, which is mechanically simple;
- Solid body presents cubic symmetries.

Further details of this assumption will be defined later. Figure 3.4 shows how free energy leads to a redistribution of atoms.

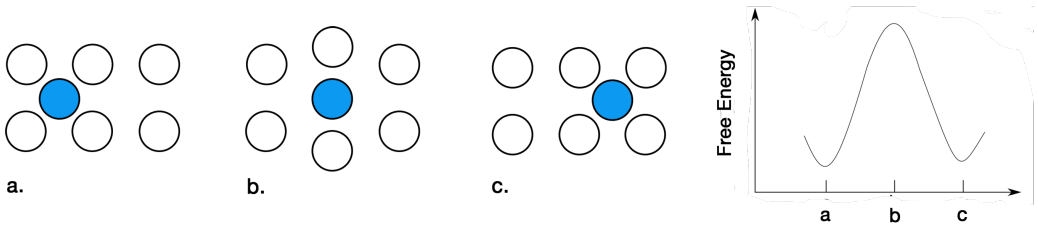

Figure 3.4: Schematic diagram showing the configuration of a set of atoms when one of them changes its position (a. b. and c.) and the corresponding free energy of the lattice (d.).

Since the diffusion is seen as an exchange between an atom and a vacancy, atom and vacancy fluxes have to satisfy:

$$\boldsymbol{j}^a + \boldsymbol{j}^v = 0 \tag{3.18}$$

and dissipation δ can be rewritten as:

$$\delta = -(\mu^{av}\nabla \cdot \boldsymbol{j}^a + \nabla\mu^{av} \cdot \boldsymbol{j}^a) + \boldsymbol{\sigma} : \boldsymbol{\varepsilon} - \rho\dot{\varphi} \geq 0 \tag{3.19}$$

where the relative chemical potential μ^{av} is the difference between atom and vacancy chemical potentials.

Difining ρ^a the atom density and ρ^v the vacancy density (number of atoms or vacancies per unit of volume) and recalling the popolation balance law (Eq. 3.10), implies that:

$$\dot{\rho}^a + \dot{\rho}^v = 0 \quad \text{and leads to lattice constraint} \quad \rho^a + \rho^v = \rho^{sites} \tag{3.20}$$

where ρ^{sites} represents the density of substitutional sites, per unit volume, available for occupation by atoms.

Following quantities are setted:

$$\varphi = \varphi(\rho^a, \varepsilon) \quad \boldsymbol{\sigma} = \boldsymbol{\sigma}(\rho^a, \varepsilon) \quad \mu^{av} = \mu^{av}(\rho^a, \varepsilon) \tag{3.21}$$

and by Fick's law mentioned in Appendix A.1, the flux has been defined as:

$$\boldsymbol{j}^a = -m^a(\rho^a)\nabla\mu^{av} \tag{3.22}$$

where m^a is the atomic mobility which is assumed to be scalar (cubic symmetry) independent of the strain (material mechanically simple).

Substituting equations Eq. 3.22 in Eq. 3.19, leads to:

$$m^a(\nabla\mu^{av})^2 + \left(\boldsymbol{\sigma} - \rho\frac{\partial\varphi}{\partial\boldsymbol{\varepsilon}}\right) : \dot{\boldsymbol{\varepsilon}} + (\frac{\partial^v\varphi}{\partial\rho^a} - \mu^{av})\dot{\rho}^a \geq 0 \tag{3.23}$$

Dissipation inequality has to be fullfilled for any strain and atomic density rates, modility must be non-negative ($m^a \geq 0$), stress and chemical potential can be defined as follow:

$$\boldsymbol{\sigma} = \rho\frac{\partial\varphi}{\partial\boldsymbol{\varepsilon}} = \frac{\partial\Psi}{\partial\boldsymbol{\varepsilon}} \qquad \mu^{av} = \rho\frac{\partial^v\varphi}{\partial\rho^a} = \frac{\partial^v\Psi}{\partial\rho^a} \tag{3.24}$$

It's simple to find now the Maxwell's relation:

$$\rho = \boldsymbol{\sigma}\frac{\partial\boldsymbol{\varepsilon}}{\partial\varphi} = \mu^{av}\frac{\partial\rho^a}{\partial^v\varphi} \quad \longrightarrow \quad \frac{\partial^v\boldsymbol{\sigma}}{\partial\rho^a} = \frac{\partial\mu^{av}}{\partial\boldsymbol{\varepsilon}} \tag{3.25}$$

and the Gibbs relation:

$$\dot{\Psi} = \boldsymbol{\sigma} : \dot{\boldsymbol{\varepsilon}} + \mu^{av}\dot{\rho}^a \tag{3.26}$$

Now, it's time to define the following important tensors:

$$\underline{\underline{\boldsymbol{C}}} \equiv \boldsymbol{C} = \frac{\partial\boldsymbol{\sigma}}{\partial\boldsymbol{\varepsilon}} = \frac{\partial^2\Psi}{\partial\varepsilon\,\partial\varepsilon} \quad \text{and} \quad \boldsymbol{A} = \frac{\partial\mu^{av}}{\partial\boldsymbol{\varepsilon}} = \frac{\partial^2\Psi}{\partial\rho^a\,\partial\varepsilon} \tag{3.27}$$

where $\boldsymbol{C}$ is the fourth-order elasticity tensor, and $\boldsymbol{A}$ is referred to as a stress-composition tensor.

The two assumptions made before, can now be clarified. By mechanical simplicity and the cubic simmetry it can be possible say that mobility is independent of strain, $\boldsymbol{C}$ and $\boldsymbol{A}$ are independent of strain and composition. Mobility and stress-composition tensors are isotropic and thus characterized by a scalar, while $\boldsymbol{C}$ is known through two parameters:

$$\boldsymbol{C}_{ijkl} = 2G\delta_{ik}\delta_{jl} + \lambda\delta_{ij}\delta_{kl} \qquad \text{and} \qquad \boldsymbol{A}^{\alpha} = \alpha^{a}\mathbf{I} \tag{3.28}$$

where G and λ are the Lame's parameters. It's also possible say that:

$$d\boldsymbol{\sigma}^{\nu} = \boldsymbol{C} : d\boldsymbol{\varepsilon} + \alpha^{a} d\rho^{a}\boldsymbol{I} \qquad \text{or} \qquad d\boldsymbol{\sigma}^{a} = \boldsymbol{C} : d\boldsymbol{\varepsilon} + \alpha^{\nu} d\rho^{\nu}\boldsymbol{I} \tag{3.29}$$

By summing up both expressions:

$$\boldsymbol{\sigma} = \boldsymbol{C} : \boldsymbol{\varepsilon} + \frac{1}{2}[\alpha^{a}(\rho^{a} - \rho_0^{a}) + \alpha^{\nu}(\rho^{\nu} - \rho_0^{\nu})]\boldsymbol{I} \tag{3.30}$$

Expressing the coupling between stress and composition.

3.2.4 Flux Equations

Recalling Eq. 3.24, it's possibile to find and expression of $\boldsymbol{\Psi}$ simply integrating, getting:

$$\boldsymbol{\Psi}(\boldsymbol{\varepsilon}, \rho^{a}) = \frac{1}{2}\boldsymbol{\varepsilon} : \boldsymbol{C}\boldsymbol{\varepsilon} + \frac{1}{2}[\alpha^{a}(\rho^{a} - \rho_0^{a}) + \alpha^{\nu}(\rho^{\nu} - \rho_0^{\nu})]tr\boldsymbol{\varepsilon} + F^{\nu}(\rho^{a}) \tag{3.31}$$

It's now possible to find an expression of chemical potential, derived as a derivative of the potential $\boldsymbol{\Psi}$ (function of ρ^{a}):

$$\alpha^{\nu} = -\alpha^{a} \qquad \longrightarrow \qquad \mu^{a\nu}(\boldsymbol{\varepsilon}, \rho^{a}) = \alpha^{a} tr(\boldsymbol{\varepsilon}) + \frac{\partial^{\nu} F(\rho^{a})}{\partial \rho^{a}} \tag{3.32}$$

Let us make a digression. Consider the free energy $\boldsymbol{\Psi}_0(\boldsymbol{\varepsilon}, \rho^{a})$ and the chemical potentials $\mu_0^{a\nu}(\rho^{a})$, at zero stress, and making the assumption that $F^{\nu}(\rho^{a}) = \boldsymbol{\Psi}_0(\boldsymbol{\varepsilon}, \rho^{a})$, equation 3.33 can also be written in the following manner:

$$\boldsymbol{\Psi}(\boldsymbol{\varepsilon}, \rho^{a}) - \boldsymbol{\Psi}_0(\boldsymbol{\varepsilon}, \rho^{a}) = \frac{1}{2}\boldsymbol{\varepsilon} : \boldsymbol{C} : \boldsymbol{\varepsilon} + \frac{1}{2}[\alpha^{a}(\rho^{a} - \rho_0^{a}) + \alpha^{\nu}(\rho^{\nu} - \rho_0^{\nu})]tr\boldsymbol{\varepsilon} \tag{3.33}$$

As shown in [23], to derive the Gibbs–Duhem equation at zero stress, atomic density, atomic volume and concentrations are used. With nontrivial algebra, the equation obtained is:

$$\boldsymbol{\Psi}_0(\boldsymbol{\varepsilon}, \rho^{a}) = \sum_{\alpha=1}^{N} \rho^{\alpha}\mu_0^{\alpha}(\boldsymbol{\varepsilon}, \rho^{a}) \tag{3.34}$$

And the term $F^{\nu}(\rho^{a})$, can now be written as:

$$F^{\nu}(\rho^{a}) = \sum_{\alpha=1}^{N} \rho^{\alpha}\mu_0^{\alpha}(\boldsymbol{\varepsilon}, \rho^{a}) \tag{3.35}$$

In order to express the chemical potential as a function of stress instead of strain, consider the identity $\boldsymbol{\sigma}(\boldsymbol{x},t) = \hat{\boldsymbol{\sigma}}(\tilde{\boldsymbol{\varepsilon}}(\boldsymbol{\sigma},\rho^a),\rho^a)$, where hat and tilde symbols are used to highlight the difference between, on one side, $\boldsymbol{\sigma}$ and $\boldsymbol{\varepsilon}$ which depend on position and time, and on the other side, the same physical quantities but considered as functions of strain and atomic density for $\hat{\boldsymbol{\sigma}}$, or of stress and atomic density for $\tilde{\boldsymbol{\varepsilon}}$. By differentiating this identity with respect to ρ^a we obtain $\boldsymbol{A} = -\boldsymbol{C} : \boldsymbol{N}^a$, where $\boldsymbol{N}^a = \partial\tilde{\boldsymbol{\varepsilon}}/\partial\rho^a = n^a\boldsymbol{I}$ (cubic symmetry). Since $\boldsymbol{C} : \boldsymbol{I} = (2G + 3\lambda)\boldsymbol{I} = 3K\boldsymbol{I}$, with K the bulk modulus, we conclude that $\boldsymbol{\alpha}^a = -3Kn^a$. Reminding that the hydrostatic pressure is defined by

$$p = -Ktr(\boldsymbol{\varepsilon}) \tag{3.36}$$

and using Eq. (7.41) of [23] in the case of a binary mixture subjected to the lattice constraint, leads to:

$$\mu^{av}(p,\rho^a) = \mu_0^{av}(\rho^a) + 3n^a p \tag{3.37}$$

here μ^{av} is the relative chemical potential at zero stress. Finally, by Fick's law leads to the atomic flux expression:

$$\boldsymbol{j}^a = -m^a(\rho^a)\left(\frac{\partial^v\mu_0^{av}(\rho^a)}{\partial\rho^a}\nabla\rho^a + 3n^a\nabla p\right) \tag{3.38}$$

The atomic mobility m^a is given by well-known expression (Eistein relation):

$$m^a(\rho^a) = \frac{D_v\rho^a}{kT} \tag{3.39}$$

where D_v is the lattice diffusion coefficient.

It was made the following assumption: at the lattice level, the exchange of an atom with a vacancy implies a change of volume (contraction) of the neighbourhood. Last thing to do is pecifying the mechanism relating strain and diffusion, that is by specifying n^a. The strain variation associated with this mechanism is then assumed to be described by

$$n^v\boldsymbol{I} = \frac{\partial\tilde{\boldsymbol{\varepsilon}}}{\partial\rho^v} = -\frac{1}{3}(1-f)\Omega_0^a\boldsymbol{I} = -n^a\boldsymbol{I} \tag{3.40}$$

where Ω_0^a is the stress-free atomin volume, and $(1-f)\Omega_0^a$ with $0 < f < 1$, the change of volume due to the exchange of an atom by a vacancy.

Finally, to summarize, the continuum formulation for stress-driven lattice diffusion in polycrystalline solids considered as atom - vacancy mixtures, is described by the set of balance and constitutive equations:

$$\nabla \cdot \boldsymbol{\sigma} = 0 \qquad \text{Momentum Balance} \tag{3.41a}$$

$$\frac{d\rho^a}{dt} + \nabla \cdot \boldsymbol{j}^a = 0 \qquad \text{Atom Population Balance} \tag{3.41b}$$

$$\boldsymbol{\sigma} = \boldsymbol{C} : \boldsymbol{\varepsilon} - (1-f)\Omega_0^a K(\rho^a - \rho_0)\boldsymbol{I} \tag{3.41c}$$

$$\boldsymbol{j} = -\frac{D_v \rho^a}{kT}\left(\frac{\partial^v \mu_0^{av}(\rho^a)}{\partial \rho^a}\nabla\rho^a + (1-f)\Omega_0^a \nabla p\right) \tag{3.41d}$$

Chapter 4

Sintering Elastic Model - FEM Formulation

4.1 Bilinear quadrilateral element (QUAD-4)

The law 4.39a, refers to an isotropic, elastic, linear material. The polymers behavior differs much from the one just described. However, it will still be a test in order to have a comparison with models probably more reliable.

For FEM simulation a QUAD-4 element it's computed. We wrote a matlab code that calculates displacements, pressure and density of each node.

Let recall some important characteristic of this element. This is the axisymmetric solid version of the well known isoparametric quadrilateral with bilinear shape functions. The element has 4 nodes and 8 displacement degrees of freedom arranged. The standard 4-node isoparametric quadrilateral is usually processed with a 2×2 Gauss integration rule for displacements and a $1x1$ Gauss integration rule for density.

4.1.1 Shape Function

It's necessary to introduce a 'parent element' to link the real coordinates of the element in a more congenial space. This element is introduced to compute shape functions more easily.

Now, a Mapping sistem is necessary to switch from real element to parent element and viceversa. For simplicity, only displacement field math steps will be shown [26].

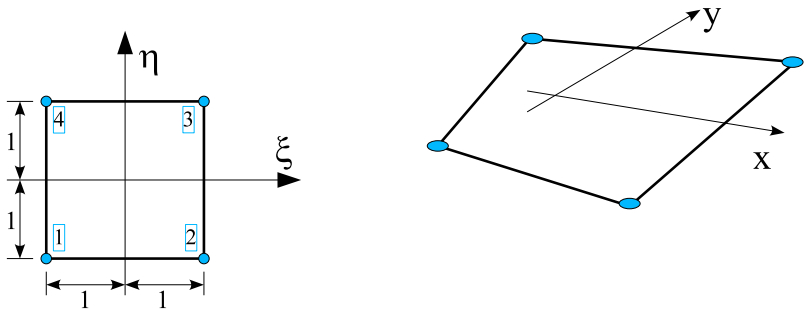

Figure 4.1: Mapping [26]

$$\xi = \xi(x) \qquad x = x(\xi) \tag{4.1}$$

In this formulation:

- $\boldsymbol{\xi}$ are the natural coordinates (parent element coordinates);
- $\boldsymbol{x}$ are the real element coordiantes.

$$\boldsymbol{\xi} \left\{ \begin{array}{c} \xi \\ \eta \end{array} \right\}; \qquad \boldsymbol{x} \left\{ \begin{array}{c} x \\ y \end{array} \right\} \tag{4.2}$$

Using the same interpolating functions both for $\boldsymbol{u}$ field of the unknowns to interpolate the field of geometric functions. The approximations are:

$$\boldsymbol{u} \left\{ \begin{array}{c} u \\ v \end{array} \right\} \quad \Rightarrow \quad \begin{array}{l} u \approx u^h = \sum_{i=1}^{4} N_i \hat{u}_i \\ v \approx v^h = \sum_{i=1}^{4} N_i \hat{v}_i \end{array} \tag{4.3}$$

$$\boldsymbol{x} \left\{ \begin{array}{c} x \\ y \end{array} \right\} \quad \Rightarrow \quad \begin{array}{l} x = \sum_{i=1}^{4} N_i \bar{x}_i \\ y = \sum_{i=1}^{4} N_i \bar{y}_i \end{array} \tag{4.4}$$

Where $\bar{x}_i$ e $\bar{y}_i$ are the nodes (x,y) coordinates..

The shape functions are now defined in the virtual space

$$N_i = N_i(\xi, \eta) = N_i(\boldsymbol{\xi}) \tag{4.5}$$

Once defined on parent element, N_i functions can be mapped to current element if or whenever necessary:

$$\boldsymbol{\xi} = \boldsymbol{\xi}(\boldsymbol{x}) \qquad \Rightarrow \qquad N_i = N_i(\boldsymbol{\xi}) = N_i(\boldsymbol{\xi}(\boldsymbol{x})) = N_i(\boldsymbol{x}) \tag{4.6}$$

The added convenience is that it's easier to define $\boldsymbol{N}$ in the parent element compared to the one with the real geometry.

One possibility is:

$$N_i = \frac{1}{4}\left(1 + \bar{\xi}_i \xi\right)\left(1 + \bar{\eta}_i \eta\right) \tag{4.7}$$

with $\bar{\xi}_i$ e $\bar{\eta}_i$ natural nodes coordinates.

$$\begin{aligned} &\bar{\xi}_1 = -1 \quad \bar{\xi}_2 = 1 \quad \bar{\xi}_3 = 1 \quad \bar{\xi}_4 = -1 \\ &\bar{\eta}_1 = -1 \quad \bar{\eta}_2 = 1 \quad \bar{\eta}_3 = 1 \quad \bar{\eta}_4 = -1 \end{aligned} \tag{4.8}$$

Finally, there will be 4 explicit expression for shape function, replacing $\bar{\xi}_i$ and $\bar{\eta}_i$ of nodes N_i:

$$\begin{aligned} N_1 &= \frac{1}{4}(1 - \xi)(1 - \eta) \\ N_2 &= \frac{1}{4}(1 + \xi)(1 - \eta) \\ N_3 &= \frac{1}{4}(1 + \xi)(1 + \eta) \\ N_4 &= \frac{1}{4}(1 - \xi)(1 + \eta) \end{aligned} \tag{4.9}$$

Shape functions depends on $\boldsymbol{\xi}$.

$$N_i(\boldsymbol{\xi}) \tag{4.10}$$

The derivatives of the shape functions are calculated from the current coordinates x, $\frac{\partial N_i}{\partial x}$.

This leads to a problem: to derive $\boldsymbol{x}$ something that depends on $\boldsymbol{\xi}$. By the link between the virtual and real field I can write that:

$$\boldsymbol{u} = \boldsymbol{u}(\boldsymbol{\xi}) = \boldsymbol{u}(\boldsymbol{\xi}(\boldsymbol{x})) \tag{4.11}$$

Then, the derivatives of $\boldsymbol{u}$ can be written as:

$$\begin{aligned} u_{,x} &= \frac{\partial u}{\partial x} = \frac{\partial u}{\partial \xi}\frac{\partial \xi}{\partial x} + \frac{\partial u}{\partial \eta}\frac{\partial \eta}{\partial x} \\ u_{,y} &= \frac{\partial u}{\partial y} = \frac{\partial u}{\partial \xi}\frac{\partial \xi}{\partial y} + \frac{\partial u}{\partial \eta}\frac{\partial \eta}{\partial y} \end{aligned} \tag{4.12}$$

In matrix form:

$$\begin{Bmatrix} u_{,x} \\ u_{,y} \end{Bmatrix} = \begin{bmatrix} \dfrac{\partial \xi}{\partial x} & \dfrac{\partial \eta}{\partial x} \\ \dfrac{\partial \xi}{\partial y} & \dfrac{\partial \eta}{\partial y} \end{bmatrix} \begin{Bmatrix} \dfrac{\partial u}{\partial \xi} \\ \dfrac{\partial u}{\partial \eta} \end{Bmatrix} \tag{4.13}$$

Introducing now the approximations derived by calculating the natural coordinates:

$$\begin{aligned} \frac{\partial u}{\partial \xi} &= \frac{\partial}{\partial \xi}\left(\sum_{i=1}^{4} N_i \hat{u}_i\right) = \sum_{i=1}^{4}\left(\frac{\partial N_i}{\partial \xi}\right)\hat{u}_i = \sum_{i=1}^{4} N_{i,\xi}\hat{u}_i \\ \frac{\partial u}{\partial \eta} &= \frac{\partial}{\partial \eta}\left(\sum_{i=1}^{4} N_i \hat{u}_i\right) = \sum_{i=1}^{4}\left(\frac{\partial N_i}{\partial \eta}\right)\hat{u}_i = \sum_{i=1}^{4} N_{i,\eta}\hat{u}_i \end{aligned} \tag{4.14}$$

Then:

$$\begin{aligned} N_i &= \frac{1}{4}\left(1 + \bar{\xi}_i\xi\right)\left(1 + \bar{\eta}_i\eta\right) \\ N_{i,\xi} &= \frac{1}{4}\bar{\xi}_i\left(1 + \bar{\eta}_i\eta\right) \\ N_{i,\eta} &= \frac{1}{4}\bar{\eta}_i\left(1 + \bar{\xi}_i\xi\right) \end{aligned} \tag{4.15}$$

Let define $\boldsymbol{F}$:

$$\boldsymbol{F} = \begin{bmatrix} \dfrac{\partial \xi}{\partial x} & \dfrac{\partial \eta}{\partial x} \\ \dfrac{\partial \xi}{\partial y} & \dfrac{\partial \eta}{\partial y} \end{bmatrix} \tag{4.16}$$

If it is the transposed of the *Jacobian* related to the change of coordinates. So to calculate it, it's can be possible to calculate the em Jacobian referring to real coordinates $\boldsymbol{x} = \boldsymbol{x}(\boldsymbol{\xi})$, transpose it and then the inverse.

To summarize

- Step from $\boldsymbol{\xi} = \boldsymbol{\xi}(\boldsymbol{x})$ to $\boldsymbol{x} = \boldsymbol{x}(\boldsymbol{\xi})$;

- Compute more easily the *Jacobian* $\boldsymbol{G}$ referred to $\boldsymbol{x} = \boldsymbol{x}(\boldsymbol{\xi})$:

$$\boldsymbol{G} = \begin{bmatrix} \dfrac{\partial x}{\partial \xi} & \dfrac{\partial x}{\partial \eta} \\ \dfrac{\partial y}{\partial \xi} & \dfrac{\partial y}{\partial \eta} \end{bmatrix} \tag{4.17}$$

- Then, compute $\boldsymbol{F} = \boldsymbol{G}^{-T}$.

Gauss integration

General Stiffness integrate formulation:

$$\int_{\Omega_e} f(x) = \int_{[]} f[x(\xi)] J d[] \tag{4.18}$$

J is the determinant of *Jacobian* matrix referred to the mapping $\boldsymbol{x} = \boldsymbol{x}(\boldsymbol{\xi})$, in formula:

$$J = \det\left(\frac{\partial \boldsymbol{x}}{\partial \boldsymbol{\xi}}\right) = \det(\boldsymbol{G}) \tag{4.19}$$

For a 2D problem:

$$G = \begin{bmatrix} \dfrac{\partial x}{\partial \xi} & \dfrac{\partial x}{\partial \eta} \\ \dfrac{\partial y}{\partial \xi} & \dfrac{\partial y}{\partial \eta} \end{bmatrix} \tag{4.20}$$

Let rewrite the general term of the element stiffness as:

$$\int_{[]} g(\boldsymbol{\xi}) d[] \tag{4.21}$$

The function $\boldsymbol{g}$ is usually complex and nonlinear. It's possible and convenient to calculate the integrals in closed form only for specific cases (linear triangles). It is not convenient or possible to calculate it in closed form for the general case. A numerical integration (quadrature) is then adopted.

$$\int_{[]} g(\boldsymbol{\xi}) d[] \approx \sum_{i=1}^{ng} g(\tilde{\boldsymbol{\xi}}) w_i \tag{4.22}$$

where:

- $\tilde{\boldsymbol{\xi}}$ it's a point in which the function can be computed;
- w_i is the weight.

This type of integration is also called integration Gauss (the most used among the various quadrature formulas).

For example, the standard stiffness formulation for a linear elastic isotropic material is defined as:

$$\boldsymbol{K} = \int_F (\boldsymbol{B}^u)^T \boldsymbol{C} \boldsymbol{B}^u dA = \int_F (\boldsymbol{B}^u)^T \boldsymbol{C} \boldsymbol{B}^u J dA_p = \sum_{i=1}^{ng} \sum_{j=1}^{ng} (\boldsymbol{B}^u)^T(\xi,\eta) \boldsymbol{C} \boldsymbol{B}^u(\xi,\eta) J_{ij} w_i w_j \tag{4.23}$$

The Gauss quadrature is generally defined in $-1 < G.Q. < 1$.

A Gaussian integration formula integrates exactly a $2n-1$ order polynomial. In 2 dimensions, the Gauss quadrature becomes:

$$\int_{-1}^{1} \int_{-1}^{1} f(\xi,\eta) d\xi d\eta \approx \sum_{j=1}^{n} \sum_{k=1}^{n} f(\xi_j,\eta_k) w_j w_k \tag{4.24}$$

For further informations, see Appendix C, section 1.

Shape functions are:

$$\{N_i\}, \qquad N[1x4] = [N_1, N_2, N_3, N_4] \tag{4.25}$$

and their derivative are:

$$\left[\frac{\partial N}{\partial \xi}\right]_{ij} = \frac{\partial N_i}{\partial \xi_i}, \qquad \left[\frac{\partial N}{\partial \xi}\right]_{[2x4]} = \begin{bmatrix} \frac{\partial N_1}{\partial \xi} & \frac{\partial N_2}{\partial \xi} & \frac{\partial N_3}{\partial \xi} & \frac{\partial N_4}{\partial \xi} \\ \frac{\partial N_1}{\partial \eta} & \frac{\partial N_2}{\partial \eta} & \frac{\partial N_3}{\partial \eta} & \frac{\partial N_4}{\partial \eta} \end{bmatrix} \tag{4.26}$$

$$\left[\frac{\partial N}{\partial x}\right]_{ij} = \frac{\partial N_i}{\partial x_i}, \qquad \left[\frac{\partial N}{\partial x}\right]_{[2x4]} = \begin{bmatrix} \frac{\partial N_1}{\partial x} & \frac{\partial N_2}{\partial x} & \frac{\partial N_3}{\partial x} & \frac{\partial N_4}{\partial x} \\ \frac{\partial N_1}{\partial y} & \frac{\partial N_2}{\partial y} & \frac{\partial N_3}{\partial y} & \frac{\partial N_4}{\partial y} \end{bmatrix} \tag{4.27}$$

where:

$$\begin{aligned} N_i &= \frac{1}{4}(1+\bar{\xi}_i\xi)(1+\bar{\eta}_i\eta) \\ N_{i,\xi} &= \frac{1}{4}\bar{\xi}_i(1+\bar{\eta}_i\eta) \\ N_{i,\eta} &= \frac{1}{4}\bar{\eta}_i(1+\bar{\xi}_i\xi) \end{aligned} \tag{4.28}$$

with:

$$\bar{\xi} = \{-1\ 1\ 11\} \qquad \bar{\eta} = \{-1\ \ -1\ 1\ 1\} \tag{4.29}$$

Now, coordinates of $\boldsymbol{N_i}$ are calculated, to do that it's necesary a formulato to switch from one to another:

$$\frac{\partial N_i}{\partial x} = \frac{\partial N_i}{\partial \xi}\frac{\partial \xi}{\partial x} + \frac{\partial N_i}{\partial \eta}\frac{\partial \eta}{\partial x} = \begin{bmatrix} \frac{\partial \eta}{\partial x} & \frac{\partial \eta}{\partial x} \end{bmatrix} \begin{Bmatrix} \frac{\partial N_i}{\partial \xi} \\ \frac{\partial N_i}{\partial \eta} \end{Bmatrix} \tag{4.30}$$

Rewrote as:

$$\begin{Bmatrix} \frac{\partial N_i}{\partial x} \\ \frac{\partial N_i}{\partial y} \end{Bmatrix} = \begin{bmatrix} \frac{\partial \xi}{\partial x} & \frac{\partial \eta}{\partial x} \\ \frac{\partial \xi}{\partial y} & \frac{\partial \eta}{\partial y} \end{bmatrix} \begin{Bmatrix} \frac{\partial N_i}{\partial \xi} \\ \frac{\partial N_i}{\partial \eta} \end{Bmatrix} \tag{4.31}$$

$$\left[\frac{\partial N}{\partial x}\right]_{[2x4]} = \left[\frac{\partial \xi}{\partial x}\right]^T_{[2x2]} \left[\frac{\partial N}{\partial \xi}\right]_{[2x4]} \tag{4.32}$$

Jacobian tranformation. (To compute it, the inverse of the transposed is necessary):

$$\begin{bmatrix} \frac{\partial \xi}{\partial x} & \frac{\partial \eta}{\partial x} \\ \frac{\partial \xi}{\partial y} & \frac{\partial \eta}{\partial y} \end{bmatrix} = \left[\frac{\partial \boldsymbol{\xi}}{\partial \boldsymbol{x}}\right]^T = \left(\left[\frac{\partial \boldsymbol{x}}{\partial \boldsymbol{\xi}}\right]^T\right)^{-1} \quad \text{con} \quad \left[\frac{\partial \boldsymbol{x}}{\partial \boldsymbol{\xi}}\right]^T = \begin{bmatrix} \frac{\partial x}{\partial \xi} & \frac{\partial x}{\partial \eta} \\ \frac{\partial y}{\partial \xi} & \frac{\partial y}{\partial \eta} \end{bmatrix} \tag{4.33}$$

Geometric map:

$$\boldsymbol{x} = \boldsymbol{x}(\boldsymbol{\xi}) \ \Rightarrow \ x = \sum_{i=1}^{4} N_i \hat{x}_i, \ y = \sum_{i=1}^{4} N_i \hat{y}_i \tag{4.34}$$

$$\begin{aligned} \left[\frac{\partial x}{\partial \xi}\right]^T_{11} &= \frac{\partial x}{\partial \xi} = \sum_{i=1}^{4} \frac{\partial N_i}{\partial \xi}\hat{x}_i \\ \left[\frac{\partial x}{\partial \xi}\right]^T_{12} &= \frac{\partial y}{\partial \xi} = \sum_{i=1}^{4} \frac{\partial N_i}{\partial \xi}\hat{y}_i \\ \left[\frac{\partial x}{\partial \xi}\right]^T_{21} &= \frac{\partial x}{\partial \eta} = \sum_{i=1}^{4} \frac{\partial N_i}{\partial \eta}\hat{x}_i \\ \left[\frac{\partial x}{\partial \xi}\right]^T_{22} &= \frac{\partial y}{\partial \eta} = \sum_{i=1}^{4} \frac{\partial N_i}{\partial \eta}\hat{y}_i \end{aligned} \tag{4.35}$$

$$J = det\left(\frac{\partial \boldsymbol{x}}{\partial \boldsymbol{\xi}}\right) = det(\boldsymbol{G}) \tag{4.36}$$

Finally, the load and stiffness matrix, are:

$$A = \begin{bmatrix} N_1 & 0 & N_2 & 0 & N_3 & 0 & N_4 & 0 \\ 0 & N_1 & 0 & N_2 & 0 & N_3 & 0 & N_4 \end{bmatrix} \tag{4.37}$$

$$B = \begin{bmatrix} \frac{\partial N_1}{\partial x} & 0 & \frac{\partial N_2}{\partial x} & 0 & \frac{\partial N_3}{\partial x} & 0 & \frac{\partial N_4}{\partial x} & 0 \\ 0 & \frac{\partial N_1}{\partial y} & 0 & \frac{\partial N_2}{\partial y} & 0 & \frac{\partial N_3}{\partial y} & 0 & \frac{\partial N_4}{\partial y} \\ \frac{\partial N_1}{\partial x} & \frac{\partial N_1}{\partial y} & \frac{\partial N_2}{\partial x} & \frac{\partial N_2}{\partial y} & \frac{\partial N_3}{\partial x} & \frac{\partial N_3}{\partial y} & \frac{\partial N_4}{\partial x} & \frac{\partial N_4}{\partial y} \end{bmatrix} \tag{4.38}$$

4.2 Mixed Variational Method

The purpose of this chapter is to solve the continuum formulation for stress-driven lattice diffusion in polycrystalline solids considered as atom - vacancy mixtures. Obtaining general closed-form solutions it's too difficult and for this reason, must resort to a numerical approximation: finite element method.

The Finite element method (FEM) is a general approach to compute approximate solution for any general differential equation (ODE).

There are three main steps to contruct a finite element method from a differential equation:

1. switch from strong to weak form (convert differential to integral form);
2. switch form integral to algebraic form (introduce approximation fields;
3. solution of the algebric problem (generally easy to solve).

The weak form is often associated to variational principles and the approximation implies problem discretization.

4.2.1 Governing Equations

Let now recall the governing equations, the strong (differential) form is:

$$\nabla \cdot \boldsymbol{\sigma} = 0 \tag{4.39a}$$

$$\frac{d\rho^a}{dt} + \nabla \cdot \boldsymbol{j}^a = 0 \tag{4.39b}$$

and let's make some manipulations. Eq. 4.39a will be associated with Eq. 4.40a:

$$\nabla \cdot \boldsymbol{\sigma} = 0 \tag{4.40a}$$

$$\boldsymbol{\sigma} = \boldsymbol{C} : \boldsymbol{\varepsilon} - (1-f)\Omega_0^a K(\rho^a - \rho_0)\boldsymbol{I} \tag{4.40b}$$

and Eq. 4.66b will be associated with Eq. 4.41b:

$$\frac{d\rho^a}{dt} + \nabla \cdot \boldsymbol{j}^a = 0 \tag{4.41a}$$

$$\boldsymbol{j} = -\frac{D_v \rho^a}{kT}\left(\frac{\partial^v \mu_0^{av}(\rho^a)}{\partial \rho^a}\nabla\rho^a + (1-f)\Omega_0^a \nabla p\right) \tag{4.41b}$$

Focusing on the above equations, you may notice that:

- To solve the system, it's necessary a mixed $(\boldsymbol{u}, \boldsymbol{\rho})$ formulation;
- there is a time dependence (density);
- there is two non linear terms.

For now, since the nonlinear term has little influence on the overall solution, it will be kept equal to one. This simplification will be justified then later.

Considering the mixed formulation used, it' s logical to expect two residual equations:

$$\boldsymbol{R}(\boldsymbol{u}, \boldsymbol{\rho}) = \boldsymbol{0}$$

In a more extended formula:

$$\begin{aligned} dR^u &= \frac{\partial \boldsymbol{R}^u}{\partial \hat{\mathbf{u}}} d\hat{\mathbf{u}} + \frac{\partial \boldsymbol{R}^u}{\partial \hat{\boldsymbol{\rho}}} d\hat{\boldsymbol{\rho}} \\ dR^\rho &= \frac{\partial \boldsymbol{R}^\rho}{\partial \hat{\mathbf{u}}} d\hat{\mathbf{u}} + \frac{\partial \boldsymbol{R}^\rho}{\partial \hat{\boldsymbol{\rho}}} d\hat{\boldsymbol{\rho}} \end{aligned} \tag{4.42}$$

4.2.2 Weak Form And Approximation

Toward a weak formulation (integral form), following steps will be done:

1. multiply the differential equations by generic 'weight' functions: $\delta \boldsymbol{u}$, $\delta \boldsymbol{\rho}$;
2. integrate product over problem domain;
3. observe that integral is equal to zero;
4. integrate by parts.

In formula:

$$\boldsymbol{R}^{u} = \delta \boldsymbol{u} \cdot \left\{ \int_{\Omega} [div(\boldsymbol{\sigma})] d\Omega \right\} = \mathbf{0} \tag{4.43a}$$

$$\boldsymbol{R}^{\rho} = \delta \boldsymbol{\rho} \cdot \left\{ \int_{\Omega} [\dot{\rho} + \nabla \cdot \boldsymbol{j}] \, d\Omega \right\} = \mathbf{0} \tag{4.43b}$$

$$\tag{4.43c}$$

Now, new field approximation will be introduced. The approximation are based on domain discretization (mesh) with elements of finite dimensions (finite elements). Field discretization are:

$$\boldsymbol{u} \approx \boldsymbol{N}^{u} \hat{\mathbf{u}} \quad \delta \boldsymbol{u} \approx \boldsymbol{N}^{u} \delta \hat{\mathbf{u}} \quad \rho \approx \boldsymbol{N}^{\rho} \hat{\boldsymbol{\rho}} \quad \delta \rho \approx \boldsymbol{N}^{\rho} \delta \hat{\boldsymbol{\rho}} \tag{4.44}$$

Field discretization derivative are:

$$\nabla \boldsymbol{u} \approx \boldsymbol{B}^{u} \hat{\mathbf{u}} \quad \delta \nabla \boldsymbol{u} \approx \boldsymbol{B}^{u} \delta \hat{\mathbf{u}} \quad \nabla \rho \approx \boldsymbol{B}^{\rho} \hat{\boldsymbol{\rho}} \quad \delta \nabla \rho \approx \boldsymbol{B}^{\rho} \delta \hat{\boldsymbol{\rho}} \tag{4.45}$$

where:

- $\hat{\mathbf{u}}$, $\hat{\boldsymbol{\rho}}$ are nodal unknown parameters;
- $\delta \hat{\mathbf{u}}$, $\delta \hat{\boldsymbol{\rho}}$ are nodal arbitrary parameters;
- $\boldsymbol{N}^{u}$, $\boldsymbol{N}^{\rho}$, ... , are shape function matrices.

More informations about shape function matrix type and dimension will be done afterwards.

4.2.3 Weak Form of Equilibrium Equation

We have to recall Eq. 4.40.

$$\delta \boldsymbol{u} \cdot \left[\int_{\Omega} [div(\boldsymbol{\sigma})] d\Omega \right] = \int_{\Omega} \delta \boldsymbol{u} \cdot [div(\boldsymbol{\sigma})] d\Omega = \int_{\Omega} \nabla \boldsymbol{u} : \boldsymbol{\sigma} - \int_{\partial\Omega} \delta \boldsymbol{u} \cdot \boldsymbol{\sigma} \boldsymbol{n} = 0 \tag{4.46}$$

Setting $\boldsymbol{\sigma} \boldsymbol{n} = \boldsymbol{t}$ on $\partial\Omega$ and replacing Eq. 4.40a into Eq. 4.39a, Eq. 6.45 becomes:

$$\int_{\Omega} \nabla \boldsymbol{u} : \left[\boldsymbol{C} \boldsymbol{\varepsilon} - (1-f)\Omega_0^a K(\rho^a - \rho_0) \boldsymbol{I} \right] - \int_{\partial\Omega} \delta \boldsymbol{u} \cdot \boldsymbol{t} = 0 \tag{4.47}$$

For simplicity, the quantity $(1-f)\Omega_0^a K$, from now, will be called k_1 and ρ^a will be called simply ρ.

$$\int_{\Omega} \nabla \boldsymbol{u} : \boldsymbol{C} \boldsymbol{\varepsilon} - \int_{\Omega} \nabla \boldsymbol{u} \boldsymbol{I} k_1 \rho + \int_{\Omega} \nabla \boldsymbol{u} \boldsymbol{I} k_1 \rho_0 - \int_{\partial\Omega} \delta \boldsymbol{u} \cdot \boldsymbol{t} = 0 \tag{4.48}$$

Before continuing, some remarks. For a $\Omega \subset \mathcal{R}^2$:

- $\boldsymbol{u}$ is a 2 component vector;
- $\nabla \boldsymbol{u} \equiv \boldsymbol{\varepsilon}$ is a 3 component vector;
- $\boldsymbol{C}$ is a $3x3$ matrix.

Substituting Eq. 4.45 in Eq. 6.47:

$$\int_{\Omega} (\boldsymbol{B}^u)^T \delta \hat{\mathbf{u}} \boldsymbol{C} \boldsymbol{B}^u \hat{\mathbf{u}} - \int_{\Omega} (\boldsymbol{B}^u)^T \delta \hat{\mathbf{u}} \boldsymbol{I} k_1 \boldsymbol{N}^\rho \hat{\boldsymbol{\rho}} + \int_{\Omega} (\boldsymbol{B}^u)^T \delta \hat{\mathbf{u}} \boldsymbol{I} k_1 \rho_0 - \int_{\partial\Omega} (\boldsymbol{N}^u)^T \delta \hat{\mathbf{u}} \cdot \boldsymbol{t} = 0 \tag{4.49}$$

Since $\delta \hat{\mathbf{u}}$ and $\delta \hat{\boldsymbol{\rho}}$ are arbitrary, whatever is their value, Eq. 4.49 must be always valid, thus:

$$\int_{\Omega} (\boldsymbol{B}^u)^T \boldsymbol{C} \boldsymbol{B}^u \hat{\mathbf{u}} - \int_{\Omega} (\boldsymbol{B}^u)^T \boldsymbol{I} k_1 \boldsymbol{N}^\rho \hat{\boldsymbol{\rho}} + \int_{\Omega} (\boldsymbol{B}^u)^T \boldsymbol{I} k_1 \rho_0 - \int_{\partial\Omega} (\boldsymbol{N}^u)^T \cdot \boldsymbol{t} = 0 \tag{4.50}$$

For a two dimensional general problem, each node has two coordinates, horizontal and vertical displacement respectively.

$$\boldsymbol{R}^{\boldsymbol{u}} = \int_{\Omega} (\boldsymbol{B}^u)^T \boldsymbol{C} \boldsymbol{B}^u \hat{\mathbf{u}} - \int_{\Omega} (\boldsymbol{B}^u)^T \boldsymbol{I} \boldsymbol{N}^\rho k_1 \hat{\boldsymbol{\rho}} + \int_{\Omega} (\boldsymbol{B}^u)^T \boldsymbol{I} k_1 \rho_0 - \int_{\partial\Omega} (\boldsymbol{N}^u)^T \boldsymbol{t} = 0 \tag{4.51}$$

In a more compact manner, Eq. 4.51, can be rewritten as:

$$\boldsymbol{K}^{uu}\hat{\mathbf{u}} - \boldsymbol{K}^{up}\hat{\boldsymbol{\rho}} = \boldsymbol{f}^{u} \tag{4.52}$$

where:

$$\begin{aligned}
\boldsymbol{K}^{uu} &= \int_{\Omega} (\boldsymbol{B}^{u})^{T}\boldsymbol{C}\boldsymbol{B}^{u} \\
\boldsymbol{K}^{up} &= \int_{\Omega} (\boldsymbol{B}^{u})^{T}\boldsymbol{I}\boldsymbol{N}^{\rho}k_1 \\
\boldsymbol{f} &= \int_{\Omega} (\boldsymbol{B}^{u})^{T}\boldsymbol{I}k_1\rho_0 - \int_{\partial\Omega} (\boldsymbol{N}^{u})^{T}\boldsymbol{t}
\end{aligned} \tag{4.53}$$

4.2.4 Weak Form of Mass Balance

The other terms will be find by Eq. 4.41. Steps are exactly the same, recall equations in a strong form, multiplying by a weight function and integrate problem over the problem domain. The time dependence is treated as follow:

$$\dot{\rho} + \nabla\cdot\boldsymbol{j} = \frac{\rho - \rho^{n}}{\Delta t} + div(\boldsymbol{j}) = 0 \tag{4.54}$$

$$\frac{1}{\Delta t}\left[\int_{\Omega}\delta\rho\rho\right] + \int_{\Omega}\nabla\delta\rho\cdot\boldsymbol{j} - \int_{\partial\Omega}\delta\rho\cdot\boldsymbol{j} = \frac{1}{\Delta t}\left[\int_{\Omega}\delta\rho\rho^{n}\right] \tag{4.55}$$

Let's step back on Eq. 4.41b:

$$\boldsymbol{j} = -\frac{D_v\rho^{a}}{kT}\left(\frac{\partial^{v}\mu_0^{av}(\rho^{a})}{\partial\rho^{a}}\nabla\rho^{a} + (1-f)\Omega_0^{a}\nabla p\right) \tag{4.56}$$

Following quantities are setted:

$$k_2 = -\frac{D_v}{kT} \qquad k_3 = -\frac{D_v}{kT}(1-f)\Omega_0^{a} \tag{4.57}$$

Eq. 4.56 becomes:

$$\boldsymbol{j} = k_2\rho\mu(\rho)\nabla\rho + k_3\rho\nabla p \tag{4.58}$$

The non linear terms $\rho\mu(\rho)$ and ρ are setted to be one. Eq. 4.58 becomes:

$$\boldsymbol{j} = k_2\nabla\rho + k_3\nabla p \tag{4.59}$$

Replacing Eq. 4.59 in Eq. 4.55:

$$\frac{1}{\Delta t}\left[\int_\Omega \delta\rho\rho\right] + \int_\Omega \nabla\delta\rho \cdot [k_2\nabla\rho + k_3\nabla p] - \int_{\partial\Omega} \delta\rho \cdot [k_2\nabla\rho + k_3\nabla p] = \frac{1}{\Delta t}\left[\int_\Omega \delta\rho\rho^n\right] \quad (4.60)$$

The pressure term p can be written as a displacement function:

$$p = K\theta = \frac{K}{3}\boldsymbol{I}^T\nabla\boldsymbol{u} = \frac{K}{3}\boldsymbol{I}^T\boldsymbol{B}^u\hat{\mathbf{u}} = \frac{K}{3}\boldsymbol{I}^T\boldsymbol{B}^u\hat{\mathbf{u}} \quad (4.61)$$

The derivative of p is more complicated and can be written as:

$$\nabla p = \begin{Bmatrix} p_{,x} \\ p_{,y} \end{Bmatrix}\hat{\mathbf{u}} = \frac{K}{3}\begin{bmatrix} (\boldsymbol{I}^T\boldsymbol{B}^u)_{,x} \\ (\boldsymbol{I}^T\boldsymbol{B}^u)_{,y} \end{bmatrix}\hat{\mathbf{u}} \quad (4.62)$$

$$\underset{2x1}{\nabla p} = \underset{2x8}{\boldsymbol{F}^u}\underset{8x1}{\hat{\mathbf{u}}} \quad (4.63)$$

The $\boldsymbol{F}^u$ matrix presents many difficulties. The displacement Laplacian cause problems with the shape functions. As seen in previous chapter, the choosen element is the bilinear quadrilatera element. To construct shape functions, it's convenient to introduce a parent element with a fixed known geometry. Contrariwise, our element, has a variable geometry (nodal coordinates depend on specific element). We'll introduce a map from current to parent element and viceversa:

$$\boldsymbol{\xi} = \boldsymbol{\xi}(\boldsymbol{x})$$

To map coordinates, we use the mapping matrix:

$$\boldsymbol{F} = \begin{bmatrix} \frac{\partial\xi}{\partial x} & \frac{\partial\eta}{\partial x} \\ \frac{\partial\xi}{\partial y} & \frac{\partial\eta}{\partial y} \end{bmatrix}$$

This matrix is obtained doing the inverse of the transpose of the Jacobian matrix.

If we have to calculate a second derivateve of a shape function, it means we have to calculate the second order mapping matrix. We can't invert an Hessian matrix such as the Jacobian.

This time, we want to isolate the $\boldsymbol{G}$ matrix from others calculations. In this manner, it's not necessary to compute the Hessian inverse but we can invert only the $\boldsymbol{G}$ and correlate to its all the others components.

Given the excessive complication due to the displacement Laplacian and the simplifying assumptions made before, we diceded to opt for a three field mixed formulation, so as to bypass the problem.

4.3 Three Fields Mixed Variational Method

4.3.1 Governing Equations

Let now recall the governing equations, the strong (differential) form is:

$$\nabla \cdot \boldsymbol{\sigma} = 0 \tag{4.64a}$$

$$\frac{d\rho^a}{dt} + \nabla \cdot \boldsymbol{j}^a = 0 \tag{4.64b}$$

Focusing on the above equations, and recalling the constitutive and flux equations (3.41c and 3.41d) you may notice that:

- To solve the system, it's necessary a mixed $(\boldsymbol{u}, \rho)$ formulation;
- there is a time dependence (density);
- there is two non linear terms.

As said before, for now, since the nonlinear term has little influence on the overall solution, it will be kept equal to one. This simplification will be justified then later.

As seen before, a 2 fields formulation, leads to some mathematical difficulties. Since, our aim is to simulate the sintering process, we can do it using a 3 fields mixed formulation. For a three fields formulation, another weak equations is needed. Since the pressure field is a hydrostatic pressure field, we can write:

$$p = K\theta = \frac{K}{3}\boldsymbol{I}^T \nabla \boldsymbol{u} \tag{4.65a}$$

In this manner, equations 4.64, becomes:

$$\nabla \cdot \boldsymbol{\sigma} = 0 \tag{4.66a}$$

$$\frac{d\rho^a}{dt} + \nabla \cdot \boldsymbol{j}^a = 0 \tag{4.66b}$$

$$p - K\theta = 0 \tag{4.66c}$$

Considering the mixed formulation used, it' s logical to expect that residual equation becomes:

$$\boldsymbol{R}(\boldsymbol{u}, \boldsymbol{\rho}) = \boldsymbol{0} \quad \Rightarrow \quad \boldsymbol{R}(\boldsymbol{u}, \boldsymbol{\rho}, \boldsymbol{p}) = \boldsymbol{0} \tag{4.67}$$

4.3.2 Weak Form And Approximation

Toward a weak formulation (integral form), following steps will be done:

1. multiply the differential equations by generic 'weight' functions: δu, $\delta \rho$ and δp;
2. integrate product over problem domain;
3. observe that integral is equal to zero;
4. integrate by parts.

In formula:

$$\boldsymbol{R}^u = \delta \boldsymbol{u} \cdot \left\{ \int_\Omega [div(\boldsymbol{\sigma})] d\Omega \right\} = \boldsymbol{0} \tag{4.68a}$$

$$\boldsymbol{R}^\rho = \delta \boldsymbol{\rho} \cdot \left\{ \int_\Omega [\dot{\rho} + \nabla \cdot \boldsymbol{j}] \, d\Omega \right\} = \boldsymbol{0} \tag{4.68b}$$

$$\boldsymbol{R}^p = \delta \boldsymbol{p} \cdot \left\{ \int_\Omega [p - K\theta] \, d\Omega \right\} = \boldsymbol{0} \tag{4.68c}$$

Now, new field approximation will be introduced. The approximation are based on domain discretization (mesh) with elements of finite dimensions (finite elements). Field discretization are:

$$\boldsymbol{u} \approx \boldsymbol{N}^{u}\hat{\mathbf{u}} \quad \delta\boldsymbol{u} \approx \boldsymbol{N}^{u}\delta\hat{\mathbf{u}} \quad \rho \approx \boldsymbol{N}^{\rho}\hat{\boldsymbol{\rho}} \quad \delta\rho \approx \boldsymbol{N}^{\rho}\delta\hat{\boldsymbol{\rho}} \quad \boldsymbol{p} \approx \boldsymbol{N}^{p}\hat{\boldsymbol{p}} \quad \delta\boldsymbol{p} \approx \boldsymbol{N}^{p}\delta\hat{\boldsymbol{p}} \tag{4.69}$$

Field discretization derivative are:

$$\nabla\boldsymbol{u} \approx \boldsymbol{B}^{u}\hat{\mathbf{u}} \quad \delta\nabla\boldsymbol{u} \approx \boldsymbol{B}^{u}\delta\hat{\mathbf{u}} \quad \nabla\rho \approx \boldsymbol{B}^{\rho}\hat{\boldsymbol{\rho}} \quad \delta\nabla\rho \approx \boldsymbol{B}^{\rho}\delta\hat{\boldsymbol{\rho}} \quad \nabla p \approx \boldsymbol{B}^{p}\hat{\boldsymbol{p}} \quad \delta\nabla p \approx \boldsymbol{B}^{p}\delta\hat{\boldsymbol{p}} \tag{4.70}$$

where:

- $\hat{\mathbf{u}}$, $\hat{\boldsymbol{\rho}}$ and $\hat{\boldsymbol{p}}$ are nodal unknown parameters;
- $\delta\hat{\mathbf{u}}$, $\delta\hat{\boldsymbol{\rho}}$ and $\delta\hat{\boldsymbol{p}}$ are nodal arbitrary parameters;
- $\boldsymbol{N}^{u}$, $\boldsymbol{N}^{\rho}$, ... , are shape function matrices.

More informations about shape function matrix type and dimension will be done afterwards.

4.3.3 Weak Form of Equilibrium Equation

For a *linear elastic isotropic material*, constitutive equations can specializes as follows:

$$\boldsymbol{\sigma} = \boldsymbol{C}\boldsymbol{\varepsilon} = \lambda tr(\boldsymbol{\varepsilon}) + 2\mu\boldsymbol{\varepsilon} \tag{4.71}$$

where λ and μ are lamè constants. And

$$tr(\boldsymbol{\varepsilon}) = \boldsymbol{\varepsilon} : \boldsymbol{I} = \epsilon_{11} + \epsilon_{22} + \epsilon_{33} \qquad \boldsymbol{C} = \lambda(\boldsymbol{I} \otimes \boldsymbol{I}) + 2\mu\boldsymbol{I} \tag{4.72}$$

It's important that, for this type of material, constitutive equations written also in different forms, splitting stress and strain into volumetric and deviatoric components:

$$\begin{aligned} \boldsymbol{\sigma} &= \boldsymbol{\sigma}^{vol} + \boldsymbol{\sigma}^{dev} = p\boldsymbol{I} + \boldsymbol{s} \\ \boldsymbol{\varepsilon} &= \frac{\theta}{3}\boldsymbol{I} + \boldsymbol{e} \end{aligned} \tag{4.73}$$

with

$$p = \frac{1}{3} tr(\boldsymbol{\sigma}) = \frac{1}{3} \boldsymbol{\sigma} : \boldsymbol{I} = \frac{1}{3}(\sigma_{11} + \sigma_{22} + \sigma_{33}) \quad \theta = tr(\boldsymbol{\varepsilon}) = \boldsymbol{\varepsilon} : \boldsymbol{I} = \epsilon_{11} + \epsilon_{22} + \epsilon_{33} \tag{4.74}$$

manipulating Eq. 4.73, we can write

$$\begin{aligned} \boldsymbol{s} &= \boldsymbol{\sigma} - p\boldsymbol{I} \\ \boldsymbol{e} &= \boldsymbol{\varepsilon} - \frac{\theta}{3}\boldsymbol{I} \end{aligned} \tag{4.75}$$

and constitutive equation simplifies as follows:

$$\begin{aligned} p &= K\theta \\ \boldsymbol{s} &= 2\mu\boldsymbol{e} \end{aligned} \tag{4.76}$$

Let us rewriting Eq. 3.41c as follow:

$$\boldsymbol{\sigma} = \boldsymbol{C} : \boldsymbol{\varepsilon} - (1-f)\Omega_0^a K(\rho^a - \rho_0)\boldsymbol{I} = \tilde{\boldsymbol{\sigma}} - (1-f)\Omega_0^a K(\rho^a - \rho_0)\boldsymbol{I} \tag{4.77}$$

We have to check if the sum of deviatoric stress plus the volumetric stress is equal to total stress tensor, in formula:

$$\tilde{\boldsymbol{\sigma}}^{dev} + \tilde{\boldsymbol{\sigma}}^{vol} = \tilde{\boldsymbol{\sigma}} \tag{4.78}$$

For simplicity, following steps will be done for a 2D problem.

$$\tilde{\boldsymbol{\sigma}} = \begin{Bmatrix} \tilde{\sigma}_{11} \\ \tilde{\sigma}_{22} \\ \tilde{\sigma}_{12} \end{Bmatrix} \tag{4.79}$$

- Volumetric stress:

  We know that:

$$\tilde{\boldsymbol{\sigma}}^{vol} = \begin{Bmatrix} \left(\frac{\tilde{\sigma}_{11} + \tilde{\sigma}_{22}}{2}\right) \\ \left(\frac{\tilde{\sigma}_{11} + \tilde{\sigma}_{22}}{2}\right) \\ 0 \end{Bmatrix} = \frac{1}{2} tr(\tilde{\boldsymbol{\sigma}})\boldsymbol{I} = \boldsymbol{I}^{vol}\tilde{\boldsymbol{\sigma}} \tag{4.80}$$

  We have to find the ^{vol} component.

$$\tilde{\boldsymbol{\sigma}}^{vol} = \begin{Bmatrix} \left(\frac{\tilde{\sigma}_{11} + \tilde{\sigma}_{22}}{2}\right) \\ \left(\frac{\tilde{\sigma}_{11} + \tilde{\sigma}_{22}}{2}\right) \\ 0 \end{Bmatrix} = \begin{bmatrix} a & b & c \\ d & e & f \\ g & h & i \end{bmatrix} \begin{Bmatrix} \tilde{\sigma}_{11} \\ \tilde{\sigma}_{22} \\ \tilde{\sigma}_{12} \end{Bmatrix} \tag{4.81}$$

Rewriting in a more extended form:

$$\begin{cases} \dfrac{\tilde{\sigma}_{11} + \tilde{\sigma}_{22}}{2} = a\tilde{\sigma}_{11} + b\tilde{\sigma}_{22} + c\tilde{\sigma}_{12} \\ \dfrac{\tilde{\sigma}_{11} + \tilde{\sigma}_{22}}{2} = d\tilde{\sigma}_{11} + e\tilde{\sigma}_{22} + f\tilde{\sigma}_{12} \\ 0 = g\tilde{\sigma}_{11} + h\tilde{\sigma}_{22} + i\tilde{\sigma}_{12} \end{cases} \tag{4.82}$$

Solving the sistem, we obtain:

$$\boldsymbol{I}^{vol} = \begin{bmatrix} \frac{1}{2} & \frac{1}{2} & 0 \\ \frac{1}{2} & \frac{1}{2} & 0 \\ 0 & 0 & 0 \end{bmatrix} \tag{4.83}$$

- Deviatoric part:

  For deviatoric stress, math steps are the same. The resulting system is a little bit more complicated, in formula:

$$\tilde{\boldsymbol{\sigma}} - \tilde{\boldsymbol{\sigma}}\boldsymbol{I}^{vol} = \tilde{\boldsymbol{\sigma}}\boldsymbol{I}^{dev} \tag{4.84}$$

  In matrix form:

$$\begin{Bmatrix} \tilde{\sigma}_{11} \\ \tilde{\sigma}_{22} \\ \tilde{\sigma}_{12} \end{Bmatrix} - \begin{Bmatrix} \tilde{\sigma}_{11} \\ \tilde{\sigma}_{22} \\ \tilde{\sigma}_{12} \end{Bmatrix} \begin{bmatrix} \frac{1}{2} & \frac{1}{2} & 0 \\ \frac{1}{2} & \frac{1}{2} & 0 \\ 0 & 0 & 0 \end{bmatrix} = \begin{bmatrix} a & b & c \\ d & e & f \\ g & h & i \end{bmatrix} \begin{Bmatrix} \tilde{\sigma}_{11} \\ \tilde{\sigma}_{22} \\ \tilde{\sigma}_{12} \end{Bmatrix} \tag{4.85}$$

  Solvign the system, we obtain the $\boldsymbol{I}^{dev}$:

$$\boldsymbol{I}^{dev} = \begin{bmatrix} \frac{1}{2} & -\frac{1}{2} & 0 \\ -\frac{1}{2} & \frac{1}{2} & 0 \\ 0 & 0 & 1 \end{bmatrix} \tag{4.86}$$

Now, we have to check if the sum is $\boldsymbol{I}$:

$$\boldsymbol{I} = \boldsymbol{I}^{vol} + \boldsymbol{I}^{dev} = \begin{bmatrix} \frac{1}{2} & \frac{1}{2} & 0 \\ \frac{1}{2} & \frac{1}{2} & 0 \\ 0 & 0 & 0 \end{bmatrix} + \begin{bmatrix} \frac{1}{2} & -\frac{1}{2} & 0 \\ -\frac{1}{2} & \frac{1}{2} & 0 \\ 0 & 0 & 1 \end{bmatrix} = \begin{bmatrix} 1 & 0 & 0 \\ 0 & 1 & 0 \\ 0 & 0 & 1 \end{bmatrix} \tag{4.87}$$

Taking into account above relations, let us recall Eq. 4.68a

$$\delta \boldsymbol{u} \cdot \left[\int_{\Omega} [div(\boldsymbol{\sigma})] d\Omega \right] = 0 \tag{4.88}$$

$$\delta \boldsymbol{u} \cdot \left[\int_{\Omega} [div(\boldsymbol{\sigma})] d\Omega \right] = \int_{\Omega} \delta \boldsymbol{u} \cdot [div(\boldsymbol{\sigma})] d\Omega = \int_{\Omega} \nabla \boldsymbol{u} : \boldsymbol{\sigma} d\Omega - \int_{\partial\Omega} \delta \boldsymbol{u} \cdot \boldsymbol{\sigma} \boldsymbol{n} d\Omega = 0 \tag{4.89}$$

Recalling Eq. 4.78, setting $\boldsymbol{\sigma} \boldsymbol{n} = \boldsymbol{t}$ on $\partial\Omega$ and replacing Eq. 3.41c into Eq. 4.66a, Eq. 4.89 becomes:

$$\int_{\Omega} \nabla \boldsymbol{u} : \left[(\tilde{\boldsymbol{\sigma}}^{dev} + \tilde{\boldsymbol{\sigma}}^{vol}) - (1-f)\Omega_0^a K(\rho^a - \rho_0)\boldsymbol{I} \right] - \int_{\partial\Omega} \delta \boldsymbol{u} \cdot \boldsymbol{t} = 0 \tag{4.90}$$

For simplicity, the quantity $(1-f)\Omega_0^a K$, from now, will be called k_1 and ρ^a will be called simply ρ.

$$\int_{\Omega} \nabla \boldsymbol{u} : (p\boldsymbol{I} + 2\mu \boldsymbol{I}^{dev} \boldsymbol{\varepsilon}) - \int_{\Omega} \nabla \boldsymbol{u} : \boldsymbol{I} k_1 \rho + \int_{\Omega} \nabla \boldsymbol{u} : \boldsymbol{I} k_1 \rho_0 - \int_{\partial\Omega} \delta \boldsymbol{u} \cdot \boldsymbol{t} = 0 \tag{4.91}$$

and thus:

$$\int_{\Omega} \nabla \boldsymbol{u} : p\boldsymbol{I} + \int_{\Omega} \nabla \boldsymbol{u} : 2\mu \boldsymbol{I}^{dev} \boldsymbol{\varepsilon} - \int_{\Omega} \nabla \boldsymbol{u} : \boldsymbol{I} k_1 \rho + \int_{\Omega} \nabla \boldsymbol{u} : \boldsymbol{I} k_1 \rho_0 - \int_{\partial\Omega} \delta \boldsymbol{u} \cdot \boldsymbol{t} = 0 \tag{4.92}$$

Now, we can proceed substituting approximations.

Substituting Eq. 4.70 in Eq. 4.91:

$$\int_{\Omega} (\boldsymbol{B}^u)^T \delta \hat{\mathbf{u}} \boldsymbol{I} \boldsymbol{N}^p \hat{\boldsymbol{p}} + \int_{\Omega} (\boldsymbol{B}^u)^T \delta \hat{\mathbf{u}} 2G \boldsymbol{I}^{dev} \boldsymbol{B}^u \hat{\mathbf{u}} - \int_{\Omega} (\boldsymbol{B}^u)^T \delta \hat{\mathbf{u}} \boldsymbol{I} k_1 \boldsymbol{N}^\rho \hat{\boldsymbol{\rho}} + \int_{\Omega} (\boldsymbol{B}^u)^T \delta \hat{\mathbf{u}} \boldsymbol{I} k_1 \rho_0 +$$
$$- \int_{\partial\Omega} (\boldsymbol{N}^u)^T \delta \hat{\mathbf{u}} \cdot \boldsymbol{t} = 0 \tag{4.93}$$

Since $\delta \hat{\mathbf{u}}$ and $\delta \hat{\boldsymbol{\rho}}$ are arbitrary, whatever is their value, Eq. 4.93 must be always valid, thus:

$$\int_{\Omega}(\boldsymbol{B}^{u})^{T}\boldsymbol{I}\boldsymbol{N}^{p}\hat{\boldsymbol{p}}+\int_{\Omega}(\boldsymbol{B}^{u})^{T}2G\boldsymbol{I}^{dev}\boldsymbol{B}^{u}\hat{\mathbf{u}}-\int_{\Omega}(\boldsymbol{B}^{u})^{T}\boldsymbol{I}k_{1}\boldsymbol{N}^{\rho}\hat{\boldsymbol{\rho}}+\int_{\Omega}(\boldsymbol{B}^{u})^{T}\boldsymbol{I}k_{1}\rho_{0}+ \\ -\int_{\partial\Omega}(\boldsymbol{N}^{u})^{T}\cdot\boldsymbol{t}=0 \tag{4.94}$$

For a two dimensional general problem, each node has two coordinates, horizontal and vertical displacement respectively.

$$\boldsymbol{R}^{\boldsymbol{u}}=\int_{\Omega}\underbrace{(\boldsymbol{B}^{u})^{T}\boldsymbol{I}\boldsymbol{N}^{p}}_{8x3\ \ 3x11x4}\hat{\boldsymbol{p}}+\int_{\Omega}\underbrace{(\boldsymbol{B}^{u})^{T}2G\boldsymbol{I}^{dev}\boldsymbol{B}^{u}}_{8x3\ \ 3x3\ \ 3x8}\hat{\mathbf{u}}-\int_{\Omega}\underbrace{(\boldsymbol{B}^{u})^{T}\boldsymbol{I}\boldsymbol{N}^{\rho}}_{8x3\ \ 3x1\ \ 1x4}k_{1}\hat{\boldsymbol{\rho}}+\int_{\Omega}\underbrace{(\boldsymbol{B}^{u})^{T}\boldsymbol{I}}_{8x3\ \ 3x1}k_{1}\rho_{0}+ \\ -\int_{\partial\Omega}\underbrace{(\boldsymbol{N}^{u})^{T}\boldsymbol{t}}_{8x2\ \ 8x1}=0 \tag{4.95}$$

In a more compact manner, Eq. 4.95, can be rewritten as:

$$\boldsymbol{K}^{uu}\hat{\mathbf{u}}-\boldsymbol{K}^{up}\hat{\boldsymbol{\rho}}+\boldsymbol{K}^{up}\hat{\boldsymbol{p}}=\boldsymbol{f}^{u} \tag{4.96}$$

where:

$$\begin{aligned}\boldsymbol{K}^{uu}&=\int_{\Omega}(\boldsymbol{B}^{u})^{T}2G\boldsymbol{I}^{dev}\boldsymbol{B}^{u}\\ \boldsymbol{K}^{up}&=\int_{\Omega}(\boldsymbol{B}^{u})^{T}\boldsymbol{I}\boldsymbol{N}^{\rho}k_{1}\\ \boldsymbol{K}^{up}&=\int_{\Omega}(\boldsymbol{B}^{u})^{T}\boldsymbol{I}\boldsymbol{N}^{p}\\ \boldsymbol{f}^{u}&=\int_{\Omega}(\boldsymbol{B}^{u})^{T}\boldsymbol{I}k_{1}\rho_{0}-\int_{\partial\Omega}(\boldsymbol{N}^{u})^{T}\boldsymbol{t}\end{aligned} \tag{4.97}$$

4.3.4 Weak Form of Mass Balance

Recalling Eq. 4.68b, steps are exactly the same, find equations in a strong form, multiplying by a weight function and integrate problem over the problem domain. The time dependence is treated as follow.

$$\dot{\rho}+\nabla\cdot\boldsymbol{j}=\frac{\rho-\rho^{n}}{\Delta t}+div(\boldsymbol{j})=0 \tag{4.98}$$

$$\frac{1}{\Delta t}\left[\int_{\Omega}\delta\rho\rho d\Omega\right]+\int_{\Omega}\nabla\delta\rho\cdot\boldsymbol{j}d\Omega-\int_{\partial\Omega}\delta\rho\cdot\boldsymbol{j}d\Omega=\frac{1}{\Delta t}\left[\int_{\Omega}\delta\rho\rho^{n}d\Omega\right] \tag{4.99}$$

Let's step back on Eq. 3.41d:

$$\boldsymbol{j} = -\frac{D_v \rho^a}{kT}\left(\frac{\partial^v \mu_0^{av}(\rho^a)}{\partial \rho^a}\nabla\rho^a + (1-f)\Omega_0^a \nabla p\right) \tag{4.100}$$

Following quantities are setted:

$$k_2 = -\frac{D_v}{kT} \qquad k_3 = -\frac{D_v}{kT}(1-f)\Omega_0^a \tag{4.101}$$

Eq. 4.100 becomes:

$$\boldsymbol{j} = k_2 \rho\mu(\rho)\nabla\rho + k_3\rho\nabla p \tag{4.102}$$

The non linear terms $\rho\mu(\rho)$ and ρ are setted to be one. Eq. 4.102 becomes:

$$\boldsymbol{j} = k_2\nabla\rho + k_3\nabla p \tag{4.103}$$

Replacing Eq. 4.103 in Eq. 4.99:

$$\frac{1}{\Delta t}\left[\int_\Omega \nabla\delta\rho\rho\right] + \int_\Omega \delta\rho\cdot[k_2\nabla\rho + k_3\nabla p] - \int_{\partial\Omega}\delta\rho\cdot[k_2\nabla\rho + k_3\nabla p] = \frac{1}{\Delta t}\left[\int_\Omega \delta\rho\rho^n\right] \tag{4.104}$$

Substituting all approximations:

$$\begin{aligned}&\frac{1}{\Delta t}\left[\int_\Omega (\boldsymbol{N}^\rho)^T\delta\hat{\boldsymbol{\rho}}\boldsymbol{N}^\rho\hat{\boldsymbol{\rho}}\right] + \int_\Omega (\boldsymbol{B}^\rho)^T\delta\hat{\boldsymbol{\rho}}k_2\boldsymbol{B}^\rho\hat{\boldsymbol{\rho}} - \int_\Omega (\boldsymbol{B}^\rho)^T\delta\hat{\boldsymbol{\rho}}k_3\boldsymbol{B}^p\hat{\boldsymbol{p}} + \\ &- \int_{\partial\Omega}(\boldsymbol{N}^\rho)^T\delta\hat{\boldsymbol{\rho}}k_2\boldsymbol{B}^\rho\hat{\boldsymbol{\rho}} - \int_{\partial\Omega}(\boldsymbol{B}^\rho)^T\delta\hat{\boldsymbol{\rho}}k_3\boldsymbol{B}^p\hat{\boldsymbol{p}} = \frac{1}{\Delta t}\left[\int_\Omega (\boldsymbol{N}^\rho)^T\delta\hat{\boldsymbol{\rho}}\rho^n\right]\end{aligned} \tag{4.105}$$

Since $\delta\hat{\boldsymbol{\rho}}$ and $\delta\hat{\boldsymbol{\rho}}$ are arbitrary, whatever is their value, Eq. 4.105 must be always valid, thus:

$$\begin{aligned}&\frac{1}{\Delta t}\left[\int_\Omega \underbrace{(\boldsymbol{N}^\rho)^T\boldsymbol{N}^\rho}_{4x1\ 1x4}\hat{\boldsymbol{\rho}}\right] + \int_\Omega \underbrace{(\boldsymbol{B}^\rho)^T k_2\boldsymbol{B}^\rho}_{4x2\ 2x4}\hat{\boldsymbol{\rho}} - \int_\Omega \underbrace{(\boldsymbol{B}^\rho)^T k_3\boldsymbol{B}^p}_{4x2\ 2x4}\hat{\boldsymbol{p}} - \int_{\partial\Omega}\underbrace{(\boldsymbol{N}^\rho)^T k_2\boldsymbol{B}^\rho}_{4x1\ 1x4}\hat{\boldsymbol{\rho}} \\ &- \int_{\partial\Omega}\underbrace{(\boldsymbol{B}^\rho)^T k_3\boldsymbol{B}^p}_{4x2\ 1x4}\hat{\boldsymbol{p}} = \frac{1}{\Delta t}\left[\int_\Omega \underbrace{(\boldsymbol{N}^\rho)^T\rho^n}_{4x1}\right]\end{aligned} \tag{4.106}$$

In a more compact manner:

$$\frac{1}{\Delta t}\left[\boldsymbol{M}^{\rho\rho}\right]\hat{\boldsymbol{\rho}} + \int_{\Omega}\boldsymbol{K}^{\rho\rho}\hat{\boldsymbol{\rho}} - \int_{\Omega}\boldsymbol{K}^{\rho\rho}\hat{\boldsymbol{\rho}} = \frac{1}{\Delta t}\left[\boldsymbol{f}^{\rho}\right] \tag{4.107}$$

where:

$$\begin{aligned}
\boldsymbol{M}^{\rho\rho} &= \frac{1}{\Delta t}\left[\int_{\Omega}(\boldsymbol{N}^{\rho})^{T}\boldsymbol{N}^{\rho}\right] \\
\boldsymbol{K}^{\rho\rho} &= \int_{\Omega}(\boldsymbol{B}^{\rho})^{T}k_2\boldsymbol{B}^{\rho} - \int_{\partial\Omega}(\boldsymbol{N}^{\rho})^{T}k_2\boldsymbol{B}^{\rho} \\
\boldsymbol{K}^{\rho p} &= \int_{\Omega}(\boldsymbol{B}^{\rho})^{T}k_3\boldsymbol{B}^{p} - \int_{\partial\Omega}(\boldsymbol{B}^{\rho})^{T}k_3\boldsymbol{B}^{p} \\
\boldsymbol{f}^{\rho} &= \frac{1}{\Delta t}\left[\int_{\Omega}(\boldsymbol{N}^{\rho})^{T}\rho^{n}\right]
\end{aligned} \tag{4.108}$$

4.3.5 Weak Form of Pressure Balance

The pressure balance combines pressure field with displacement field.

Recalling

$$p = K\theta = \frac{1}{3}Ktr(\boldsymbol{\varepsilon}) = \frac{K}{3}\boldsymbol{I}^{T}\nabla\boldsymbol{u} \tag{4.109a}$$

Rewriting Eq. 4.109a as

$$p = k\theta = \frac{1}{3}tr(\boldsymbol{\varepsilon}) = \frac{1}{3}\boldsymbol{I}^{T}\nabla u \tag{4.110}$$

The steps are the same saw before. We have to use an appropriate weight function δp:

$$\int_{\Omega}\delta p\,(p - K\theta)\,d\Omega = \int_{\Omega}\delta p\left(p - \frac{1}{3}K\boldsymbol{I}^{T}tr(\boldsymbol{\varepsilon})\right)d\Omega = \int_{\Omega}\delta p\left(p - K\boldsymbol{I}^{T}\nabla u\right)d\Omega = 0 \tag{4.111}$$

Recalling Eqs. 4.70, Eq. 4.111 becomes:

$$\int_{\Omega}(\boldsymbol{N}^{p})^{T}\delta\hat{\boldsymbol{p}}\left(\boldsymbol{N}^{p}\hat{\boldsymbol{p}} - K\boldsymbol{I}^{T}\boldsymbol{B}^{u}\hat{\mathbf{u}}\right) = \delta\hat{\boldsymbol{p}}\left\{\int_{\Omega}(\boldsymbol{N}^{p})^{T}\left(\boldsymbol{N}^{p}\hat{\boldsymbol{p}} - K\boldsymbol{I}^{T}\boldsymbol{B}^{u}\hat{\mathbf{u}}\right)\right\} = 0 \tag{4.112}$$

and thus

$$\boldsymbol{R}^p = \int_\Omega \underbrace{(\boldsymbol{N}^p)^T \boldsymbol{N}^p}_{4x1\ \ 1x4} \hat{\boldsymbol{p}} - \int_\Omega \underbrace{(\boldsymbol{N}^p)^T K \boldsymbol{I}^T \boldsymbol{B}^u}_{4x1\ \ 1x3\ \ 3x8} \hat{\mathbf{u}} = \mathbf{0} \tag{4.113}$$

In a more compact manner:

$$\boldsymbol{K}^{pp} + \boldsymbol{K}^{pu} = 0 \tag{4.114}$$

where:

$$\begin{aligned} \boldsymbol{K}^{pp} &= \int_\Omega (\boldsymbol{N}^p)^T \boldsymbol{N}^p \\ \boldsymbol{K}^{pu} &= \int_\Omega (\boldsymbol{N}^p)^T K \boldsymbol{I}^T \boldsymbol{B}^u \end{aligned} \tag{4.115}$$

4.4 Global Residual

Finally, the solving sistem is:

$$\frac{1}{\Delta t} \begin{bmatrix} \mathbf{0} & \mathbf{0} & \mathbf{0} \\ \boldsymbol{M}^{\rho u} & \mathbf{0} & \mathbf{0} \\ \mathbf{0} & \mathbf{0} & \mathbf{0} \end{bmatrix} \begin{Bmatrix} \hat{\mathbf{u}} \\ \hat{\boldsymbol{\rho}} \\ \hat{\boldsymbol{p}} \end{Bmatrix} + \begin{bmatrix} \boldsymbol{K}^{uu} & \boldsymbol{K}^{u\rho} & \boldsymbol{K}^{up} \\ \boldsymbol{K}^{\rho u} & \boldsymbol{K}^{\rho\rho} & \boldsymbol{K}^{\rho p} \\ \boldsymbol{K}^{pu} & \boldsymbol{K}^{p\rho} & \boldsymbol{K}^{pp} \end{bmatrix} \begin{Bmatrix} \hat{\mathbf{u}} \\ \hat{\boldsymbol{\rho}} \\ \hat{\boldsymbol{p}} \end{Bmatrix} = \begin{Bmatrix} \boldsymbol{f}^u \\ \boldsymbol{f}^\rho \\ \boldsymbol{f}^p \end{Bmatrix} \tag{4.116}$$

where:

- The $\boldsymbol{M}$ contribute is:

$$\boldsymbol{M}^{\rho\rho} = \frac{1}{\Delta t} \left[\int_\Omega \underbrace{(\boldsymbol{N}^\rho)^T \boldsymbol{N}^\rho}_{4x4} \hat{\boldsymbol{\rho}} \right] \tag{4.117}$$

- The $\boldsymbol{K}$ contributes are :

$$\boldsymbol{K}^{\rho\rho} = \int_{\Omega} \underbrace{(\boldsymbol{B}^{\rho})^T k_2 \boldsymbol{B}^{\rho}}_{4x4} - \int_{\partial\Omega} \underbrace{(\boldsymbol{N}^{\rho})^T k_2 \boldsymbol{B}^{\rho}}_{4x4} \tag{4.118a}$$

$$\boldsymbol{K}^{pp} = \int_{\Omega} \underbrace{(\boldsymbol{N}^{p})^T \boldsymbol{N}^{p}}_{4x4} \tag{4.118b}$$

$$\boldsymbol{K}^{pp} = \int_{\Omega} \underbrace{(\boldsymbol{B}^{p})^T k_3 \boldsymbol{B}^{p}}_{4x4} - \int_{\partial\Omega} \underbrace{(\boldsymbol{B}^{p})^T k_3 \boldsymbol{B}^{p}}_{4x4} \tag{4.118c}$$

$$\boldsymbol{K}^{uu} = \int_{\Omega} \underbrace{(\boldsymbol{B}^{u})^T 2G \boldsymbol{I}^{dev} \boldsymbol{B}^{u}}_{8x8} \tag{4.118d}$$

$$\boldsymbol{K}^{pu} = \int_{\Omega} \underbrace{(\boldsymbol{N}^{p})^T K \boldsymbol{I}^T \boldsymbol{B}^{u}}_{4x8} \tag{4.118e}$$

$$\boldsymbol{K}^{u\rho} = \int_{\Omega} \underbrace{(\boldsymbol{B}^{u})^T \boldsymbol{I} \boldsymbol{N}^{\rho} k_1}_{8x4} \tag{4.118f}$$

$$\boldsymbol{K}^{up} = \int_{\Omega} \underbrace{(\boldsymbol{B}^{u})^T \boldsymbol{I} \boldsymbol{N}^{p}}_{8x4} \tag{4.118g}$$

- The $\boldsymbol{f}$ contributes are:

$$\boldsymbol{f}^{\rho} = \frac{1}{\Delta t} \left[\int_{\Omega} \underbrace{(\boldsymbol{N}^{\rho})^T \rho^n}_{4x1} \right] \tag{4.119a}$$

$$\boldsymbol{f}^{u} = \int_{\Omega} \underbrace{(\boldsymbol{B}^{u})^T \boldsymbol{I} k_1 \rho_0}_{8x1} - \int_{\partial\Omega} \underbrace{(\boldsymbol{N}^{u})^T \boldsymbol{t}}_{8x1} \tag{4.119b}$$

Now, we can have an idea of elementary stiffness matrix ($\boldsymbol{K}_{el}$), Mass matrix ($\boldsymbol{M}_{el}$) and force vector ($\boldsymbol{f}_{el}$) dimension, i.e.

- Elementary stiffness matrix:

$$\boldsymbol{K}_{el} = \begin{bmatrix} \boldsymbol{K}^{uu}\ [8x8] & \boldsymbol{K}^{u\rho}\ [8x4] & \boldsymbol{K}^{pu}\ [8x4] \\ \boldsymbol{0}\ [4x8] & \boldsymbol{K}^{\rho\rho}\ [4x4] & \boldsymbol{K}^{pp}\ [4x4] \\ \boldsymbol{K}^{pu}\ [4x8] & \boldsymbol{0}\ [4x4] & \boldsymbol{K}^{pp}\ [4x4] \end{bmatrix} \tag{4.120}$$

- elementary mass matrix:

$$\boldsymbol{M}_{el} = \begin{bmatrix} \mathbf{0}\ [8x8] & \mathbf{0}\ [8x4] & \mathbf{0}\ [4x4] \\ \boldsymbol{M}^{\rho u}\ [4x4] & \mathbf{0}\ [4x4] & \mathbf{0}\ [4x4] \\ \mathbf{0}\ [4x8] & \mathbf{0}\ [4x4] & \mathbf{0}\ [4x4] \end{bmatrix} \tag{4.121}$$

- elementary forces vector:

$$\boldsymbol{f}_{el} = \begin{Bmatrix} \boldsymbol{F}^{u}\ [8x1] \\ \boldsymbol{F}^{\rho}\ [4x1] \\ \mathbf{0}\ [4x1] \end{Bmatrix} \tag{4.122}$$

4.5 Mapping

Recalling section 4.1, we want to transform the general quad-4 formulation into a specific formulation, referred to our case.

4.5.1 Implementation

The bilinear quadrilateral shape functions are:

$$N_i = \frac{1}{4}\left(1 + \bar{\xi}_i \xi\right)\left(1 + \bar{\eta}_i \eta\right) \tag{4.123}$$

with $\bar{\xi}_i$ e $\bar{\eta}_i$ natural nodes coordinates, i.e.

$$\begin{aligned} \bar{\xi}_1 = -1 \quad \bar{\xi}_2 = 1 \quad \bar{\xi}_3 = 1 \quad \bar{\xi}_4 = -1 \\ \bar{\eta}_1 = -1 \quad \bar{\eta}_2 = 1 \quad \bar{\eta}_3 = 1 \quad \bar{\eta}_4 = -1 \end{aligned} \tag{4.124}$$

Finally, there will be 4 explicit expression for shape function, replacing $\bar{\xi}_i$ and $\bar{\eta}_i$ of nodes N_i:

$$\begin{aligned} N_1 &= \frac{1}{4}(1-\xi)(1-\eta) \\ N_2 &= \frac{1}{4}(1+\xi)(1-\eta) \\ N_3 &= \frac{1}{4}(1+\xi)(1+\eta) \\ N_4 &= \frac{1}{4}(1-\xi)(1+\eta) \end{aligned} \tag{4.125}$$

Shape function derivative are:

$$\begin{aligned} N_i &= \frac{1}{4}\left(1+\bar{\xi}_i\xi\right)\left(1+\bar{\eta}_i\eta\right) \\ N_{i,\xi} &= \frac{1}{4}\bar{\xi}_i\left(1+\bar{\eta}_i\eta\right) \\ N_{i,\eta} &= \frac{1}{4}\bar{\eta}_i\left(1+\bar{\xi}_i\xi\right) \end{aligned} \tag{4.126}$$

Shape functions derivative are:

$$\boldsymbol{B}^u = \begin{bmatrix} \frac{\partial N_1}{\partial x} & 0 & \frac{\partial N_2}{\partial x} & 0 & \frac{\partial N_3}{\partial x} & 0 & \frac{\partial N_4}{\partial x} & 0 \\ 0 & \frac{\partial N_1}{\partial y} & 0 & \frac{\partial N_2}{\partial y} & 0 & \frac{\partial N_3}{\partial y} & 0 & \frac{\partial N_4}{\partial y} \\ \frac{\partial N_1}{\partial x} & \frac{\partial N_1}{\partial y} & \frac{\partial N_2}{\partial x} & \frac{\partial N_2}{\partial y} & \frac{\partial N_3}{\partial x} & \frac{\partial N_3}{\partial y} & \frac{\partial N_4}{\partial x} & \frac{\partial N_4}{\partial y} \end{bmatrix} \tag{4.127}$$

and

$$\boldsymbol{B}^p = \boldsymbol{B}^p = \begin{bmatrix} \frac{\partial N_1}{\partial x} & \frac{\partial N_2}{\partial x} & \frac{\partial N_3}{\partial x} & \frac{\partial N_4}{\partial x} \\ \frac{\partial N_1}{\partial y} & \frac{\partial N_2}{\partial y} & \frac{\partial N_3}{\partial y} & \frac{\partial N_4}{\partial y} \end{bmatrix} \tag{4.128}$$

The unknown quantities are setted on the quad element as shown in figure 4.2.

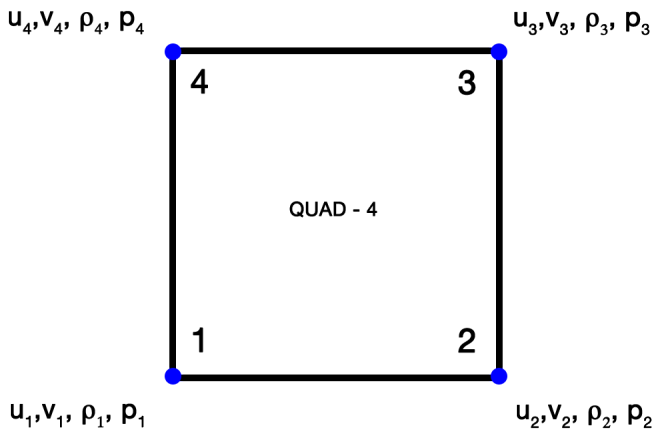

Figure 4.2: Quad quantities distributions

A 2*x*2 Gaussian Integration is used to calculate the shape functions integral. For further details see C.1.

4.6 Algorithm and Results

It's important to emphasize that, the present program has been developed with a significant amount of simplifications. We create a Matlab code to simulate the sintering process. For simplicity, only the major algorithm structure will be shown in present work.

Load material mechanical and chemical characteristics

Set $t = 0$

Choose Δt **and tollerance** $t_{toll} = t_{max}$

Do while $t \leq t_{toll}$

    Loop over the elements

        Compute stiffness matrix

        Compute force vector

        Assembly global stiffness matrix and force vector

    End loop

    Store displacement, density and pressure

    Set $t = t + \Delta t$

End do while

Plot displacement, density and pressure versus time

After running code, we can say that the major nodal displacement of the external nodes is about 2.2 e^{-4} mm. Recalling filament dimensions, we can calcualte the percentage of displacement. By relating the two quantities can be seen that the relative displacement is about 1‰. This value corresponds to a sintering angle of practically zero. As expected, numerical results of numerical analysis described above, in the present work, have no physical meaning. As we shall see in the next chapters, eliminating non-linearity, assume an elastic behavior and imposing geometry, make results not significant.

Chapter 5

Sintering Elastic Model - Analytical Model

5.1 Modeling different routes of sintering phenomena

Recalling chapter 3, now the particle system is assumed to be at chemical equilibrium at any time. Characteristic time of chemical diffusion is much more smaller than the characteristic time associated at the mechanical strin rate [10]. This fact, simplifying, leads to a quasi-static equilibrium. In formula:

$$\frac{\partial \rho^a}{\partial t} = 0 \qquad \longrightarrow \qquad \rho^a = \rho_0^a = \frac{a}{(1-f)\Omega_0^a} \tag{5.1}$$

Considerations made before, lead to assuming that the matter can not be accumulated, to a normal motion of these interfaces. This motion is then characterized by a displacement rate, referred to as diffusion velocity, but which does not correspond necessarily to the velocity of particles. Now, all assumptions have to be applied to the diffusion routes described in table 3.1.

Let set some notation. It's possible to split well-known boundary of set of grains, denoted by $\partial\Omega$, in two distinct parts:

1. Γ_{sf}, the set of free boundaries, that is the set of the interfaces between solid bodies and the surrounding medium (considered as a fluid medium);

2. Γ_{gb}, the set of the grain boundaries, that is the set of the interfaces between two adjacent

solid grains;

It's now obvious that $\partial\Omega = \Gamma_{sf} \cup \Gamma_{gb}$. Let γ_{sf} and γ_{gb} be the constant surface tension parameter defined over the two before mentioned boundaries.

By Eq. 3.36, Eq. 3.41, Eq. 5.1 and since $\boldsymbol{C} : \boldsymbol{I} = (2G + 3\lambda)\boldsymbol{I} = 3K\boldsymbol{I}$, it's possible to write:

$$\nabla \cdot (2G\boldsymbol{\varepsilon} + \lambda tr(\boldsymbol{\varepsilon})\boldsymbol{I}) = 2\nabla \cdot \boldsymbol{\varepsilon} - \left(1 - \frac{2G}{3K}\right)\nabla p = 0 \tag{5.2}$$

and then:

$$2G\nabla \cdot \boldsymbol{\varepsilon}(u) - \left(1 - \frac{2G}{3K}\right)\nabla p = 0 \quad \text{in} \quad \Omega \tag{5.3a}$$

$$\nabla \cdot u + \frac{p}{K} = 0 \quad \text{in} \quad \Omega \tag{5.3b}$$

$$[\boldsymbol{\sigma}\boldsymbol{n}]_{\Gamma sf} = \gamma_{sf}\kappa\boldsymbol{n} \quad \text{over} \quad \Gamma sf \tag{5.3c}$$

$$[\boldsymbol{\sigma}\boldsymbol{n}]_{\Gamma gb} = \gamma_{gb}\kappa\boldsymbol{n} \quad \text{over} \quad \Gamma gb \tag{5.3d}$$

where κ is the surface curvature and the last two eqs. express the Laplace Law of surface tension.

Let f be a funcion possibly to discontinuous across a surface S; for any point $\boldsymbol{x} \in S$, $f^+(\boldsymbol{x})$ and $f^-(\boldsymbol{x})$ the value of f on each side of S are defined by the limits:

$$f^{\pm}(\boldsymbol{x}) = \lim_{\epsilon \to 0} f(\boldsymbol{x} \pm \epsilon\boldsymbol{n}) \quad \text{con} \quad \epsilon > 0 \tag{5.4}$$

The symbols $[\cdot]_{\Gamma sf}$ and $[\cdot]_{\Gamma gb}$ are the operators of jump across the two surfaces. They are defined as follow:

$$[f]_S(\boldsymbol{x}) = f^+(\boldsymbol{x}) - f^-(\boldsymbol{x}) \quad \text{for any } x \in S \tag{5.5}$$

5.1.1 Surface Diffusion

Consider a pure solid substance in which vacancies are the only defect present. If the local equilibrium between vacancies and atom is assumed, the *Gibbs-Duhem* relation is satisfied:

$$G = \mu_a N_a + \mu_v N_v \tag{5.6}$$

where μ_a is the chemical potential of the atoms, μ_v is the chemical potential of the vacancies, N_a si the number of atoms, N_v is the number of vacancies and G is the Gibbs free energy which is defined as a function of temperature T, pressure p and internal energy U as follow:

$$G = U + pV - TS \tag{5.7}$$

where V is the volume and S is the entropy. The chemical potential which represent the energy brought by and atom, μ_a, and by a vacancy, μ_v can be derived from the previous equations:

$$\begin{aligned} \mu_a &= \left(\frac{\partial G}{\partial N_a}\right)_{N_v,T,p} \\ \mu_v &= \left(\frac{\partial G}{\partial N_v}\right)_{N_a,T,p} \end{aligned} \tag{5.8}$$

The internal energy U can be written as a function of the change of the extensive quantities $S,\ V,\ N_a,\ N_v$:

$$dU = TdS - pdV + \mu_a dN_a + \mu_v dN_v \tag{5.9}$$

as well-known, temperature T, pressure P, chemical potential of the atoms μ_a and vacancies μ_v, are the intensive quantities of the system (do not depend on the amount of material).

Eq. 5.9 means that the free energy of a system can change in different ways: by changing its entropy, its volume, the amount of atoms or the amount of vacancies. The intensive quantity ($T,\ p,\ \mu_a,\ \mu_v$) determine the magnitude of the energy change related to the change of corresponding extensive quantities ($S,\ V,\ N_a,\ N_v$).

Now, a set of thermodynamical expressions are presented:

$$\left(\frac{\partial \mu_a}{\partial p}\right)_{N_v,T} = \left(\frac{\partial G}{\partial p \partial N_a}\right)_{N_v,T} = \Omega$$

$$\left(\frac{\partial \mu_v}{\partial p}\right)_{N_v,T} = \left(\frac{\partial G}{\partial p \partial N_v}\right)_{N_v,T} = f\Omega \tag{5.10}$$

where the volume of a vacancy is supposed to be the fraction of the atomic volume Ω. Because of the presence of vacancies, the lattice is distorted as shown in figure 5.1.

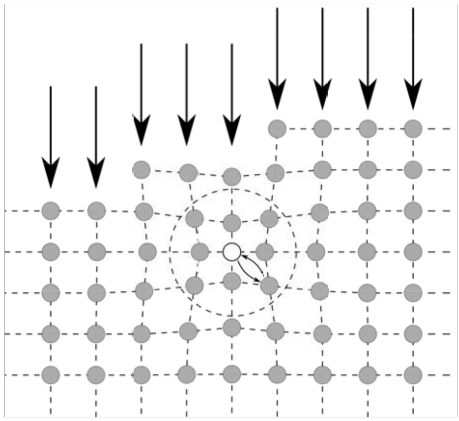

Figure 5.1: Rearrangement of the lattice around a vacancy

The change in chemical potentials with respect to the change in vacancies concentration C_v is mainly due to the entropy mixing of the atoms and vacancies. Vacancies concentration is defined as a function of the number of atoms N_a and the number of lattice sites N_L in a given volume: $C_v = (N_L - N_a)/N_L$ and, since $C_v \ll 1$ it's possible to write:

$$\left(\frac{\partial \mu_v}{\partial C_v}\right)_{p,T} = \frac{kT}{C_v} + O(1)$$

$$\left(\frac{\partial \mu_a}{\partial C_v}\right)_{p,T} = -kT + O(C_v) \tag{5.11}$$

The diffusional transport can take place only by migration of interstitial atoms or lattice vacancies and neither of these process changes the number of lattice sites in the region. In other words the number of atoms and the number of vacancies change by equal and opposite amounts. Under those conditions, the change of free energy of a region is therefore equal to

the number of atoms entering or leaving it multiplied by the difference of chemical potential involved in the atom vacancies switching ($\mu_a - \mu_v$). The diffusional flux is given by:

$$\boldsymbol{j}_{diff} = -\frac{D}{kT\Omega}(\nabla\mu_a - \nabla\mu_v) \tag{5.12}$$

Previous expressions will be used in the following sections in order to find the surface and ground boundary diffusion.

The specific surface free energy (γ_{sf}) of a crystalline solid is defined as the increase of energy when the area of the free surface $\partial\omega$ of the crystal is increased by a unit amount. It comes that the surface free energy E_s of the sistem is given by:

$$E_s = \int_{\partial\omega} \gamma_{sf}\, dA \tag{5.13}$$

where γ_{sf} is constant along the free surface. Considering this equation and referring to figure 5.2, it's possible say that the first solid has more free energy that the second. It follows that a way to reduce energy is to reduce the surface of the solid. This is possible by transporting matter from the convex surface to the concave surface to tend a surface of lower curvature. An expression of the chemical potential can be found by establishing that the free energy is a minimum with respect to any infinitesimal virtual change in which the local shape of the surface is altered by removing atoms from the interior and placing them on the surface, or vice versa.

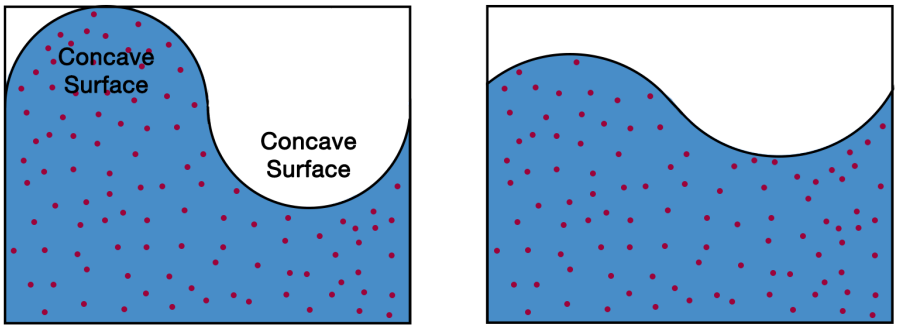

Figure 5.2: Concave and convex surface (in ω_0 and in ω)

Referring to figure 5.3, considering a smoothly curved surface, the change of the surface free energy is given by:

$$\delta\left(\int_{\partial\omega}\gamma_{sf}\,dA\right)=\int_{\partial\omega_0}\delta(\gamma_{sf})dA_0+\int_{\partial\omega}\gamma_{sf}\,\delta(dA) \tag{5.14}$$

where δ represent the small change of the quantity. dA_0 is the area of an element of the original surface and $dA_0+\delta dA$ the area of the element of the final surface. The term $\delta\gamma_{sf}$ is equal to zero beacuse $\gamma_{sf}=const$.

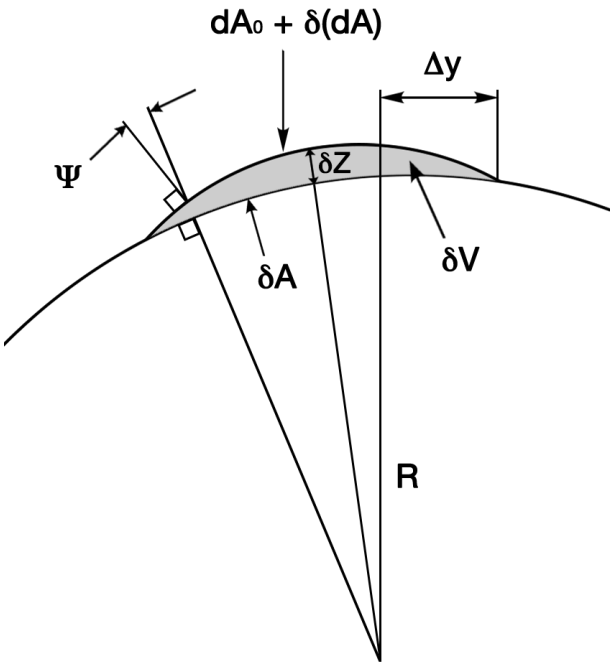

Figure 5.3: Infinitesimal hump formed building up a curved surface

Quantity $\delta(dA)$ is given by:

$$\delta(dA)=\left(\frac{1}{\cos\Psi}-1\right)dA_0+\delta Z\left(\frac{1}{R_1}+\frac{1}{R_2}\right)dA_0 \tag{5.15}$$

in which R_1 and R_2 are the two principal radii of curvature at dA_0. If Δy is small, the radii can be considered constant in the hump and $(1/\cos\Psi-1)\simeq 0$. Eq. 5.14 can be simplified as:

$$\delta\left(\int_{\partial\omega}\gamma_{sf}\,dA\right)=\gamma_{sf}\left(\frac{1}{R_1}+\frac{1}{R_2}\right)\delta V \tag{5.16}$$

with $\delta V=\int_{\partial\omega}\delta Z\,dA_0$ that is the volume of the hump.

From Eq. 5.9, and considering an isothermal process where only a vacancy is brought (no change of number of atoms), the change of the volume term of free energy due to the hump is:

$$\delta U = -p\delta V + \mu_v \frac{\delta V}{\Omega} \tag{5.17}$$

where quantity $\frac{\delta V}{\Omega}$ represent the number of atoms which must be brought into this portion of the crystal to build up the hump.

To ensure that this phenomenon occurs, the internal and external variation must vanish, substituting Eq. 5.17 in Eq. 5.14, i.e.

$$-p\delta V + \mu_v \frac{\delta V}{\Omega} + \gamma_{sf}\left(\frac{1}{R_1} + \frac{1}{R_2}\right)\delta V = 0 \tag{5.18}$$

From this equation, vacancies chemical potential can be write as:

$$\mu_v = p\Omega - \gamma_{sf}\left(\frac{1}{R_1} + \frac{1}{R_2}\right)\Omega = p\Omega - \gamma_{sf}\kappa\Omega \tag{5.19}$$

The aim of this section is to find an expression of the diffusional flux on the surface $\boldsymbol{j}^s$. It's necessary infact, to compute the atoms chemical potential.

The second equation of 5.11 shows the variations in μ_a due to variations of C_v will be negligible compared to the corresponding variation of μ_v. By Eq. 5.10, it's possible to write:

$$\mu_a = \mu_{a0} + p\Omega \tag{5.20}$$

where μ_{a0} is the atoms chemical potential under no stress.

Finally, the atoms flux $\boldsymbol{j}^s$ is given by:

$$\boldsymbol{j}^s = -\frac{D_s\gamma_{sf}}{kT}\nabla\kappa \tag{5.21}$$

Surface diffusion is assumed to occur in a layer of width δ_s. Surface motion can occur by atoms moving along the surface. The diffusive flux $\boldsymbol{j}_s$ is proportional to the gradients of the curvature:

$$\boldsymbol{j}_s = -\frac{\delta D_s}{kT}\frac{1}{\Omega}\nabla_s\mu = \frac{\gamma_s\delta D_s}{kT}\nabla_s\kappa \tag{5.22}$$

5.1.2 Grain Boundary Diffusion

Graind boundary diffusion is a very important path of sintering and the theory related to the matter transport by this mechanism is presented.

Free energy of the system is given by the sum of two contribution, the change of internal energy δU and the change of the surface free energy. The main difference is related to the internal enrgy that can be lowered by the migration of matter from one particle to its neighbor. If the internal energy of one of the particle forming the grain boundary in higher than the internal energy of its neighbor, matter migrate and the particle of lower energy will grow at the expense of the other particle.

Making developments similar to those made in the previous section, it's possible to show that chemical potential at the grain boundary between the particles can be written as a function of the normal stress σ_{nn}:

$$\boldsymbol{j}^{gb} = -\frac{D_{gb}}{kT}\nabla_{gb}\sigma_{nn} \tag{5.23}$$

where D_{gb} is the grain boundary diffusion coefficient. Like in surface diffusion, ∇_{gb} corresponds to a gradient computed along the grain boundary.

5.1.3 Volume Diffusion

Considering a solide where the lattice is deformed because of the presence of a vacancy. The deformation of the lattice due to the presence of lattice is supposed to be isotropic. The presence of new vacancies induce a virtual change of the volume δV. The number of vacancies require to generate that volume change of the internal energy $\delta U/f\Omega$.

If the system should be in equilibrium with respect to this virtual volume change, the change of the internal energy δU must equal to zero:

$$\delta U = -d\delta V + \mu_v \frac{\delta V}{f\Omega} \qquad \longrightarrow \qquad \mu_v = fp\Omega \tag{5.24}$$

Chemical potential μ_a is considered not to depend on the vacancies concentration C_v as $C_v \ll 1$. The atoms chemical potential is given by Eq. 5.20. According to Eq. 3.41 and Eq. 5.1, the atomic flux for volume diffusione is:

$$\boldsymbol{j}_v = -(1-f)\frac{D_v}{kT}\nabla p \tag{5.25}$$

where D_v is the volume diffusion coefficient.

5.1.4 Diffusion Induced Velocity

According to the path chosen, there are different way to compute induced velocity. The surface and grain boundary diffusions, matter is transported along the interfaces. For surface diffusion, the flux follows the free surface and do the flux along the grain boundary and the flux on the grain boundary, the flux appears along the grain boundary between the particles. Those transport paths result in a deposition or removal of material over correspondending interface, which gives raise to a displacement rate assumed to be normal to the interface: $\boldsymbol{v}_n = v\boldsymbol{n}$.

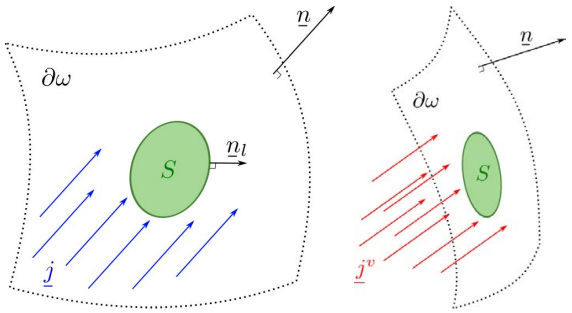

Figure 5.4: Surface or grain boundary diffusion and volume diffusion

Referring to figure 5.4, as the density of the material is constant, then it's possible to say that the matter transported by the induced velocity $\boldsymbol{v}_n$ is equal to $\frac{\boldsymbol{v}_n}{\Omega}$. Since matter is transported along the surface, the balance of matteri is given by:

$$\begin{aligned} \int_{\partial S} \boldsymbol{j} \cdot n_l dL = -\int_S \frac{1}{\Omega}\boldsymbol{v}_n \cdot \boldsymbol{n} dS \quad &\longrightarrow \quad \int_S \left(\nabla_s \cdot \boldsymbol{j} + \frac{1}{\Omega}\boldsymbol{v}_n \cdot \boldsymbol{n}\right) dS = 0 \\ \int_{\partial S} \boldsymbol{j} \cdot n_l dL = -\int_S \frac{\boldsymbol{v}_n}{\Omega} dS \quad &\longrightarrow \quad \int_S \left(\nabla_s \cdot \boldsymbol{j} + \frac{\boldsymbol{v}_n}{\Omega}\boldsymbol{n} \cdot \boldsymbol{n}\right) dS = 0 \end{aligned} \tag{5.26}$$

By the Divergence theorem and by the equation 5.26 holds for any $S \subset \partial\Omega$, it's possible to fine some expressions for the diffusion velocity for surface diffusion v^s and grain boundary diffusion v^{gb}:

$$\begin{aligned} v_s &= -\Omega\nabla_s \cdot \boldsymbol{j}^s \\ v_{gb} &= -\Omega\nabla_{gb} \cdot \boldsymbol{j}^{gb} \end{aligned} \tag{5.27}$$

In contrast with the two previous velocities, matter flux due to volume diffusion is not transported along the interfaces. In fact, this matter comes from the lattice, and therefore the balance of matter has to be established in different way:

$$\int_S \boldsymbol{j}^v \cdot \boldsymbol{n} = \int_S \frac{1}{\Omega} \boldsymbol{v}^c \cdot \boldsymbol{n} dS \qquad \longrightarrow \qquad \boldsymbol{v}^v = \Omega \boldsymbol{j}^v \cdot \boldsymbol{n} \tag{5.28}$$

Surface Diffusion Velocity - Developments

Figure 5.4, where n_l is the normal to $\partial\omega$, shows the surface flux.

Flux in Eq. (5.22) results in a deposition or removal of matter on the surface $\boldsymbol{S}$. Because the mass can not be accumulated, this gives rise to a normal displacement of the surface.The displacement rate is velocity $\boldsymbol{v_s}$, which verifies:

$$-\int_{\partial S} (\Omega_0^a \boldsymbol{j}_s^a \cdot \boldsymbol{n}_l + f\Omega_0^a \boldsymbol{j}_s^v \cdot \boldsymbol{n}_l) dl = \int_S \boldsymbol{v_s} \cdot \boldsymbol{n} dA = -\int_S \Omega_0^a (1-f) \nabla_s \cdot \boldsymbol{j}_s dA \tag{5.29}$$

where it's applied the Divergence theorem. Since $\boldsymbol{v_s}$, it will be:

$$-(1-f)\Omega_0^a (\nabla_s \cdot \boldsymbol{j}_s)\boldsymbol{n} = (1-f)\Omega_0^a \frac{\delta_s D_s}{kT} \nabla^2 (\gamma_{sf}\kappa)\boldsymbol{n} \tag{5.30}$$

Note that the transport of Γ_{sf} with this velocity keeps the volume of Ω unchanged. Indeed, since the surface Γ_{sf} is closed, divergence theorem gives:

$$\frac{d|\Omega_s|}{dt} = \int_{\Gamma_{sf}} \boldsymbol{v_s} \cdot \boldsymbol{n} dA = (1-f)\Omega_0^a \frac{\delta_s D_s \gamma_s f}{kT} \int_{\Gamma_{sf}} \nabla^2 \kappa dA = 0 \tag{5.31}$$

Grain Boundary Diffusion Velocity - Developments

Doing the same popolation balance as for surface diffusion provides, when applied over Γ_{gb}:

$$v_{gb} = -(1-f)\Omega_0^a (\nabla_s \cdot \boldsymbol{j}_{gb})\boldsymbol{n} = (1-f)\Omega_0^a \frac{D_{gb}\delta_{gb}}{kT} (\nabla^2 \sigma_{nn})\boldsymbol{n} \tag{5.32}$$

Volume Diffusion Velocity - Developments

Population balance in Eq. 3.41, combined with the assumption that mass can not be accumulated, says that the volume of species passing "through" $\boldsymbol{S}$ during a time interval δt is equal to the local change of volume induced by the normal displacement of ω. In formula:

$$\delta t \int_S (\Omega_0^a \boldsymbol{j}_v^a \cdot \boldsymbol{n} + f\Omega_0^a \boldsymbol{j}_v^v \cdot \boldsymbol{n}) dA = \delta t \int_S \boldsymbol{v}_{\boldsymbol{V}} \cdot \boldsymbol{n} dA \tag{5.33}$$

where the volume vacancy flux is such that $\boldsymbol{j}_v^v = -\boldsymbol{j}_v^a$. The above equation holds for any surface $S \subset \Gamma_{sf}$, the rate of displacement of Γ_{sf} associated with the flux is given by:

$$\boldsymbol{v}_{\boldsymbol{V}} = (1-f)\Omega_0^a (\boldsymbol{j}_v \cdot \boldsymbol{n})\boldsymbol{n} = -\frac{(1-f)\Omega_0^a D_v}{kT} (\nabla p \cdot \boldsymbol{n})\boldsymbol{n} \tag{5.34}$$

It's important to say that from Eq. 5.1, atom population balance of Eq. 3.41 should imply $\nabla \cdot \boldsymbol{j}_v = 0$ which means that the volume of grains is preserved by lattice diffusion. Observing Eq. 5.25 that it's also true, we note that $\nabla^2 p = 0$ which has no reason to be satisfied (it depends on the mechanical state of this system). For this reason, bulk atomic balance of Eq. (3.41) is replaced by the population balance Eq. (5.33). The grain volume has no reason to remain unchanged during the diffusion process, but global volume has to be constant. For this reason, an additional 'correction' velocity is considered in order to preserve global volume in solid phase:

$$\boldsymbol{v}^{\boldsymbol{C}} = v_n^c \boldsymbol{n} \tag{5.35}$$

where v_n^c is a constant. By serveral consideration shown in [10], the correction velocity that ensures the volume conservation can be written as:

$$\boldsymbol{v}^{\boldsymbol{C}} = -\frac{|\Omega| - |\Omega|_0}{S\delta t} \boldsymbol{n} \tag{5.36}$$

Relation between grain boundary diffusion and surface diffusion

The total surface motion in sintering is the sum of the surface motion, and the rigid body motion:

$$\boldsymbol{v} = v_n \boldsymbol{n} \pm \frac{1}{2} v_{gb} \boldsymbol{e} \tag{5.37}$$

where $\boldsymbol{e}$ is the grain boundary normal vector. The diffusive flux along the grain boundary J_{gb} and that along the surface J_s must be continuous at the triple junction:

$$J_{gb} = 2J_s \tag{5.38}$$

5.2 Sintering of Two Elastic Spheres

The aim of this section is to validate numerical models arising from continuum formulation. In order to find an analytical model for the phenomenon of sintering, it is necessary to make certain assumptions, above all to simplify the geometry of the problem. Usually, analytical models of sintering are referred a two spheres with the same radius. And those models are developed to study the diffusion phenomena by just one diffusion path for time. Firstly, the geometry of the bodies considered is assumed to remain unchanged and the real shape of the contact area is replaced by a geometry were the curvature of the neck is constant. All those geometrical approaches are complemented with some hypoteses related to the diffusion path that is being modeled. This simplifications are generally accepted **??**, **??**, **??**.

In present work it's analyzed the sintering of two spheres, as shown in figure 5.5:

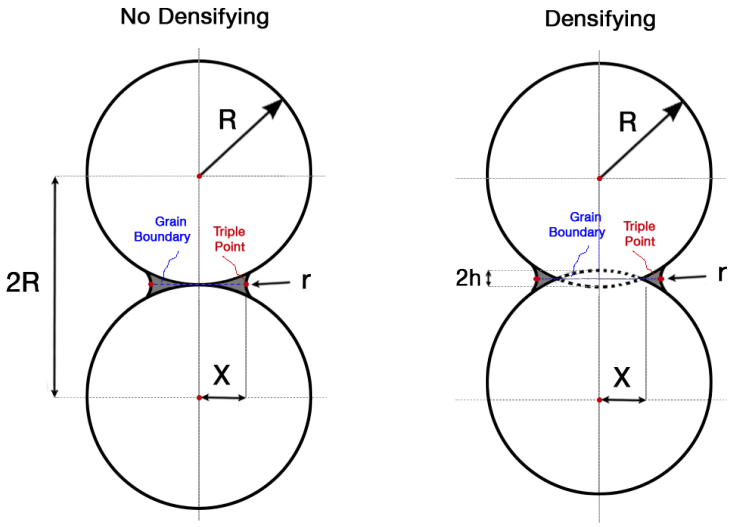

Figure 5.5: Geometrical model of two particles.

5.2.1 Grain Boundary diffusion

Now, the grain boundary is analyzed. It's important to note that grain boundary diffusion is a densifying path, and is assumed to occur over a constant thickness δ_{gb}. A general, form of the diffusion flux equations is:

$$\boldsymbol{j}_{gb} = -D\nabla \boldsymbol{C} \tag{5.39}$$

Making some hypothesis that the matter flux is parallel to the normal at the triple junction. The volume of matter transported by unit of time into the neck, is given by:

$$\frac{dV_{neck}}{dt} = D\|\nabla \boldsymbol{C}\|A_{gb}\Omega \tag{5.40}$$

where Ω is the molar volume and A_{gb} is the area of the grain boundary surface at the triple point and can be calculated as $A_{gb} = 2\pi X\delta_{gb}$. Assuming that the system is axisymmetric with respect to the axis formed by the centers of the two particles. Eq. 5.40 becomes one-dimensional and becomes:

$$\frac{dV_{neck}}{dt} = 2\pi X\delta_{gb}\Omega D_{gb}\frac{dC}{dr} \tag{5.41}$$

It's important to say that at this point, an important hypothesis should be made. This simplification concern the concentration gradient dC/dr. The derative of the concentration (C) with respect to the radius (r) is considered to be constant [32], [49], therefore:

$$\frac{dC}{dr} = \frac{\Delta C}{\Delta r} = \frac{C - C_0}{X} = -\frac{\gamma_{sf}}{kTX}\left(\frac{1}{r_1} + \frac{1}{r_2}\right) \tag{5.42}$$

where C_0 is a reference concentration value, usually correspondending to the concentration under flat surface. γ_{sf} is the surface tension, k is the Boltzmann's constant, T is the temperature, r_1 and r_2 are the two principal radii of curvature which are, respectively, $r_1 = -r$ and $r_2 = X$ (5.5), and it's assumed that $X \ll r$.

It's important to highlight that parameters expression are different if the diffusion path load whether or not densification. Next table shows the expression for V_{neck}, A_{neck}, r, h in the two chases:

The expressions in table 5.1, are accurate up to $X \sim R/3$. Since, it can be shown that for higher values of X, those expressions lead to serious deviation from the real value.

For simplicity, it will be done an example of rate of variation of the neck volume. The aim is to find a relation between volume variation and evolution of parameter X.

Parameter	No Densifying	Densifying
h	0	$X^2/4R$
r	$X^2/2R$	$X^2/4R$
V_{neck}	$\pi X^3/R$	$\pi X^3/2R$
A_{neck}	$\pi X^4/2R$	$\pi X^4/8R$

Table 5.1: Expression of V_{neck}, A_{neck}, r, h referring to figure 5.5

$$\frac{dV_{neck}}{dt} = \frac{d}{dt}\left(\frac{\pi X^4}{8R}\right) = 2\pi X \delta_{gb}\Omega D_{gb}\frac{dC}{dr} = \tag{5.43}$$

$$= \frac{dX}{dt}\left(\frac{\pi 4X^3}{8R}\right) = -2\pi X \delta_{gb}\Omega D_{gb}\frac{\gamma_{sf}}{kTX}\left(\frac{1}{r_1}+\frac{1}{r_2}\right)$$

and, since $r_1 = -r$, $r_2 = X$ and $X \ll r \longrightarrow 1/X \approx 0$, Eq. 5.43 become:

$$\frac{dX}{dt}\left(\frac{\pi X^3}{2R}\right) = 2\pi\delta_{gb}\Omega D_{gb}\frac{\gamma_{sf}}{kT}\left(\frac{1}{r}\right) = 2\pi\delta_{gb}\Omega D_{gb}\frac{\gamma_{sf}}{kT}\left(\frac{4R}{X^2}\right) = \tag{5.44}$$

$$= 8\pi R\delta_{gb}\Omega D_{gb}\frac{\gamma_{sf}}{kTX^2} \quad \longrightarrow \quad X^5 dX = 16R^2\delta_{gb}\Omega D_{gb}\frac{\gamma_{sf}}{kT}dt$$

Integrating the above equation:

$$X^6 = \left(\frac{96R^2\delta_{gb}\Omega D_{gb}\gamma_{sf}}{kT}\right)t \tag{5.45}$$

Since the aim is to relate X to a fixed parameter, like R, Eq. 5.45 can be rewritten as:

$$\left(\frac{X}{R}\right)^6 = \left(\frac{96R^2\delta_{gb}\Omega D_{gb}\gamma_{sf}}{kT}\right)R^{-4}t \tag{5.46}$$

Generally, using the same procedure, it's possible to find expressions for the neck growth as a function of time for all the others diffusion path. In this work, only the 3 cases analyzed in previous sections was been calculated. The other values are from [34]. However, those models are almost always a power-lay type:

$$\left(\frac{X}{R}\right)^n = BR^{-m}t \tag{5.47}$$

where R is the radius of the particles, t is the time, n,m and B are constants. In table 5.2 are summarized some of plausible values of the mentioned constants.

DIFFUSION PATH	**RANGE (VALUES)**		
	n	**m**	**B**
Surface diffusion	3-7 (7)	2-4 (4)	$\frac{23\delta_s\Omega D_s\gamma_{sf}}{kT}$
Volume diffusion from surface	4-5 (4)	(4)	$\frac{20\Omega D_s\gamma_{sf}}{kT}$
Vapor transport	3-7 (3)	2-4 (2)	$3\sqrt{\frac{2}{\pi}}\frac{v\gamma_{sf}p_g\Omega^{3/2}\rho^{1/2}}{(kT)^{3/2}}$
Grain boundary diffusion	3-7 (7)	2-4 (4)	$\frac{96\delta_{gb}\Omega D_{gb}\gamma_{sf}}{kT}$
Volume diffusion from grain boundary	4-5 (5)	(3)	$\frac{16\Omega D_v\gamma_{sf}}{kT}$
Volume diffusion from dislocation	(2)	(1)	$\frac{3\gamma_{sf}}{2\eta}$

Table 5.2: Paths and a set of plausible values of n, m and B. (p_g is the gas pressure, ρ is the specific density and η is the viscosity.)

Previous equations are based on some strong simplifications. Their validity is limited to reck radii: $X < 0.33R$ and limited to the study of the sintering of two particles. Then, these assumptions are well suited to study first stage of polymer sintering on Fused Deposition Modeling. Because of this, in future comparisons, the values of X obtained by other methods, will be calculated by considering a time less than that required for the complete fusion of the particles, in particular, in all computations, it will be placed a condition on the increase of X, so that is always less than $X/3$.

5.2.2 Analytical Models Resuls

In table 5.6 are shown results of grain boundary diffusion obtained with a rigosous continuum elastic approach:

Time	Radius	Diffusivity	δ_{gb}	Atomic Volume Ω	X/R	θ
$[s]$	$[m]$	$[m^2/s]$	$[m]$	$[M^3/mol]$	$[-]$	$[Deg]$
0.01	2.00E-05	1.00E-08	5.56E-07	5.53E-07	0.09	5.41
0.05	2.00E-05	1.00E-08	5.56E-07	5.53E-07	0.12	7.09
0.1	2.00E-05	1.00E-08	5.56E-07	5.53E-07	0.14	7.96
0.2	2.00E-05	1.00E-08	5.56E-07	5.53E-07	0.16	8.94
0.3	2.00E-05	1.00E-08	5.56E-07	5.53E-07	0.17	9.57
0.4	2.00E-05	1.00E-08	5.56E-07	5.53E-07	0.17	10.05
0.5	2.00E-05	1.00E-08	5.56E-07	5.53E-07	0.18	10.43
0.6	2.00E-05	1.00E-08	5.56E-07	5.53E-07	0.19	10.76
0.7	2.00E-05	1.00E-08	5.56E-07	5.53E-07	0.19	11.04
0.8	2.00E-05	1.00E-08	5.56E-07	5.53E-07	0.20	11.29
0.9	2.00E-05	1.00E-08	5.56E-07	5.53E-07	0.20	11.52
1	2.00E-05	1.00E-08	5.56E-07	5.53E-07	0.20	11.73
1.1	2.00E-05	1.00E-08	5.56E-07	5.53E-07	0.21	11.92
1.2	2.00E-05	1.00E-08	5.56E-07	5.53E-07	0.21	12.09
1.3	2.00E-05	1.00E-08	5.56E-07	5.53E-07	0.21	12.26
1.4	2.00E-05	1.00E-08	5.56E-07	5.53E-07	0.21	12.41
1.5	2.00E-05	1.00E-08	5.56E-07	5.53E-07	0.22	12.56
1.6	2.00E-05	1.00E-08	5.56E-07	5.53E-07	0.22	12.70
1.7	2.00E-05	1.00E-08	5.56E-07	5.53E-07	0.22	12.83
1.7504	2.00E-05	1.00E-08	5.56E-07	5.53E-07	**0.22**	**12.84**

Table 5.3: Dimensionless radius and sintering angle θ $[Deg]$: Continuum elastic approach

In figure 5.6 is shown the grain boundary diffusion sintering angle versus time:

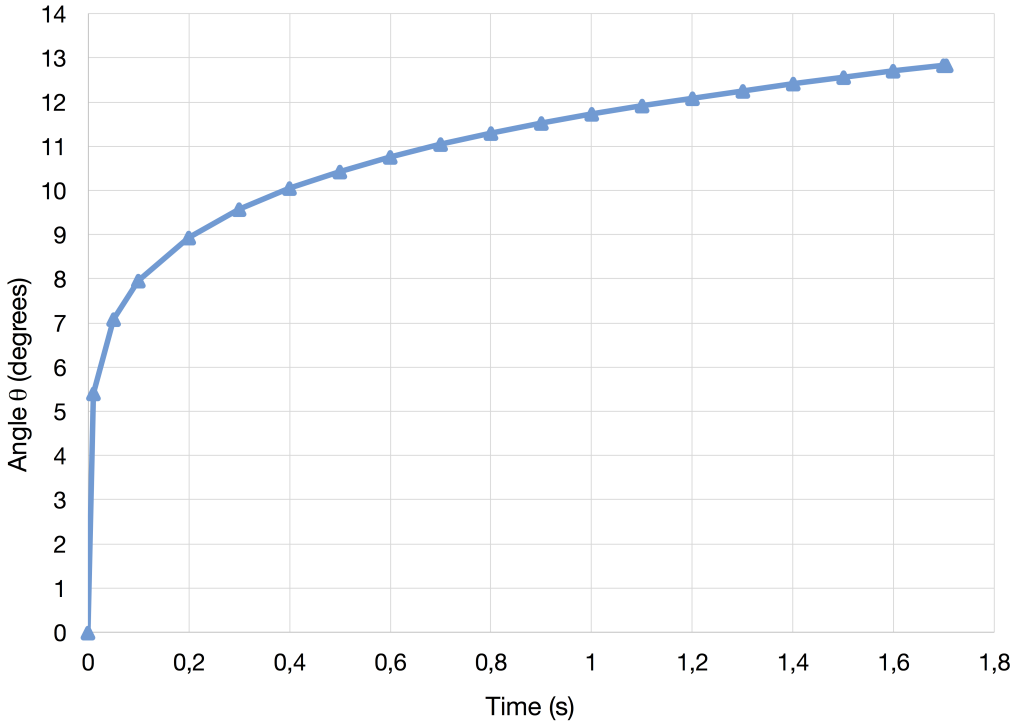

Figure 5.6: Continuum approach: grain boundary diffusion

Chapter 6

Sintering Viscous Model - Frenkel Approach

Until the 1930's, sintering was defined as a technological process of obtaining sintered materials from powder systems, now, in the present work, it can be described as *formation of a homogeneous melt from the coalescence of solid particles under the action of surface tension.* [48].

The figure 6.1 show the 3 steps, explained below, of Frenkel Sintering:

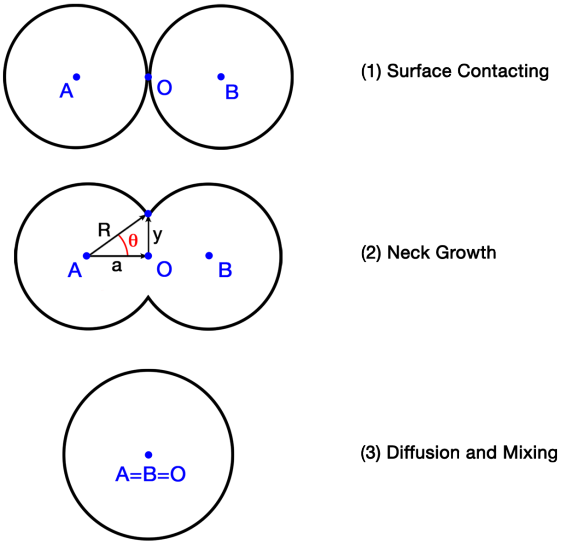

Figure 6.1: Sintering steps

The sintering phenomenon describes the bond formation process between two filaments,

it consists in 3 phases [48], [53]:

1. surface contacting;
2. neck growth;
3. diffusion and randomization.

Particularly, the sintering quality, depends on the second step.

6.1 Sintering Model for Viscous Flows

Let us consider a Newtonian fluid. The stress tensor can be decomposed into spherical and deviatoric parts:

$$\boldsymbol{\sigma} = \boldsymbol{\tau} - p\boldsymbol{I} \quad \text{or} \quad \sigma_{ij} = \tau_{ij} - p\delta_{ij} \tag{6.1}$$

where $p = -\frac{1}{3}\sigma_{ii}$ is the (mechanical) pressure and $\boldsymbol{\tau}$ is the sress deviator (shear stress tensor).

Consitutive relation for Newtonian fluid is:

$$\boldsymbol{\sigma} = \eta\left(\nabla\boldsymbol{v} + (\nabla\boldsymbol{v})^T\right) - p\boldsymbol{I} = 2\eta\dot{\boldsymbol{\varepsilon}} - p\boldsymbol{I} \tag{6.2}$$

where:

$$\dot{\boldsymbol{\varepsilon}} = \frac{1}{2}\left(\nabla\boldsymbol{v} + (\nabla\boldsymbol{v})^T\right) \tag{6.3}$$

is the volumetric strain rates. The above relations are valid for incompressive fluid ($\nabla\cdot\boldsymbol{v} = 0$).

Let us now consider the mechanism of viscous flow. We will recall for this mechanism, the energy balance concept, which can be stated as:

Rate of energy dissipation by viscous flow = rate of energy gained by reduction in surface area

In formula:

$$dW_\sigma = dW_\tau - dW_p = 0 \tag{6.4}$$

Referring to dW_τ as work of viscous forces, to dW_p as mechanical work and thanks to eq 6.12, we can write:

$$\dot{W}_v = \dot{W}_s \quad \longrightarrow \quad \Gamma \frac{dS}{dt} = \tau : \boldsymbol{D} dV \tag{6.5}$$

The above mentioned formula aims to ensure that the global equilibrium at the interface is observed, i.e. surface forces equal to viscous forces.

6.1.1 Work of Viscous Forces

The work of viscous forces can be expressed in both of the following relations:

$$\dot{W}_v = -\int_A \boldsymbol{\tau} \cdot \boldsymbol{v} dA = \int_V \boldsymbol{\tau} : \boldsymbol{D} dV = \int_V \eta \nabla v : \left(\nabla v + \nabla v^T\right) dV \tag{6.6}$$

where V is the volume of the sintering sistem and $\boldsymbol{D}$ is the strain tensor:

$$\boldsymbol{D} = \frac{1}{2}\left(\nabla \boldsymbol{v} + (\nabla \boldsymbol{v})^T\right) \tag{6.7}$$

The flow field is assumed to be only extensional, thus:

$$\nabla u = \begin{pmatrix} \dot{\varepsilon} & 0 & 0 \\ 0 & -2\dot{\varepsilon} & 0 \\ 0 & 0 & \dot{\varepsilon} \end{pmatrix} \tag{6.8}$$

Frenkel hypothesizes that the strain rate $\dot{\varepsilon}$ is assumed to be constant throughout the complete domain and was approximated by:

$$-2\dot{\varepsilon} = \frac{\partial u_y(A)}{\partial y} \approx \frac{u_y(A) - u_y(0)}{a} \quad \longrightarrow \quad \boldsymbol{\tau} = -2\eta\dot{\varepsilon} \tag{6.9}$$

Once made assumptions, the viscous work can be expressed as:

$$\dot{W}_v = -\int_V 2\eta\dot{\varepsilon}^2 dV = -2\eta\dot{\varepsilon}^2 V \tag{6.10}$$

6.1.2 Work of Surface Tension

Increasing the area of an interface with energy density, by a tiny amount dS requires an amount of work equal to the surface energy contained in the extra piece of interface:

$$dW = \alpha dS \tag{6.11}$$

Except for the sign, this is quite analocous to the mechanical work $dW = -pdV$ performed agains bulk pressure when the volume of the system is expanded by dV, i.e.:

$$dW = \alpha dA + \Delta p dV = 0 \longrightarrow \alpha dA = -\Delta p dV \tag{6.12}$$

The resistance against extension of a free surface shows that the surface has an internal surface tension which we shall now see equals the surface energy density α, then we can rewrite eq 6.11 as:

$$dW = \Gamma dS \tag{6.13}$$

where Γ is the surface tension.

The rate of change of energy due to the reduction in surface area (or surface tension work), can be written as:

$$d\dot{W} = -\Gamma \frac{dS}{dt} \tag{6.14}$$

6.1.3 Frenkel Model for Sintering - Coalescence Between Two Spheres

Hypothesizing analyze sintering process between two spheres with the same radius, referring to figure 6.2:

neck growth y is:

$$y = a \sin\theta \tag{6.15}$$

where a is the radius of the spherical part of the drop, which is determined by the starting value a_0 from the constant volume condition:

$$\frac{\pi}{3} a^3 (2 + \cos\theta - \cos^3\theta) = \frac{4\pi}{3} a_0^3 \tag{6.16}$$

and thus

$$S - S_0 = 8\pi a^2 (1 + \cos\theta) \tag{6.17}$$

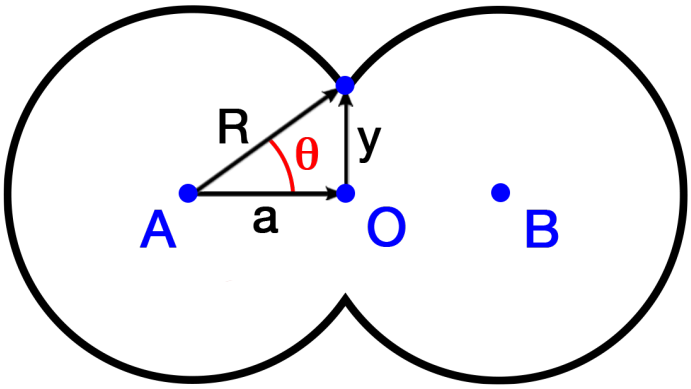

Figure 6.2: Coalescence of two spheres - Frenkel model

For small values of θ, i.e. for small neck radius, $\cos\theta \approx 1 - \frac{\theta^2}{2}$, so that, eq 6.17 becomes:

$$S - S_0 = 2\pi a_0 \theta^2 \tag{6.18}$$

The rate of chanfe of energy due to the reduction in surface area becomes:

$$\dot{W}_s = -\Gamma \frac{dS}{dt} = 4\Gamma\pi a^3 \frac{d}{dt}\left(\frac{\theta^2}{2}\right) \tag{6.19}$$

Mentioning eq 6.9, and replacing general volume V with the sphere volume, eq 6.10 becomes:

$$\dot{W}_v = \frac{16}{3}\pi a^3 \eta \dot{v}^2 \tag{6.20}$$

where $\dot{v}$ is the velocity of motion for viscous flow given by:

$$\dot{v} = \frac{1}{a}\frac{d}{dt}\left(\frac{a\theta^2}{2}\right) = \frac{d}{dt}\left(\frac{\theta^2}{2}\right) \tag{6.21}$$

and then

$$\dot{W}_v = \dot{W}_s \longrightarrow \frac{16}{3}\pi a^3 \eta \dot{v}^2 = 4\Gamma\pi a^3 \frac{d}{dt}\left(\frac{\theta^2}{2}\right) \tag{6.22}$$

and semplifying

$$\dot{v} = \frac{3}{4}\frac{\Gamma}{\eta a} \tag{6.23}$$

and integrating subject to the boundary condition , we obtain:

$$\theta^2 = \frac{3}{2}\left(\frac{\Gamma t}{\eta a}\right) \tag{6.24}$$

and, remembering that $y = a\sin\theta$, we obtain:

$$\frac{y}{a} = \left(\frac{3\Gamma t}{2\eta a}\right)^{\frac{1}{2}} \tag{6.25}$$

6.1.4 Modification of Frenkel Model for Sintering

Frenkel's model (1945), which is based on Newtonian viscous flow under the action of surface tension, was corrected by Elsheby (1949) to satisfy the continuity equation and will subsequently be referred to as the Frenkel-Eshelby model.

We want to develop a sintering model which describes the complete sintering process of two spherical particles [53]. The approach is similar to that of Frenkel and Eshelby but goes beyond the description of initial stages. In order to reduce the number of parameters, the flow is approximated to be viscous extensional and the evolution of the particle shape is restricted. However, unlike Frenkel, the variation of the particle radius with time in the coalescence[1] process is considered.

The model is based on the balance of work of surface tension and the viscous dissipation. All other forces, including gravity, are negleted. We assume that the shape of two spheres evolves as shown in 6.2. At time $t = 0$, two equale sized spheres of radius a_0, centered at points A and B, have only one contact point O. At time $t = t$, both centers have moved towards point O and a shape of two intersecting spheres of radius $a(t)$ has been created.

The angle of the intersection and the radius of the neck are denoted by $\theta(t)$ and $x(t)$, respectively. In the final stage, only one sphere of radius a_f remains and all three points A, B, and O coincide. The following relation for $a(t)$ vs. $\theta(t)$ is obtained form the conservation of mass with the assumption of a constant density:

$$a(t) = a_0\left(\frac{4}{[1+\cos[\theta(t)]]^2\,[2-cos[\theta(t)]]}\right)^{\frac{1}{3}} \tag{6.26}$$

For simplicity, the functions $\theta(t)$, $a(t)$ and $x(t)$ will be subsequently denoted θ, a and x.

[1] Coalescence is the process by which two or more droplets, bubbles or particles merge during contact to form a single daughter droplet, bubble or particle.

Unlike Frenkel, that assumed the particle radius to be constant [that is, $a(t) = a_0$] and made an approximation for small angles [that is, $\cos(\theta) = 1 - \frac{\theta^2}{2}$], the totale surface of particles varies with the angle θ, i.e.

$$S = 4\pi a^2[1 + \cos(\theta)] = \frac{8\pi a_0^2 2^{\frac{1}{3}}}{[1 + \cos(\theta)]^{\frac{1}{3}}[2 - \cos(\theta)]^{\frac{2}{3}}} \tag{6.27}$$

Remembering eq. 6.9, the term $u_y(O)$ is the velocity of the fluid at the plane of contact of the two particles and is equal to zero. The term $u_y(A)$ is defined as follows:

$$u_y(A) = \frac{d}{dt}[a\cos(\theta)] = -\frac{2^{\frac{5}{3}} a_0 \sin(\theta)}{[1 + \cos(\theta)]^{\frac{5}{3}}[2 - \cos(\theta)]^{\frac{4}{3}}}\frac{d\theta}{dt} \tag{6.28}$$

for semplicity, $\frac{d\theta}{dt}$ will be denote θ'.

Consequently:

$$\dot{\varepsilon} = \frac{u_y(A)}{a} = -\frac{2\sin(\theta)}{[1 + \cos(\theta)][2 - \cos(\theta)]}\theta' \tag{6.29}$$

For a Newtonian fluid, the viscous model is:

$$W_v = 32\pi a^3 \eta \dot{\varepsilon}^2 \tag{6.30}$$

which leads to the formula for dissipated energy

$$W_v = 32\pi a_0^3 \eta \frac{1 - \cos(\theta)}{[1 + \cos(\theta)][2 - \cos(\theta)]^2}(\theta')^2 \tag{6.31}$$

The work of surface tensione W_s is defined as

$$W_s = -\Gamma\frac{dS}{dt} \tag{6.32}$$

where Γ is the coefficient of surface tensione and S is the surface of the sintering system. Applying the chain rule on (6.27), the term $\frac{dS}{dt}$ can be derived and the expression for the work of surface tension becomes

$$W_s = \Gamma\frac{8\pi a_0^2 2^{\frac{1}{3}} \cos(\theta)\sin(\theta)}{[1 + \cos(\theta)]^{\frac{4}{3}}[2 - \cos(\theta)]^{\frac{5}{3}}}\theta' \tag{6.33}$$

Under the assumption that θ' is always positive, by equating the work of surface tension to the viscous dissipation, we obtain

$$\theta' = \frac{\Gamma}{a_0\theta}\frac{2^{-\frac{5}{3}}\cos(\theta)\sin(\theta)[2-\cos(\theta)]^{\frac{1}{3}}}{[1-\cos(\theta)][1+\cos(\theta)]^{\frac{1}{3}}} \tag{6.34}$$

with the initial condition

$$\theta(0) = \theta_0 = 0 \tag{6.35}$$

Equation (6.34) is singular near zero and a special numerical treatment is necessary to solve it. For $\theta \to 0$, the following approximation are made: $\sin(\theta) = \theta$ and $1 - \cos(\theta) = \frac{\theta^2}{2}$, respectively. Hence, the asymptotic behavior of (6.34) is

$$\theta' = \frac{1}{2}\frac{\Gamma}{\eta a_0\theta} \tag{6.36}$$

Considering that $\theta > 0$ and applying the initial condition (6.35), the solution of (6.36) is

$$\theta(t) = \left(\frac{t\Gamma}{\eta a_0}\right)^{\frac{1}{2}} \tag{6.37}$$

which corrispond to the Frenkel-Eshelby model. Once a solution for the evolution of the sintering angle with time is obtained, the evolution of the neck radius with time can easily be derived, replacing $\theta(t)$ in

$$\frac{y}{a} = \sin(\theta) \tag{6.38}$$

6.2 Isothermal - Non Isothermal Comparison

Equations 6.34 and consequently 6.36 and 6.38 refer to an isothermal condition, i.e. the surface tension and viscosity are fixed and their value is referred to a exact temperature. In the next sections it will be shown how in reality, the surface tension and viscosity, strongly depend on temperature and will be proposed a model of sintering angle variation in non-isothermal conditions. It will be also made a comparison between the two models.

6.2.1 Temperature Influence on Surface Tension

The value of the surface tension depends on the temperature. The first empirical equation for the surface tension dependence on temperature was given by Eotvos in 1886. Observing that the surface tension goes to zero when the temperature tends to the critical temperature T_C. Eotvos proposed a semi-empirical relation:

$$\Gamma = \left(\frac{1}{v_L}\right)(T - T_C) \tag{6.39}$$

where v_L is the molar volume. Later, Katayama (1915) and Guggenheim (1945) proposed have improved Eotvos relation, obtain:

$$\Gamma(T) = \Gamma^* \left(1 - \frac{T}{T_C}\right)^n \tag{6.40}$$

where Γ^* is a constant for each liquid, n is an empirical factor that depends on liquid (11/9 for organic liquid), T_C is the imaginary critical temperature of polymer.

Surface tension vanishes at the critical point:

$$-\frac{d\Gamma}{dT} = \frac{11}{9}\frac{\Gamma^*}{T_{cr}}\left(1 - \frac{T}{T_{cr}}\right)^{\frac{2}{9}} \tag{6.41}$$

for low values of T/T_{cr}, $d\Gamma/dT$ will be constant.

Katayama (1915) and Guggenheim (1945) model will be used in present work.

6.2.2 Temperature Influence on Viscosity

For the temperature dependence of viscosity, many important authors proposed reasonable models, as Reynolds and Arrhenius. Nevertheless, in this work, it will be used the Williams-Landel-Ferry model, that better approximates polymer melts behavior or other fluids that have

a glass transition temperature. Equation 6.42 show the the temperature dependence given by WLF:

$$\mu(T) = \mu_0 e^{\left(\frac{-C_1(T-T_r)}{C_2+T-T_r}\right)} \tag{6.42}$$

where T is the temperature, C_1, C_2, T_r and μ_0 are patameters(only three of them are independent from each other).

6.2.3 Non-Isothermal Model

To take stock of the situation, 4 equations were obtained:

$$T = T_\infty + (T_0 - T_\infty)e^{-mvt} \tag{6.43a}$$

$$\Gamma(T) = \Gamma^* \left(1 - \frac{T}{T_C}\right)^n \tag{6.43b}$$

$$\mu(T) = \mu_0 \cdot Exp\left(\frac{-C_1(T-T_r)}{C_2+T-T_r}\right) \tag{6.43c}$$

$$\theta' = \frac{1}{2}\frac{\Gamma}{\eta a_0 \theta} \tag{6.43d}$$

The aim is to find a way to take into account the temperature dependence of viscosity and surface tension and conseguently, to find the temperature dependence of sintering angle:

$$\Gamma,\ \mu \longrightarrow\ \Gamma(T),\ \mu(T)\ \longrightarrow\ \theta \rightarrow\ \theta(T)$$

As shown in previous chapter, since the velocity is constant, the temperature can be expressed as function of time. Substituting eq. 6.43a in eqs. 6.43b and 6.43c we can obtain the viscosity and surface tension as function of time. Subsequently, we can also obtain, the variation of sintering angle as function of time:

$$\frac{d\theta}{dt} = \frac{1}{2}\frac{\Gamma(t)}{\eta(t)a_0\theta} \tag{6.44}$$

Through some algebric tricks, a closed-form solution is possible to obtain:

$$\theta'\theta = \frac{1}{2}\frac{\Gamma(t)}{\eta(t)a_0}dt \longrightarrow\ \int_{t_0}^{t} \theta\frac{d\theta}{dt}dt = \int_{t_0}^{t} \frac{1}{2}\frac{\Gamma(t)}{\eta(t)a_0}dt \tag{6.45}$$

It can be demonstrated that:

$$\int_{t_0}^{t} \theta d\theta = \int_{\theta_0}^{\theta} \theta d\theta = \frac{\theta^2}{2} \tag{6.46}$$

Thus:

$$\theta(t) = \sqrt{2 \cdot \int_{t_0}^{t} \frac{1}{2} \frac{\Gamma(t)}{\eta(t) a_0} dt} \tag{6.47}$$

This can be confirmed by the fact that, hypothesizing Γ and η as constants, equation 6.47 returns equation 6.37.

Referring to [43], parameters were set up. Table 6.1 swow their values.

Table 6.1: Necessary parameters for sintering model

C_1	C_2	T_r	μ_0	γ_0	T_{cr}	n
$[-]$	$[K]$	$[K]$	$[Pa \cdot s]$	$[N/m]$	$[K]$	$[-]$
8.86	101.6	410.15	5500	0.055	573.15	1.2

The experiments conducted by Bellehumeur et al. in [43] show that the sintering process, for the considered material, is negligible below $473.15\ K$. Despite the isothermal curve already takes into account that after a certain temperature the angle θ no longer growing, it's possible to calculate a critical time τ which corresponds to the temperature of $473.15\ K$:

$$\frac{473.15 - T_\infty}{T_0 - T_\infty} = e^{-mv\tau} \longrightarrow \tau = -\frac{1}{mv} \ln\left[\frac{473.15 - T_\infty}{T_0 - T_\infty}\right] \tag{6.48}$$

Using a Heaviside function, it's possible to set that at time τ, $\theta(t)$ continue as a constant.

$$\theta(t) = \theta(t)H(\tau - t) + \theta(\tau)H(t - \tau) \tag{6.49}$$

Solving numerically equations 6.47 and 6.49 in mathematica, evolution of $\theta(t)$ is shown in the following figure:

It was also made a comparison between isothermal and non-isothermal curves, as shown in the following pictures:

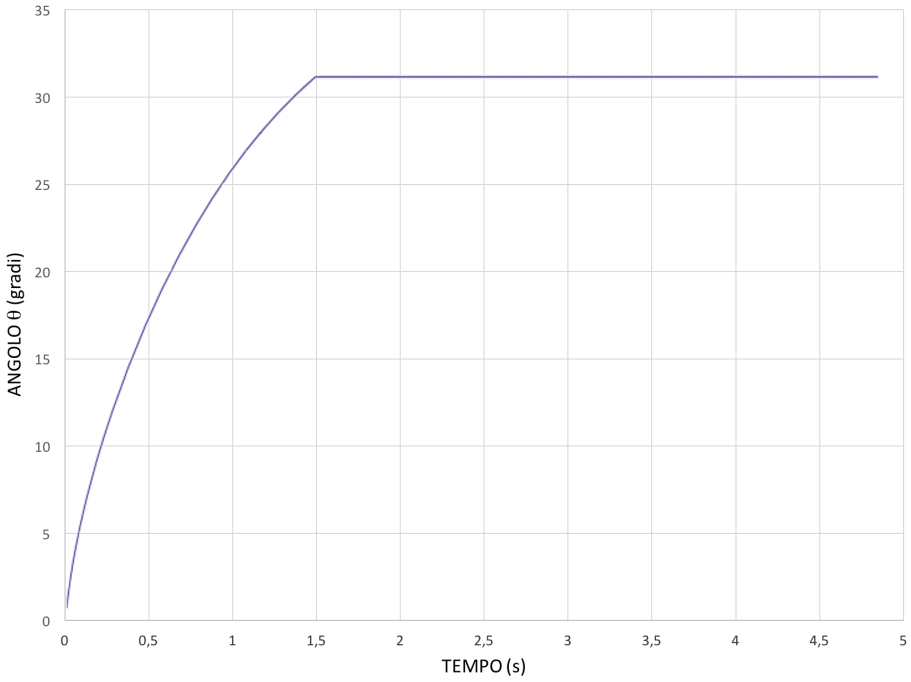

Figure 6.3: Non-isothermal evolution of θ

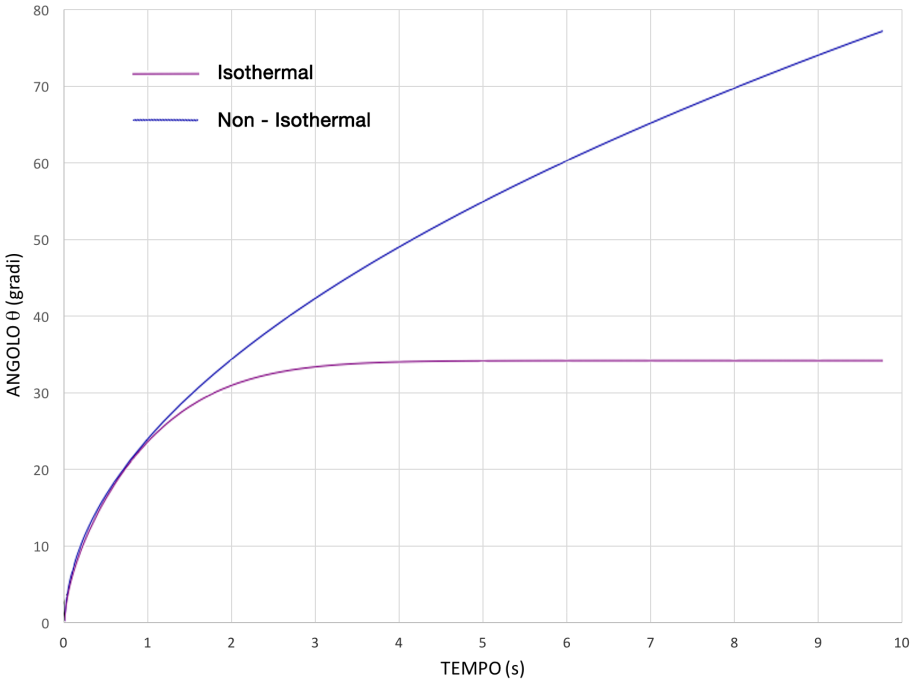

Figure 6.4: Isothermal - Non-isothermal comparison

Figures 6.4 and 6.5 show that the differences between isothermal and non-isothermal model are negligible up to the achievement of 473.15 K. Subsequently, the differences begin to be

marked, but anyway, the process of sintering does not occur, then the equations describing the phenomenon, lose physical meaning.

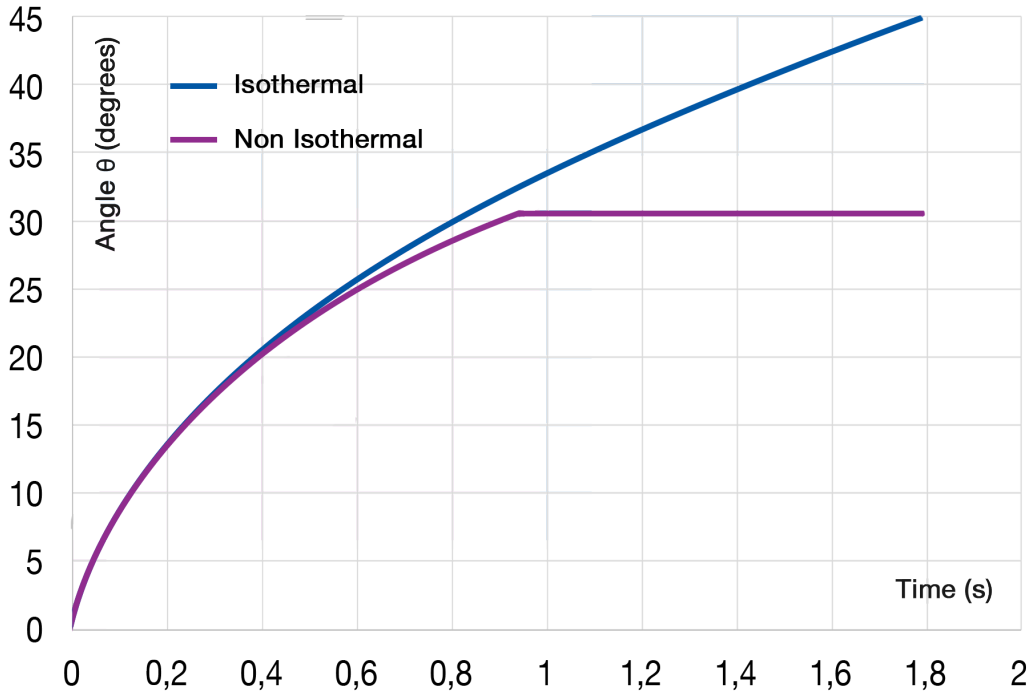

Figure 6.5: Isothermal - Non-isothermal comparison

Despite in our case, the non-isothermal and isothermal comparison are equal, changing parameters, curves take differents form. Given the numerous uncertainties related to non-isothermal parameters, in this work, it will always refer to isotherms situations.

6.3 Frenkel Sintering Resuls

Modeling ABS polymer as a pure viscous material leads to results shown in table 6.3. Frenkel Approach is the most diffused method to study polymer sintering process.

Time	Radius	γ	η	X/a	θ
$[s]$	$[m]$	$[N/mm]$	$[MPa \cdot s]$	$[-]$	$[Deg]$
0.01	0.2	0.02709	0.0005	0.05	3.09
0.05	0.2	0.02709	0.0005	0.12	6.90
0.1	0.2	0.02709	0.0005	0.17	9.76
0.2	0.2	0.02709	0.0005	0.24	13.80
0.3	0.2	0.02709	0.0005	0.29	16.90
0.4	0.2	0.02709	0.0005	0.33	19.51
0.5	0.2	0.02709	0.0005	0.37	21.82
0.6	0.2	0.02709	0.0005	0.41	23.90
0.7	0.2	0.02709	0.0005	0.44	25.81
0.8	0.2	0.02709	0.0005	0.46	27.60
0.9	0.2	0.02709	0.0005	0.49	29.27
1	0.2	0.02709	0.0005	0.51	30.85
1.1	0.2	0.02709	0.0005	0.54	32.36
1.2	0.2	0.02709	0.0005	0.56	33.80
1.3	0.2	0.02709	0.0005	0.58	35.18
1.4	0.2	0.02709	0.0005	0.59	36.51
1.5	0.2	0.02709	0.0005	0.61	37.79
1.6	0.2	0.02709	0.0005	0.63	39.03
1.7	0.2	0.02709	0.0005	0.65	40.23
1.7504	0.2	0.02709	0.0005	0.65	**40.82**

Table 6.2: Frenkel Model results: dimensionless radius and sintering angle θ $[Deg]$

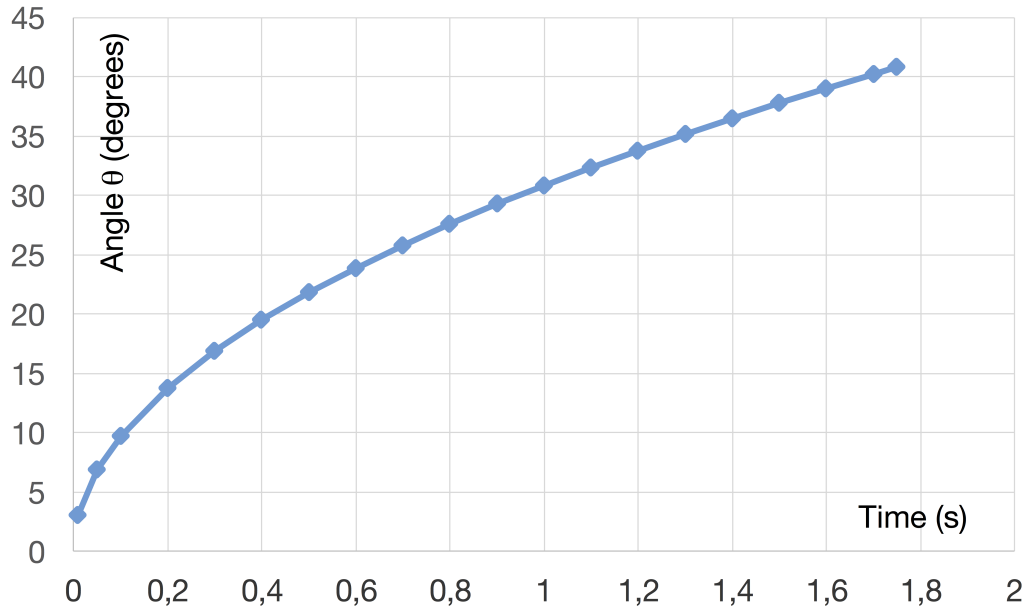

Figure 6.6: Frenkel sintering angle values as a function of time

In figure 6.6, is shown the sintering angle evolution for the Frenkel modified Model.

Chapter 7

Sintering Viscoelastic Model - Maxwell Approach

Before introducing the Maxwell Model used in this section, it's necessary to recall some notes about Viscoelasticy. Although polymers have their distinct transitions and may be considered liquid when above the glass transition or melting temperatures, or solid when below those temperatures, in reality they are neither liquid nor solid, but viscoelastic. In fact, at any temperature, a polymer can be either a liquid or a solid, depending on the time scale or the speed at which its molecules are being deformed.

7.1 Solids - Fluids Comparison

In solid bodies, the stress state, is always accompanied by a strain deformation [30]. Furthermore, when the causes of the stress state end, the solid body turn back to its undeformed shape. A body defined 'solid body', has its own form.

For a homogeneous, isotropic, elastic solid, the relation between stress and strain is a linear relation and constitutive equations are:

$$
\begin{aligned}
\sigma_x &= \frac{E}{(1+\nu)(1-2\nu)}[(1-\nu)\varepsilon_x + \nu(\varepsilon_y + \varepsilon_z)] \\
\sigma_y &= \frac{E}{(1+\nu)(1-2\nu)}[(1-\nu)\varepsilon_y + \nu(\varepsilon_x + \varepsilon_z)] \\
\sigma_z &= \frac{E}{(1+\nu)(1-2\nu)}[(1-\nu)\varepsilon_z + \nu(\varepsilon_x + \varepsilon_y)] \\
\tau_{xy} &= \frac{E}{2(1+\nu)}\gamma_{xy} \\
\tau_{xz} &= \frac{E}{2(1+\nu)}\gamma_{xz} \\
\tau_{yz} &= \frac{E}{2(1+\nu)}\gamma_{yz}
\end{aligned}
\tag{7.1}
$$

Considering a uniaxial strain, it's possibile to write:

$$
\sigma = E\varepsilon \tag{7.2}
$$

Regarding fluids, they haven't an own shape and, when they are subject to a state of rest, at each point, only normal stresses are present, in particular, the stress is the same in each principal direction. When a varation of strain is applied, some shear stresses raise. If the fluid is a Newtonian fluid, the shear stresses are proportional to strain velocity. General constitutive equations are:

$$
\begin{aligned}
\sigma_x &= p - 2\mu\dot{\varepsilon}_x + \frac{2}{3}\mu(\dot{\varepsilon}_x + \dot{\varepsilon}_y + \dot{\varepsilon}_z) \\
\sigma_y &= p - 2\mu\dot{\varepsilon}_y + \frac{2}{3}\mu(\dot{\varepsilon}_x + \dot{\varepsilon}_y + \dot{\varepsilon}_z) \\
\sigma_z &= p - 2\mu\dot{\varepsilon}_z + \frac{2}{3}\mu(\dot{\varepsilon}_x + \dot{\varepsilon}_y + \dot{\varepsilon}_z) \\
\tau_{xy} &= \mu\dot{\gamma}_{xy} \\
\tau_{xz} &= \mu\dot{\gamma}_{xz} \\
\tau_{yz} &= \mu\dot{\gamma}_{yz}
\end{aligned}
\tag{7.3}
$$

The simplest model is:

$$
\sigma = \mu\dot{\varepsilon} \tag{7.4}
$$

7.1.1 Different Resposes to Stress and Strain Input

In linear elasticity, to a finite load step with initial time $t = t_0$ and end time $t = t_1$, follows an instantaneous proportional strain. When load ends, the strain return to its initial state.

Assuming a viscous material, the system response to an instant load σ_0 increases linearly in accordance with the consitutive law until the laod is applied. When stress ceases, elongation remains constant.

Figure 7.1 shows the difference mentioned above:

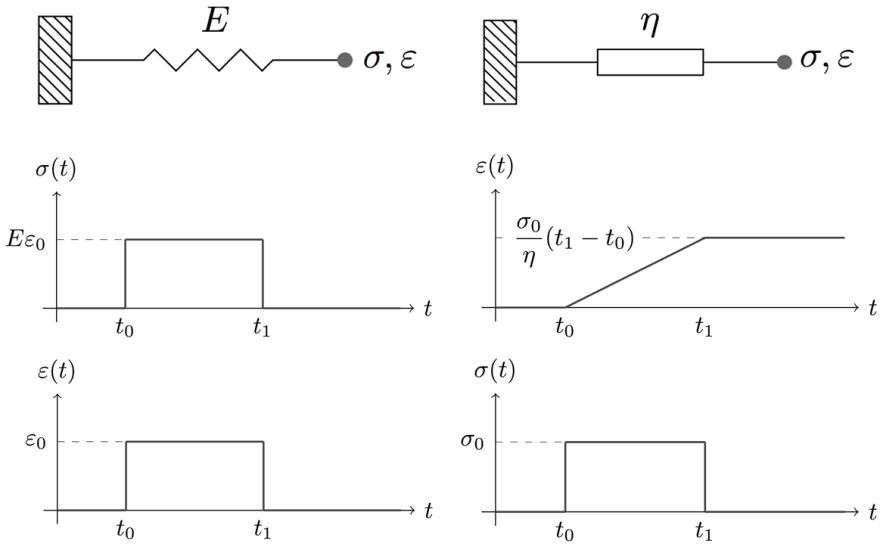

Figure 7.1: Pure Elastic - Pure Viscous Behavior

7.2 Linear Viscoelasticity

In many engineering applications, materials can be considered in linear-elastic regime, because they obey to Hooke's Law, thus, stress is proportional to the applied strain. Fluids, as it's know, don't present a proportionality between the applied stress and strain. Their constitutive behaviour can be described through a relationship between stress and strain rate by viscosity parameter.

Real behaviour of materials, in many times, deflect from Hookean and present both elastic and fluid characteristics. Immagine, for example, to hang a weight at the end of a thin lead wire. After the first instantaneous strain, if the observation lasts for a sufficiently long time,

elongation will no stop untile the wire get to rupture. Materials that obey to this behaviour are called viscoelastic materials.

Visco-elastic materials characteristic depends on time and load application (or strain application) velocity.

This behaviour lead to important phenomena:

- Creep: when, with a constant load applied, strain growth with time:

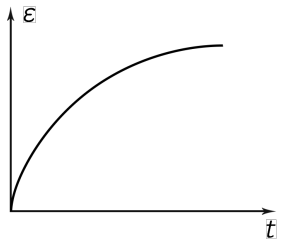

Figure 7.2: Creep phenomenon

- Relaxation: when, with a constant strain applied, stress decreases with time;

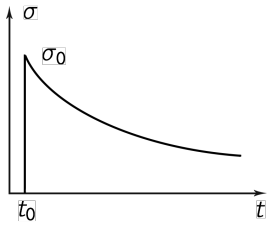

Figure 7.3: Stress Relaxation

- Stiffness depends on load application velocity;

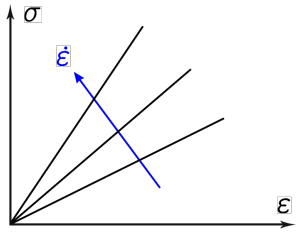

Figure 7.4: Stiffness Dependence of load application speed

The concept of linear viscosity is applied to the stress-strain response obtained at a fixed time $t = t_0$, for different applied stresses. Infact, if the strain is $\varepsilon(t_0)$, for different values of $\sigma = \sigma_1,\ \sigma_2,\ \sigma_3$ and denoting:

$$\epsilon_1 = [\epsilon(t_0)]_{\sigma=\sigma_1} \qquad \epsilon_2 = [\epsilon(t_0)]_{\sigma=\sigma_2} \qquad \epsilon_3 = [\epsilon(t_0)]_{\sigma=\sigma_3}$$

the corresponding strains, if the material behaviour is viscoelastic, following equation must be valid :

$$\frac{\epsilon_1}{\sigma_1} = \frac{\epsilon_2}{\sigma_2} = \frac{\epsilon_3}{\sigma_3} \tag{7.5}$$

In a more efficient manner (figure 7.5):

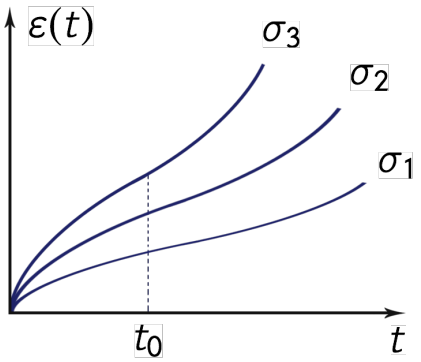

Figure 7.5: Linear Viscoelasticity

The most common, linear viscoelastic model is the Maxwell model. A Maxwell material is a viscoelastic material having the properties both of elasticity and viscosity. The Maxwell model can be represented by a purely viscous damper and a purely elastic spring connected in series, as shown in figure 7.6.

In this configuration, under an applied axial stress, the total stress, σ_{Total} and the total strain, $\varepsilon_{\text{Total}}$ can be defined as follows [30]:

$$\sigma_{\text{Total}} = \sigma_D = \sigma_S \qquad \varepsilon_{\text{total}} = \varepsilon_D + \varepsilon_S$$

where the subscript D indicates the stress/strain in the damper and the subscript S indicates the stress/strain in the spring. Taking the derivative of strain with respect to time, we obtain:

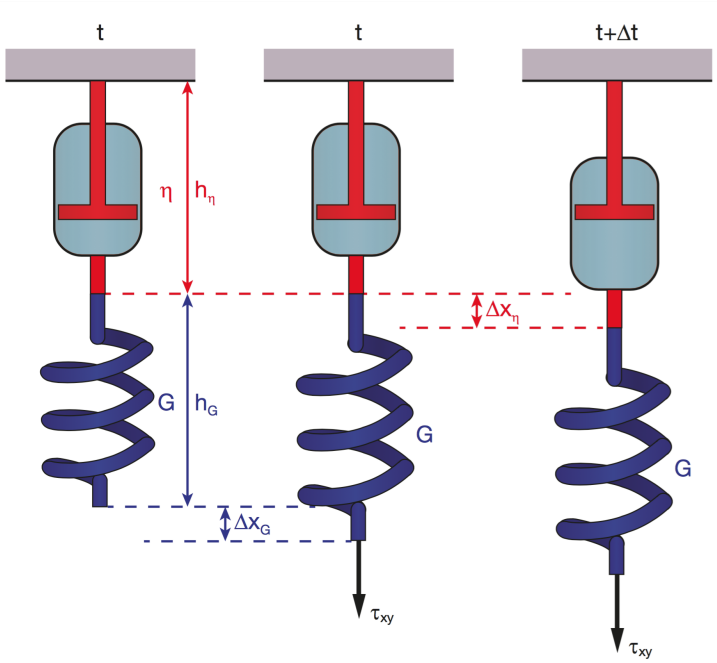

Figure 7.6: Maxwell Model

$$\frac{d\varepsilon_{\text{Total}}}{dt} = \frac{d\varepsilon_D}{dt} + \frac{d\varepsilon_S}{dt} = \frac{\sigma}{\eta} + \frac{1}{E}\frac{d\sigma}{dt}$$

where E is the elastic modulus and η is the material coefficient of viscosity. This model describes the damper as a Newtonian fluid and models the spring with Hooke's law.

If we connect these two elements in parallel, we get a generalized model of Kelvin–Voigt material.

In a Maxwell material, stress σ, strain ϵ and their rates of change with respect to time t are governed by equations of the form:

$$\frac{\dot{\sigma}}{E} + \frac{\sigma}{\eta} = \dot{\varepsilon}$$

Or by:

$$\tau_{xy} + \lambda\frac{d\tau_{xy}}{dt} = -\eta_0\dot{\gamma_{xy}} \tag{7.6}$$

Linear viscoelasticty refers to small strains.

7.3 Stress Relaxation

In materials science, stress relaxation is the observed decrease in stress in response to the same amount of strain generated in the structure. This is primarily due to keeping the structure in a strained condition for some finite interval of time and hence causing some amount of plastic strain. This should not be confused with creep, which is a constant state of stress with an increasing amount of strain.

Since relaxation relieves the state of stress, it has the effect of also relieving the equipment reactions. Thus, relaxation has the same effect as cold springing, except it occurs over a longer period of time. The amount of relaxation which takes place is a function of time, temperature and stress level, thus the actual effect it has on the system is not precisely known, but can be bounded.

Stress relaxation describes how polymers relieve stress under constant strain. Because they are viscoelastic, polymers behave in a nonlinear, non-Hookean fashion. This nonlinearity is described by both stress relaxation and a phenomenon known as creep, which describes how polymers strain under constant stress.

Viscoelastic materials have the properties of both viscous and elastic materials and can be modeled by combining elements that represent these characteristics. Maxwell model is good at predicting stress relaxation, it is fairly poor at predicting creep.

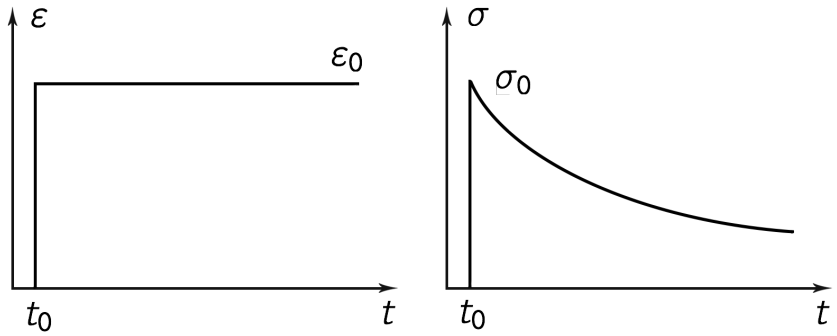

Figure 7.7: Stress Relaxation

7.4 Relaxation Time

In the physical sciences, relaxation usually means the return of a perturbed system into equilibrium. Each relaxation process can be characterized by a relaxation time τ. The simplest theoretical description of relaxation as function of time t is an exponential law $exp(-t/\tau)$.

7.4.1 Weissemberg Number

The Wi is a dimensionless number used in the study of viscoelastic flows. The dimensionless number compares the viscous forces to the elastic forces. It can be variously defined, but it is usually given by the relation of stress relaxation time of the fluid and a specific process time. In simple steady shear, the Weissenberg number, often abbreviated , is defined as the shear rate $\dot{\gamma}$ times the relaxation time λ. In formula:

$$Wi = \frac{\text{Viscous Forces}}{\text{Elastic Forces}} = \frac{\eta\dot{\gamma}}{E\varepsilon} = \lambda\dot{\gamma} \tag{7.7}$$

It's then clear that, the relaxation time it's related to stress a kind of parameter that defines the important of viscosity compared to elastic forces.

7.4.2 Deborah Number

The Deborah number (De) is a dimensionless number, often used in rheology to characterize the fluidity of materials under specific flow conditions. It is based on the premise that given enough time even a solid-like material will flow. The flow characteristics are not inherent properties of the material alone, but a relative property which depends on two fundamentally different characteristic times. Formally, the Deborah number is defined as the ratio of the relaxation time characterizing the time it takes for a material to adjust to applied stresses or strains, and the characteristic time scale of an experiment (or a computer simulation) probing the response of the material:

$$De = \frac{\text{Stress Relaxation Time}}{\text{Observation Time}} = \frac{\lambda}{tp} = \lambda\omega \tag{7.8}$$

Technically, this incorporates both the elasticity and viscosity of the material. At lower Deborah numbers, the material behaves in a more fluidlike manner, with an associated Newto-

nian viscous flow. At higher Deborah numbers, the material behavior enters the non-Newtonian regime, increasingly dominated by elasticity and demonstrating solidlike behavior.

This hypothesis will be confermed with the results comparison developed in next sections.

7.5 Non-Linear Viscoelasticity

A non-linear viscoelastic response in a polymer occurs when the strain or the rate of strain is large. In the course of polymer processing operations, large strains are always imposed on the material, requiring the use of non-linear viscoelastic models. In figure **??**, compared to linear case, is shown the non linear behaviour:

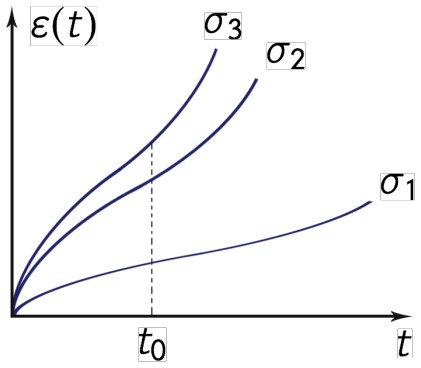

Figure 7.8: Linear Viscoelasticity

There are two types of general, non-linear, viscoelastic flow models: the differential type and the integral type. The one used in the present work is a differential model. Differential models have traditionally been the tool of choice to describe the viscoelastic behavior of polymers when simulating complex flow systems. Many differential viscoelastic models can be described in the general form:

$$Y\tau + \lambda_0\tau_0 + \lambda_1\tau_1 + \lambda_2\left[\dot{\gamma}\cdot\tau + \tau\cdot\dot{\gamma}\right] + \lambda_3\left[\tau\cdot\tau\right] = \eta_0\left[\dot{\gamma} + \lambda_4\dot{\gamma}_0 + \lambda_5\dot{\gamma}_1\right] \tag{7.9}$$

where τ_0 is the corotational or Jaumann derivative of the stress tensor defined as:

$$\tau_0 = \frac{\mathcal{D}}{\mathcal{D}t}\tau = \frac{D}{Dt}\tau - \frac{1}{2}\left[\omega\cdot\tau - \tau\cdot\omega\right] \tag{7.10}$$

and $D\tau/Dt$ is the substantial derivative and ω is the vorticity tensor given by:

$$\omega = \nabla u - (\nabla u)^T \tag{7.11}$$

where ∇u is the velocity gradient. τ_1 is the first controvariant convected time derivative of the deviatoric stress tensor and represent rates of change with respect to a convected coordinate system that moves and deforms with the fluid. The convected derivative of the deviatoric stress tensor is defined as:

$$\tau_1 = \frac{D\tau}{Dt} - \left[(\nabla u)^T \cdot \tau + \tau \cdot (\nabla u)\right] \tag{7.12}$$

and similarly, $\dot{\gamma}_0$ is the Jaumann derivative of the rate of strain tensor and $\dot{\gamma}_1$ is the first contravariant convected time derivative of the rate of strain tensor.

The constants in Eq. 7.9 are defined in Table 7.1 for various common viscoelastic models commonly used to simulate polymer flows [64].

Constitutive Models	**Y**	λ_0	λ_1	λ_2	λ_3	λ_4	λ_5
Generalized Newtonian	1	0	0	0	0	0	0
Upper Convected Maxwell	1	0	λ_1	0	0	0	0
Corotation Maxwell	1	λ_0	0	0	0	0	0
Convected Jeffrey's	1	0	λ_1	0	0	0	λ_5
Corotation Jeffrey's	1	λ_0	0	0	0	λ_4	0
White-Metzner	1	0	$\lambda_1(\dot{\gamma})$	0	0	0	0
Phan-Thien-Thanner-1	$e^{[\varepsilon(\lambda/\eta_0)tr\tau]}$	0	λ	$\lambda\xi/2$	0	0	0
Phan-Thien-Thanner-2	$1-\varepsilon(\lambda/\eta_0)tr\tau$	0	λ	$\lambda\xi/2$	0	0	0
Giesekus	1	0	λ_1	0	0	$-\alpha\lambda_1/\eta_0$	0

Table 7.1: Definition of constant presented in Eq. 7.9

Although, in next section, will be analyzed only the Upper Convected Model, value of all models are only for generalize this work.

7.6 Upper Convected Maxwell Model

For the large strains, the simplest way to combine time-dependent phenomena and rheological nonlinearity is to incorporate nonlinearity into the simple Maxwell equation. This modified

model is the Upper Convected Model (UCM).

This can be done by replacing the substantial time derivative in a tensor version, with the upper-convected time derivative of $\boldsymbol{\tau}$, in formula:

$$\lambda\tilde{\boldsymbol{\tau}} + \boldsymbol{\tau} = 2\eta\boldsymbol{D} \tag{7.13}$$

where $\boldsymbol{\lambda}$ is the relaxation time and $\tilde{\boldsymbol{\tau}}$ represents a general form of the invariant derivate of the extra-stress-tensor (upper-convected derivative):

$$\tilde{\boldsymbol{\tau}} = \frac{D\boldsymbol{\tau}}{Dt} - \boldsymbol{\omega}\cdot\boldsymbol{\tau} + \boldsymbol{\tau}\cdot\boldsymbol{\omega} - a(\boldsymbol{D}\cdot\boldsymbol{\tau} + \boldsymbol{\tau}\cdot\boldsymbol{D}) \tag{7.14}$$

where $\frac{D\boldsymbol{\tau}}{Dt}$ is the substantial derivative of extra-stress-tensor and $\boldsymbol{\omega}$ is the rotational tensor.

It's important to say that for elastic material and small strain amplitudes,the non-linear terms disappear and the upper-convected time derivative reduces to the substantial time derivative.

Assuming quasi-steady state flow as a first approximation:

$$\boldsymbol{\tau} + \lambda a(\boldsymbol{D}\cdot\boldsymbol{\tau} + \boldsymbol{\tau}\cdot\boldsymbol{D}) = 2\eta\boldsymbol{D} \tag{7.15}$$

By Eq. 6.7 and Eq. 6.8, it's possible to write:

$$\begin{pmatrix} \tau_{11} & 0 & 0 \\ 0 & \tau_{22} & 0 \\ 0 & 0 & \tau_{33} \end{pmatrix} + 2\lambda a \begin{pmatrix} \dot{\varepsilon}_{11}\tau_{11} & 0 & 0 \\ 0 & -2\dot{\varepsilon}_{22}\tau_{22} & 0 \\ 0 & 0 & \dot{\varepsilon}_{33}\tau_{33} \end{pmatrix} = 2\eta \begin{pmatrix} \dot{\varepsilon}_{11} & 0 & 0 \\ 0 & -2\dot{\varepsilon}_{22} & 0 \\ 0 & 0 & \dot{\varepsilon}_{33} \end{pmatrix} \tag{7.16}$$

the principal components of extra-stress-tensor can be deteminated as:

$$\tau_{yy} = \frac{-4\eta\dot{\varepsilon}}{1 - 4a\lambda\dot{\varepsilon}} \tag{7.17}$$

$$\tau_{xx} = \tau_{zz} = \frac{2\eta\dot{\varepsilon}}{1 - 2a\lambda\dot{\varepsilon}} \tag{7.18}$$

For viscoelastic model, eq. 6.30, the stresses are now replaced by above expressions to give:

$$W_v = \int_V \boldsymbol{\tau} : \boldsymbol{D} dV = \begin{pmatrix} \frac{2\eta\dot{\varepsilon}}{1-2a\lambda\dot{\varepsilon}} & 0 & 0 \\ 0 & \frac{-4\eta\dot{\varepsilon}}{1-4a\lambda\dot{\varepsilon}} & 0 \\ 0 & 0 & \frac{2\eta\dot{\varepsilon}}{1-2a\lambda\dot{\varepsilon}} \end{pmatrix} : \begin{pmatrix} \dot{\varepsilon}_{11} & 0 & 0 \\ 0 & -2\dot{\varepsilon}_{22} & 0 \\ 0 & 0 & \dot{\varepsilon}_{33} \end{pmatrix} \tag{7.19}$$

$$W_v = \int_V \boldsymbol{\tau} : \boldsymbol{D} dV = \frac{32\pi a^3 \eta \dot{\varepsilon}^2}{(1-4a\lambda\dot{\varepsilon}(1+2a\lambda\dot{\varepsilon})} \tag{7.20}$$

Now, by equating visco-elastic force work and surface work (Eq.6.14), as shown:

$$W_s = \Gamma \frac{8\pi a_0^2 2^{\frac{1}{3}} \cos(\theta)\sin(\theta)}{[1+\cos(\theta)]^{\frac{4}{3}}[2-\cos(\theta)]^{\frac{5}{3}}}\theta' = \frac{32\pi a^3\eta\dot{\varepsilon}^2}{(1-4a\lambda\dot{\varepsilon}(1+2a\lambda\dot{\varepsilon})} = W_v \tag{7.21}$$

and after some manipulations, a non-linear differential equation is obtained:

$$8(a\lambda K_1\theta')^2 + \left(2a\lambda K_1 + \frac{\eta a_0}{\Gamma}\frac{K_1^2}{K_2^2}\right)\theta' - 1 = 0 \tag{7.22}$$

where:

$$K_1 = \frac{\sin\theta}{(1+\cos\theta)(2-\cos\theta)} \tag{7.23}$$

$$K_2 = \frac{2^{-\frac{5}{3}}\cos\theta\sin\theta}{(1+\cos\theta)^{\frac{4}{3}}(2-\cos\theta)^{\frac{5}{3}}} \tag{7.24}$$

Once a solution for the sintering angle is obtained, the evolution of the neck radius with time can easily be derived from eq. 6.38.

It is interesting to note that for the initial stage of sintering, assuming $a = a_0$, the term θ^2 can be approximated as $(x/a)^2$ and after some manipulations eq. 7.22 simplifies to the following expression:

$$\frac{d(x/a)^2}{dt} = \frac{-a\lambda - 2\frac{\eta a_0}{\Gamma} + \left[(3a\lambda)^2 + 4a\lambda\frac{\eta a_0}{\Gamma} + 4\left(\frac{\eta a_0}{\Gamma}\right)^2\right]^{\frac{1}{2}}}{2(a\lambda)^2} \tag{7.25}$$

where $\frac{d(x/a)^2}{dt}$ represent an initial sintering rate.

7.7 Maxwell Model Results

Before continuing with the results of the Maxwell model, it's necessary to step back. Let recall Eq. 7.13.

The λ term is the relaxation time mentioned in 7.4. The meaning of this parameter is very complex and it's important to weigh the model results.

In Eq. 7.25, the value of λ has an importan influence and in this section, a comparison between some values of such parameter will be evaluated. As will be shown, the value of the dimensionless radius, and conseguently, of the sintering angle, changes so far from negligible. Values of parameters λ used in the analysis are 4: $\lambda = 0.1$, $\lambda = 10$, $\lambda = 20$ and $\lambda = 50$.

In table 8.4, there will be shown the dimensionless radius and sintering angle values as function of time and of different λ values:

Tempo [s]	$\lambda = 0.1$		$\lambda = 10$		$\lambda = 20$		$\lambda = 50$	
	X/a	θ	X/a	θ	X/a	θ	X/a	θ
0.01	0.05	3.08	0.05	2.60	0.04	2.22	0.03	1.62
0.05	0.12	6.91	0.10	5.82	0.09	4.97	0.06	3.63
0.1	0.17	9.79	0.14	8.25	0.12	7.04	0.09	5.14
0.2	0.24	13.91	0.20	11.70	0.17	9.99	0.13	7.28
0.3	0.29	17.13	0.25	14.39	0.21	12.26	0.16	8.93
0.4	0.34	19.88	0.29	16.67	0.25	14.20	0.18	10.32
0.5	0.38	22.35	0.32	18.71	0.27	15.91	0.20	11.56
0.6	0.42	24.62	0.35	20.57	0.30	17.48	0.22	12.68
0.7	0.45	26.74	0.38	22.30	0.32	18.93	0.24	13.71
0.8	0.48	28.75	0.41	23.94	0.35	20.29	0.25	14.68
0.9	0.51	30.67	0.43	25.49	0.37	21.58	0.27	15.59
1	0.54	32.53	0.45	26.98	0.39	22.81	0.28	16.46
1.1	0.56	34.33	0.48	28.41	0.41	24.00	0.30	17.28
1.2	0.59	36.09	0.50	29.80	0.42	25.14	0.31	18.08
1.3	0.61	37.81	0.52	31.14	0.44	26.24	0.32	18.84
1.4	0.64	39.51	0.54	32.46	0.46	27.31	0.34	19.58
1.5	0.66	41.19	0.56	33.75	0.47	28.35	0.35	20.30

Table 7.2: continued on next page

Table 7.2: continued from previous page

Tempo [s]	$\lambda = 0.1$		$\lambda = 10$		$\lambda = 20$		$\lambda = 50$	
	X/a	θ	X/a	θ	X/a	θ	X/a	θ
1.6	0.68	42.86	0.57	35.01	0.49	29.37	0.36	21.00
1.7	0.70	44.52	0.59	36.26	0.51	30.37	0.37	21.68
1.7504	0.71	**45.35**	0.60	**36.88**	0.51	**30.86**	0.37	**22.01**

Table 7.2: Maxwell Model results: sintering angle θ [Deg] function of λ

It can be noted that the λ paraemter, as already mentioned above, it affects the value of sintering angle. Image 8.10 shows the values of sintering angle in the form of curves versus time.

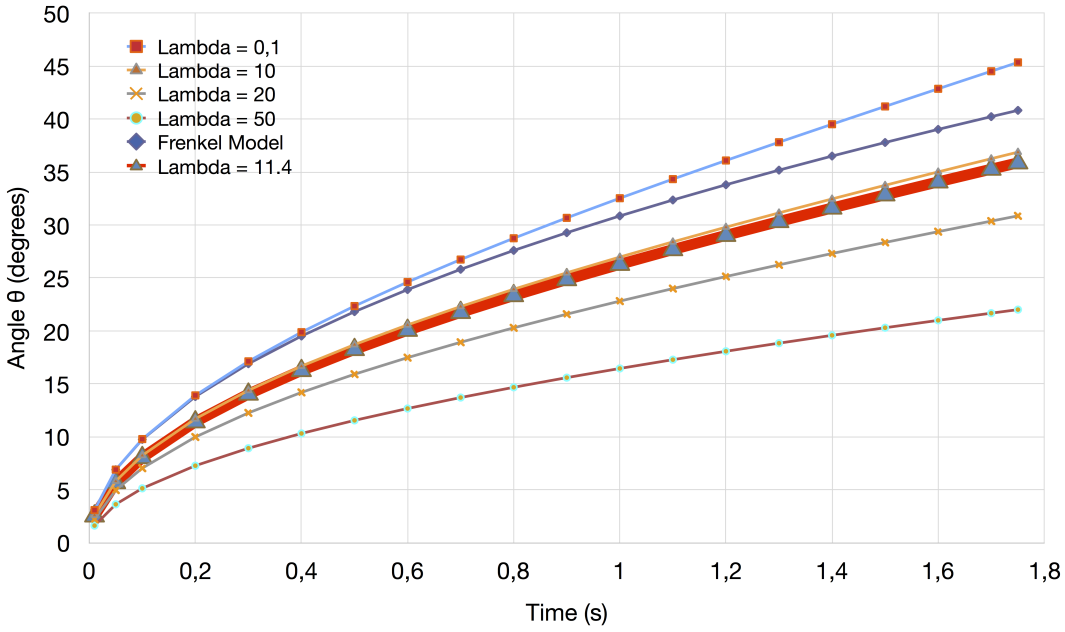

Figure 7.9: Maxwell Model results: sintering angle θ [Deg] function of time t at different values of λ

Image 8.11 shows the values of dimensionless radius in the form of curves versus time.

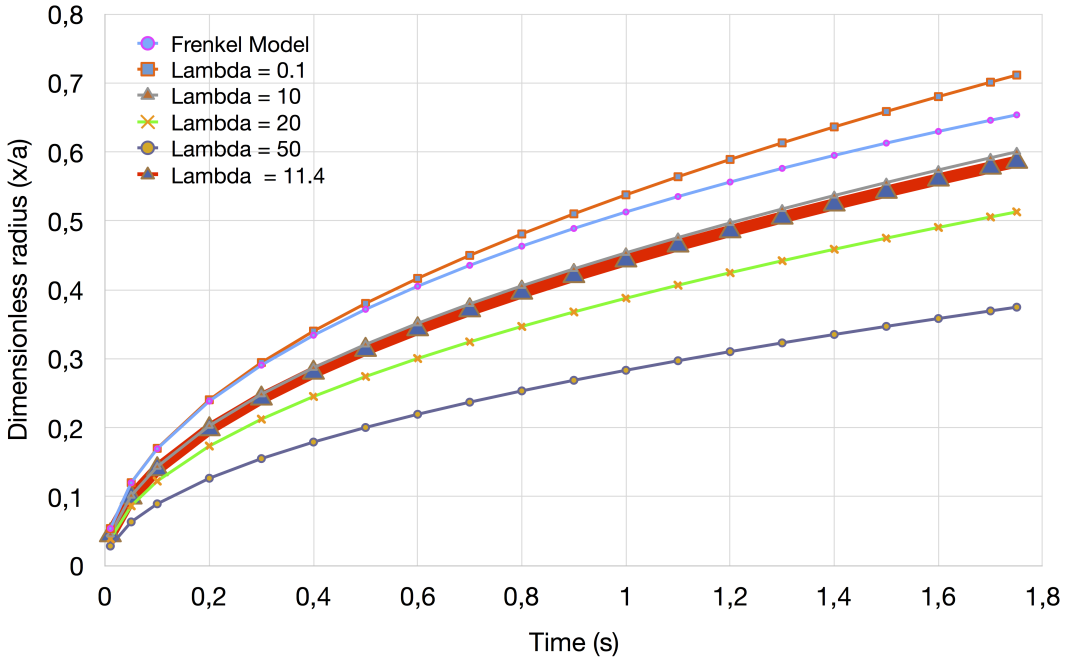

Figure 7.10: Maxwell Model results: Dimensionless radius X/a function of time t at different values of λ

Chapter 8

Sperimental Test: Relaxation Time Estimation

In previous section, it's shown how sintering angle is heavily influenced by the λ parameter. To get an idea of what is the relaxation time of the ABS 400 an experiment test has been done.

8.1 Testing Machine: MTS Insight Electromechanical Testing Systems

The MTS Insight Electromechanical Testing Systems (figure 8.1) is designed to provide test laboratories with capabilities to meet a full spectrum of static testing needs, easily and affordably. The MTS model is a twin-column table-top models for medium-force applications. The software used to perform tests is TestWorks (figure 8.2). For further informations, see [51].

8.2 Test Procedure

Generally, polymer tensile tests, measure the force required to break a plastic sample specimen and the extent to which the specimen stretches or elongates to that breaking point. Tensile tests produce stress-strain diagrams used to determine tensile modulus. The resulting tensile test data can help specify optimal materials, design parts to withstand application forces, and provide key quality control checks for materials.

In this work, tensile test, it's used to estimate the stress relaxation time and, more impor-

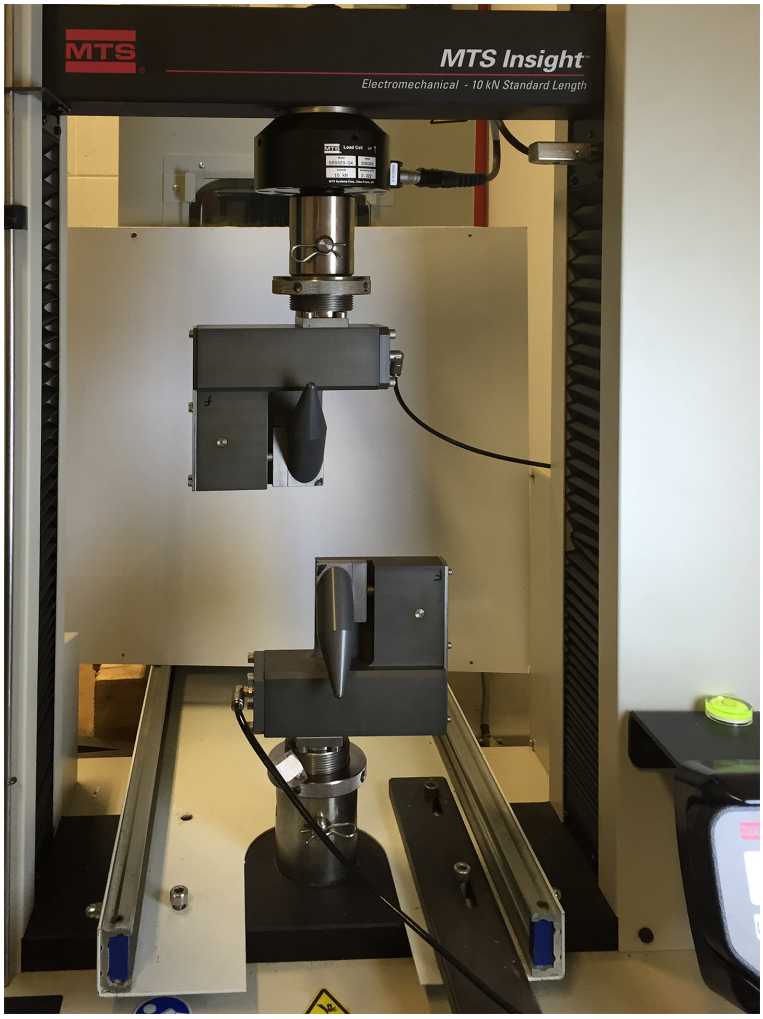

Figure 8.1: MTS testing machine

tant, the test is made with a polymer filaments used for 3D printing. The filament is a white ABS polymer piece with the following characteristics:

- diameter of 2.85 *mm*;
- length of 500 *mm*;

The specimen is wound on the supports and fixed with compressed air clamps (figure 8.1). The temperature chamber is about 20 Celsius degrees. The distance between the two grips is about 400 *mm*. Two markers were put at the distance of 30 *mm* from each others (figure 8.3). Markers must be of a color that contrasts with that of the filament and they serve to define the measurement area, which will be defined thanks to an optical sensor that detects the color contrast (8.3).

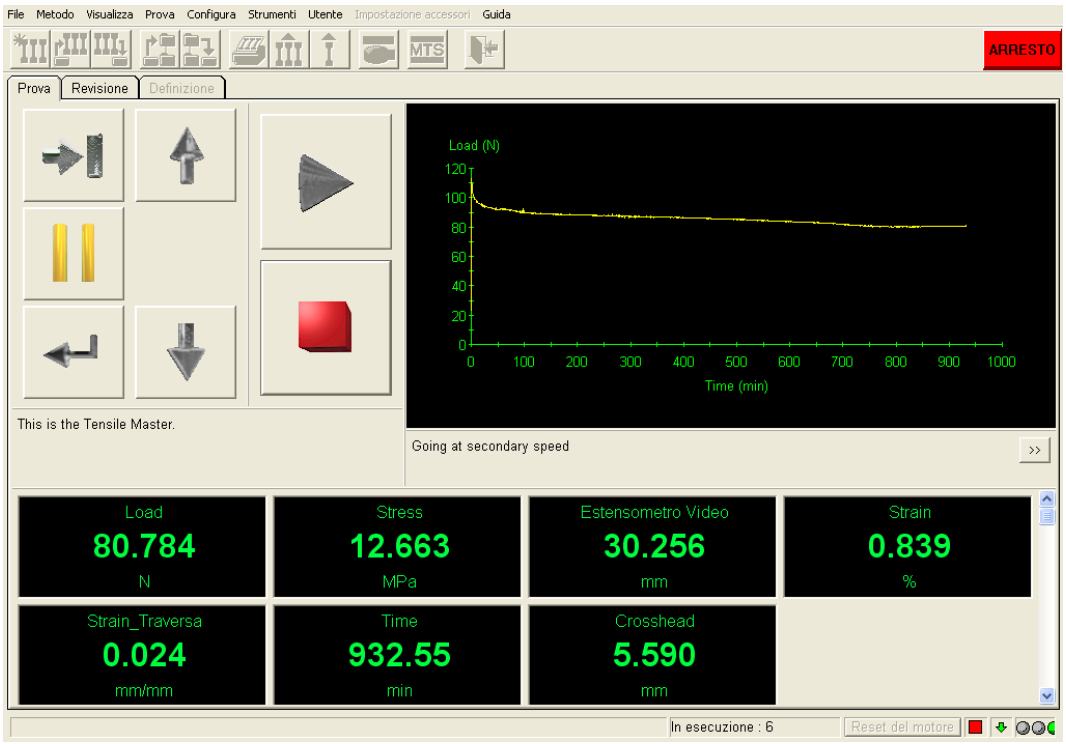

Figure 8.2: Test Software: TestWorks

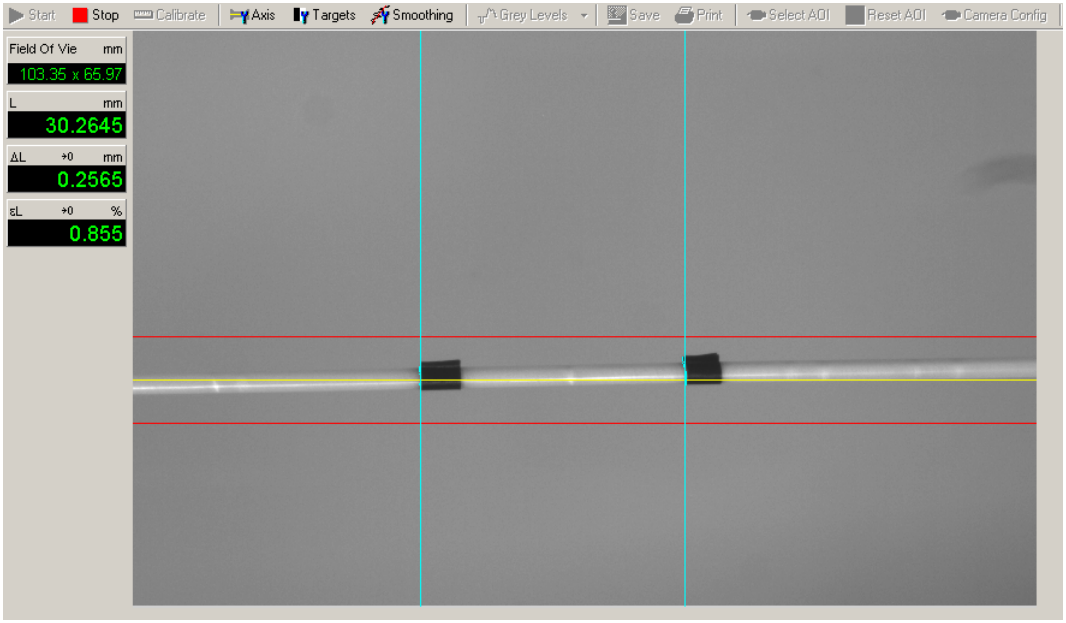

Figure 8.3: Test Software: TestWorks

After setting TestWorks for testing and setting the optical sensor to the limit of the markers we can proceed with the experiment. The test took place imposing at the sample a

dislacement story and thus, deformation history, equal to 1 %. The deformation speed increase was set 100 mm/min so as to emulate in the best possible way the response a solicitation to theoretical instantaneous step (figure 8.6). At the end of tests, data are saved in a txt file and can be exported. The sampling frequency is setted to 5 Hz and 1000 points for the ascent portion, and to 5 Hz and 40000 points for the descending portion.

We did a total of 8 tests. The first two, of which are not reported results, have been done to get a clearer idea of what were the timing of the relaxation and what was the model that best describe the phenomenon. Once learned that a 80-minute time was sufficient to describe at least the part of more rapid relaxation, we proceeded. The subsequent five tests, with duration of 80 minutes, have the aim to validate our data, so as not to incur any randomness. In fact, as it will be shown after, the curves have the same trend and reflect the relaxation of the material in a very good manner. Once validated the experiment, and based on the experience of the first seven tests, we proceeded to the final experiment.

Based on the information available in the literature and on the assumption that in reality, the relaxation time of a viscoelastic material, exceeds 80 minutes, the eighth test was prolonged to 16 hours. Based on the results obtained in the latter, the relaxation time λ will be calculated.

8.3 Test Results

In figures 8.5, 8.6 and 8.7 are shown the tests results. The trend of the curves describes with good approximation the material behaviour. The vertical jump from one curve to another is due to the initial load peak required to obtain the required deformation value. Setting in slightly different manner the air clamps, a different load is needed to obtain a deformation of 1%.

As shown in figure 8.5, curves are affected by noise. The load noise is probably due to some disorder around the test room. For further informations, by the TestWorks software, we plotted the load and deformation trend, in a smaller timeframe.

As shown in figure 8.4, the load noise is clearly evident. Looking at the top left figure, we see that the strain traverse is not afflicted by noise problem, while the speciment strain, yes. The linearity of the first means that the test machine is correctly setted. The noise in strain curve is probably due the distance between grips and markers while the initial decrease of strain is due local deformations in union with material viscoelasticity.

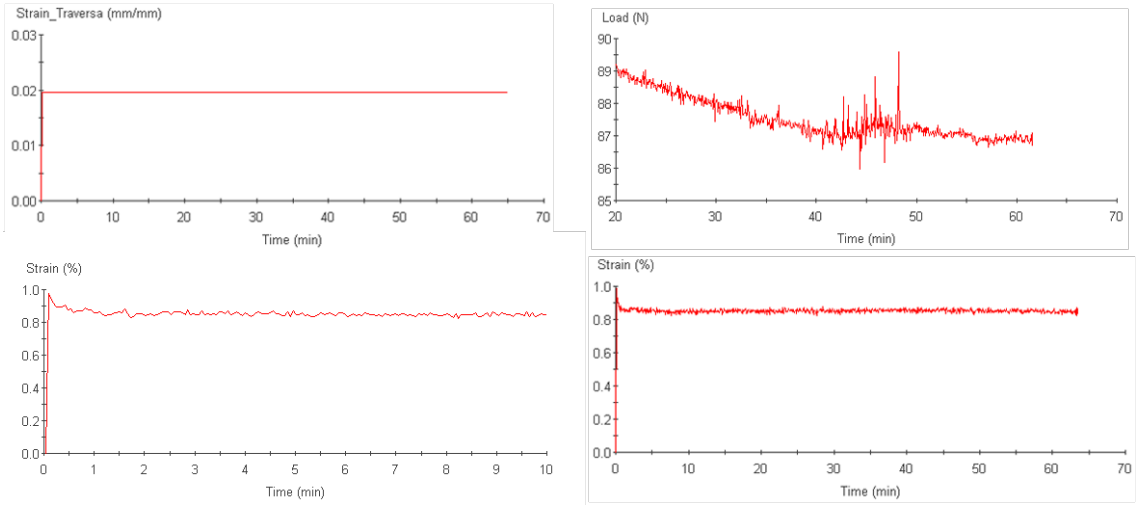

Figure 8.4: TestWorks plotted graphics: strain traversa, load, small timeframe strain, strain

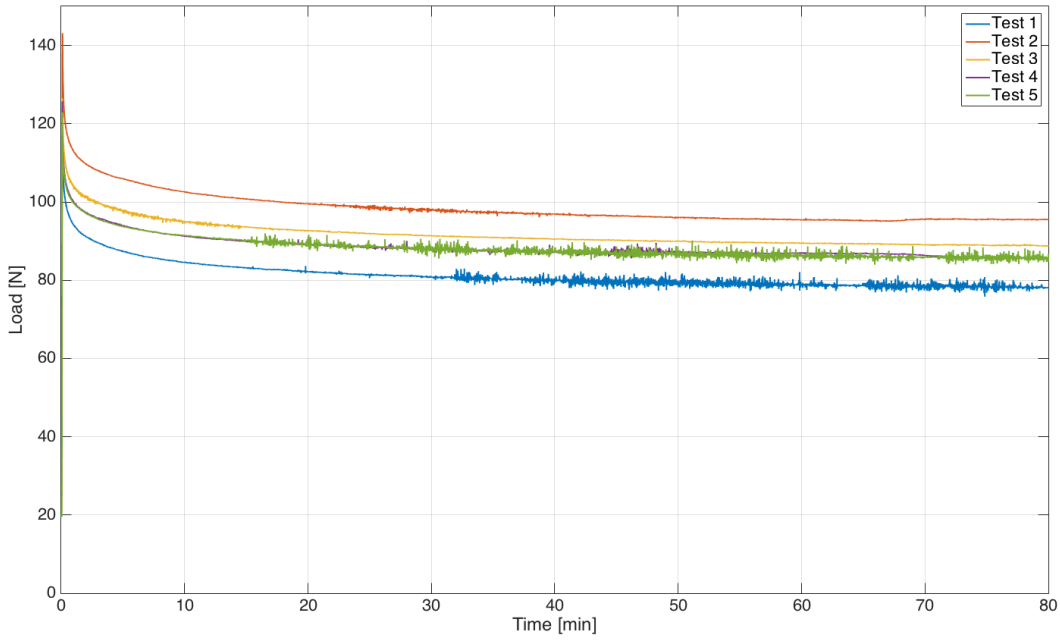

Figure 8.5: Comparison between all tests: total time

In figure 8.7, is shown the final test. As we predict, the relaxation phenomenon really end only after about 15 hours and the load remains stable at 80 N.

We focused on physical meaning of the curve and we found that the real behaviout material at the room temperature, doesn't follow that the Maxwell model. From the first sisignificant six tests, we see that load factor didn't decrease more, while theoretically, in Maxwell model, the relaxation phenomenon leads to a zero stress situation. A model that better reflects our

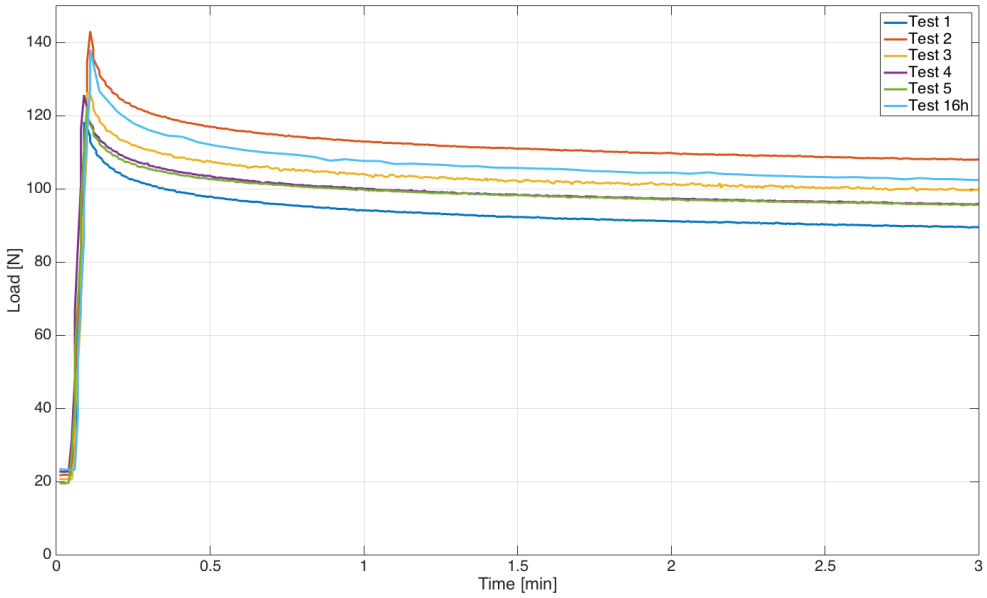

Figure 8.6: Comparison between all tests: first three minutes

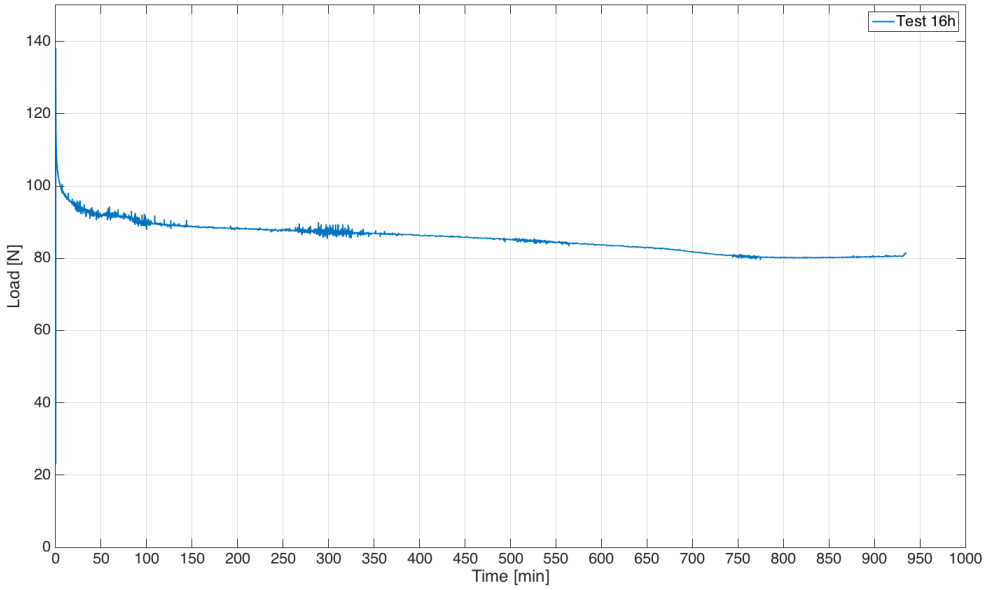

Figure 8.7: Comparison between all tests: first three minutes

speciment behaviour is the Zener model, also known as standard linear solid (SLS) model.

8.3.1 Zener Model

The Zener Model (standard linear solid model), shown in figure 8.8, is a commonly used model to simulate the short-term behavior of solid polymer components. The momentum balance of

the standard linear solid model is expressed with two equations as

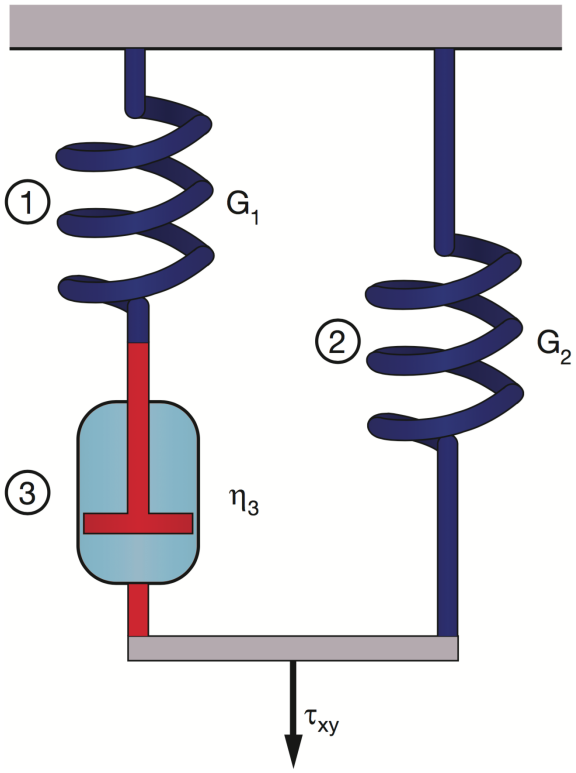

Figure 8.8: Schematic diagram of the standard linear solid model

continuity and deformation are represented by

$$\gamma_{xy} = \gamma_{xy_1} + \gamma_{xy_3} \qquad \gamma_{xy} = \gamma_{xy_2} \tag{8.1}$$

Combining Eqs. 8.1 and use the constitutive equations for the spring and dashpot elements, we get the governing equation for the standard linear solid model:

$$\eta\dot{\tau}_{xy} + G_1\tau_{xy} = \eta(G_1 + G_2)\dot{\gamma}_{xy} + G_1G_2\gamma_{xy} \tag{8.2}$$

Using Eq. 8.2 , the strain in a creep test in the standard linear solid model can be solved for as

$$\gamma_{xy} = \frac{\tau_0}{G_2}\left(\frac{\tau_0}{G_1 + G_2} - \frac{\tau_0}{G_2}\right)e^{-[G_1G_2/\eta(G_1+G_2)]t} \tag{8.3}$$

which is plotted in figure 8.9. The stress relaxation in the standard linear solid model can be derived by integrating Eq. 8.2 and is represented by

$$\tau_{xy} = \gamma_0(G_2 + G_1)e^{-(G_1/\eta)t} \tag{8.4}$$

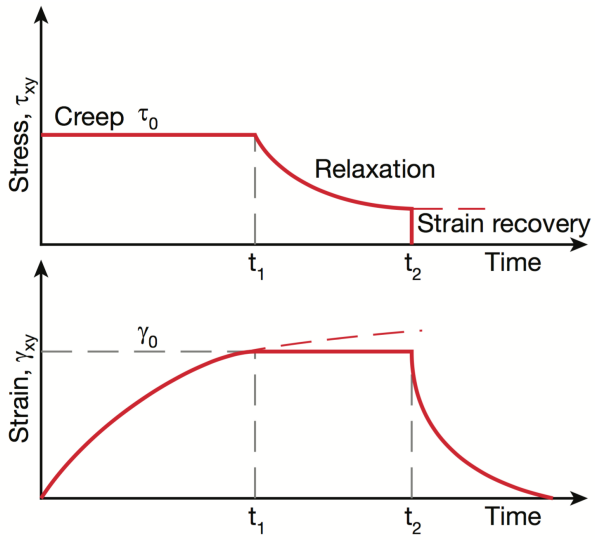

Figure 8.9: Creep, relaxation, and recovery response in the standard linear solid model

8.3.2 Relaxation Time Calculation

In our tests, referring to figure 8.9 and 8.7, we can define:

- Time $t_1 = 3/10\ s$;
- Time $t_2 = 100\ s$;
- Load $G_1 = 80.5\ N$
- Load $G_1 + G_2 = 140.8\ N$

Relaxion time is calculated when the load decreases by 50% compared to the total pressure drop. The total pressure drop is:

$$G^1_{max} - G^1_1 = \Delta G^1 = 140.8 - 80.5 = 60.3\ N \tag{8.5}$$

Then, the 50% of the total drop is:

$$\frac{\Delta G^1}{2} = 30.15\ N \tag{8.6}$$

From txt data, we can find the time when $G_1^1 + \Delta G^1 = 110.65\ N$ is reached. The time is 22.3 s

Assuming that the initial portion of curves presented in figure8.6 are exponential curves, we can write the following equation:

$$\sigma = \sigma_0 e^{-\frac{t^*}{\lambda}} \tag{8.7}$$

where t^* is the time when it reaches the fixed stress. Setting $\sigma = 0.5\sigma_0$, we obtain:

$$\sigma = \frac{\sigma_0}{2} = \sigma_0 e^{-\frac{t^*}{\lambda}} \quad \Rightarrow \quad 0.5 = e^{-\frac{t^*}{\lambda}} \tag{8.8}$$

$$\sigma = \frac{\sigma_0}{2} = \sigma_0 e^{-\frac{t^*}{\lambda}} \quad \Rightarrow \quad 0.5 = e^{-\frac{t^*}{\lambda}} \quad \Rightarrow \quad -\frac{t^*}{\lambda} = ln(0.5) \quad \Rightarrow \quad \frac{t^*}{\lambda} = ln(2) \tag{8.9}$$

and we can find the value of relaxation time as:

$$\lambda = \frac{t*}{ln(2)} = \frac{22.3}{ln(2)} = 32.2s \tag{8.10}$$

The relaxation time is $\lambda = 32.2\ s$ at temperature $T_{room} = 20°C$. Recalling Time-Temperature Superposition:

$$\log(a_T) = \frac{\eta_0}{\eta} = \frac{\lambda_0}{\lambda} \tag{8.11}$$

where η_0 and λ_0 are the viscosity and time relaxation values at $T = T_{room}$. As seen before, the visosity at melt temperature is $5100\ Pa \cdot s$ and visosity at room temperature is $300\ Pa \cdot s$. Now, we can find the λ values at melt temperature:

$$\lambda = \frac{\lambda_0}{\log\left(\frac{\eta_0}{\eta}\right)} \approx \frac{32.2}{2.83} = 11.4\ s \tag{8.12}$$

Finally, the λ parameter is equal to $11.4\ s$.

8.4 Sintering Angle: UCM with Calculated Relaxation Time

Recalling Eq. 7.25, we can calculate the values of sintering angle using the effective calculated relaxation time. In the following table is shown sintering angle evolution with a $\lambda = 11.4$.

Tempo [s]	$\lambda = 0.1$		$\lambda = 10$		$\lambda = 20$		$\lambda = 50$		$\lambda = 11.4$	
	X/a	θ	X/a	θ	X/a	θ	X/a	θ	X/a	θ
0.01	0.05	3.08	0.05	2.60	0.04	2.22	0.03	1.62	0.04	2.54
0.05	0.12	6.91	0.10	5.82	0.09	4.97	0.06	3.63	0.10	5.68
0.1	0.17	9.79	0.14	8.25	0.12	7.04	0.09	5.14	0.14	8.05
0.2	0.24	13.91	0.20	11.70	0.17	9.99	0.13	7.28	0.20	11.42
0.3	0.29	17.13	0.25	14.39	0.21	12.26	0.16	8.93	0.24	14.04
0.4	0.34	19.88	0.29	16.67	0.25	14.20	0.18	10.32	0.28	16.27
0.5	0.38	22.35	0.32	18.71	0.27	15.91	0.20	11.56	0.31	18.25
0.6	0.42	24.62	0.35	20.57	0.30	17.48	0.22	12.68	0.34	20.06
0.7	0.45	26.74	0.38	22.30	0.32	18.93	0.24	13.71	0.37	21.75
0.8	0.48	28.75	0.41	23.94	0.35	20.29	0.25	14.68	0.40	23.34
0.9	0.51	30.67	0.43	25.49	0.37	21.58	0.27	15.59	0.42	24.84
1	0.54	32.53	0.45	26.98	0.39	22.81	0.28	16.46	0.44	26.29
1.1	0.56	34.33	0.48	28.41	0.41	24.00	0.30	17.28	0.46	27.68
1.2	0.59	36.09	0.50	29.80	0.42	25.14	0.31	18.08	0.49	29.02
1.3	0.61	37.81	0.52	31.14	0.44	26.24	0.32	18.84	0.50	30.33
1.4	0.64	39.51	0.54	32.46	0.46	27.31	0.34	19.58	0.52	31.60
1.5	0.66	41.19	0.56	33.75	0.47	28.35	0.35	20.30	0.54	32.85
1.6	0.68	42.86	0.57	35.01	0.49	29.37	0.36	21.00	0.56	34.07
1.7	0.70	44.52	0.59	36.26	0.51	30.37	0.37	21.68	0.58	35.27
1.7504	0.71	45.35	0.60	36.88	0.51	30.86	0.37	22.01	**0.59**	**35.87**

Table 8.1: Maxwell Model results with the λ parameter obtained by sperimental tests. Angle θ in Degrees

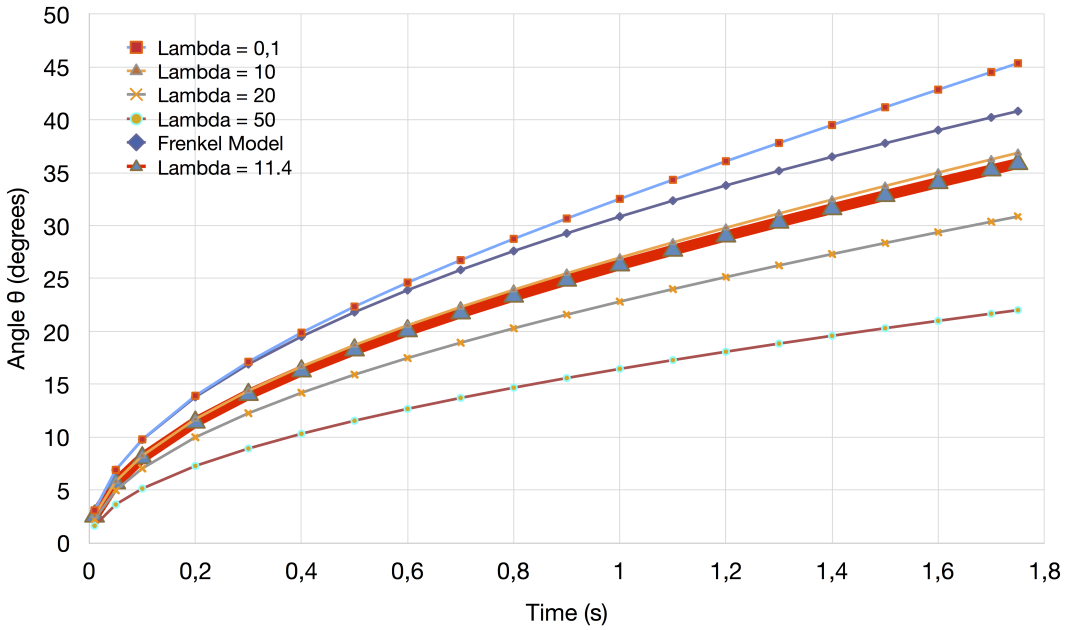

Figure 8.10: Maxwell Model results: sintering angle θ $[Deg]$ function of time t at different values of λ

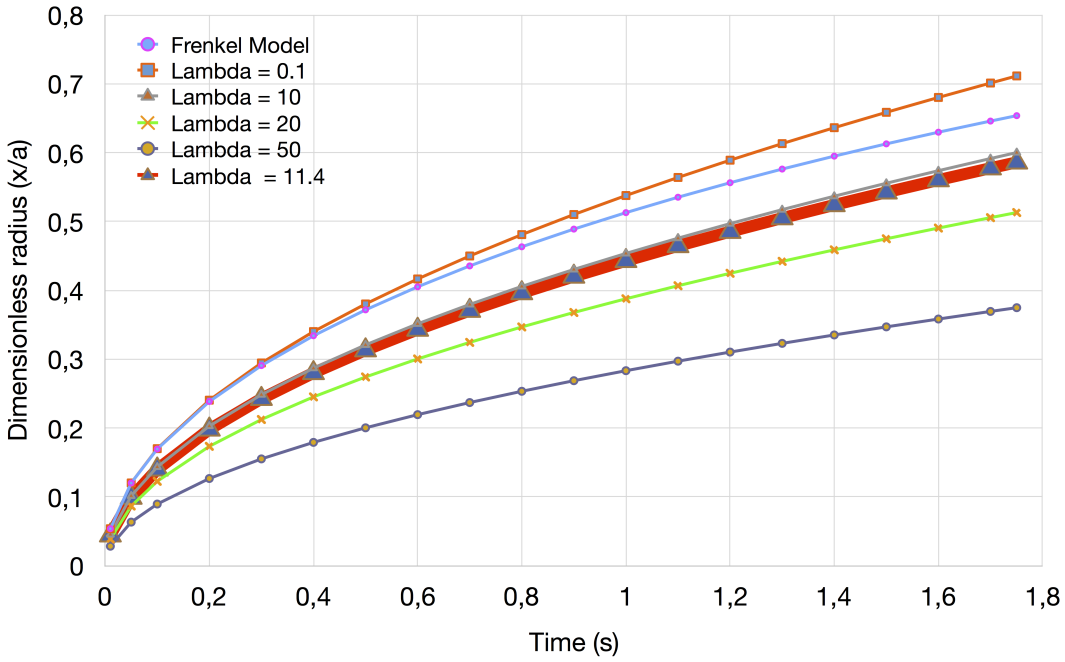

Figure 8.11: Maxwell Model results: Dimensionless radius X/a function of time t at different values of λ

Chapter 9

Elastic, Viscous and Visco-elastic Model Comparison

Deformation γ_0, and Deborah number, can be used to summarize how the system can be most accurately modeled. The magnitude of De defines the difference between solids and fluids. At small Deborah numbers, the polymer can be modeled as a Newtonian fluid, and at very high Deborah numbers, the material can be modeled as a Hookean solid [64]. Figure 9.1 helps visualize relation between time scale, deformation, and applicable material behavior.

In order to compare results in an efficient way, it's necessary to have an idea of what to expect by each model. In the present work, three models have been used:

1. Elastic Diffusion Model;
2. Pure Viscous Model;
3. Viscoelastic Upper Convected Maxwell Model.

It's logical to expect that the model developed assuming that the polymer is an elastic material will be less accurate. Simplifying ABS polymer as an elastic material, lots of informations of its real behavior will be lost. Furthermore, it's expected that the sintering angle developed, will increase more gradually than that developed with other models. If material viscosity is not taked into account, creep and stress relaxation effects are negleted.

Although the purely viscous model (Frenkel Model) describes the sintering phenomenon in a more accurate way, it not takes into account that the material, before reaching his transition

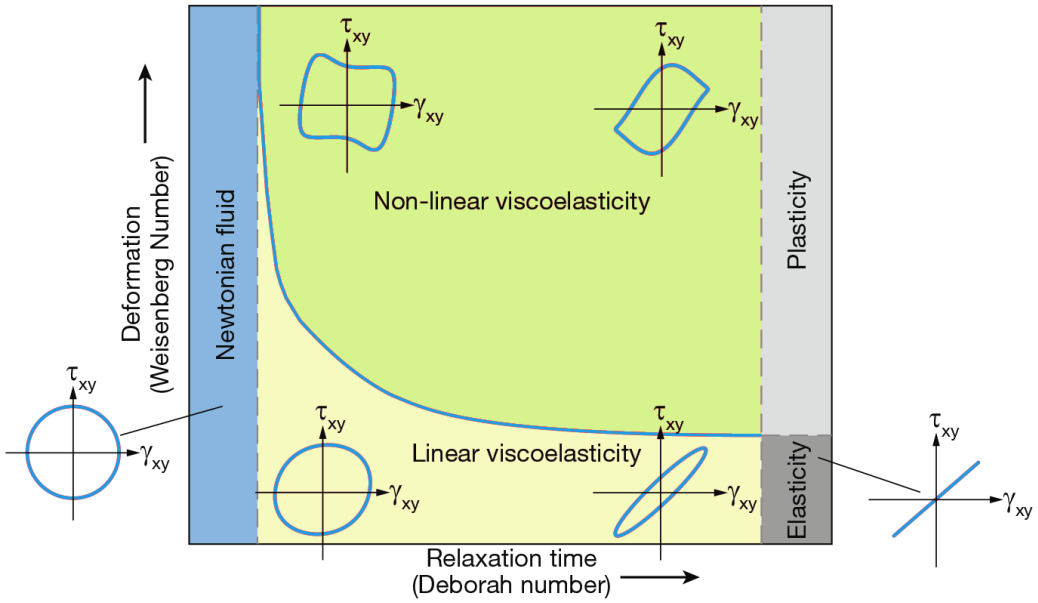

Figure 9.1: Schematic of Newtonian, elastic, linear, and non-linear viscoelastic regimes as a function of deformation and relaxation time during deformation of polymeric materials

temperature ($\approx 353.15\ K$) behaves as a solid. It's therefore suitable if analysis are referred to high temperatures and just after fusion occurred.

The Maxwell model takes into account the importance of both components: elastic and viscous, mostly, through creep and stress relaxation phenomenon via the λ parameter. Therefore, it's suppose to be the model that describes in a most accurate way the ABS behaviour.

The following table and in the following figures are shown sinter angle.

Tempo	Elastic	$\lambda = 0.1$	$\lambda = 10$	$\lambda = 20$	$\lambda = 50$	$\lambda = 11.4$	Frenkel
$[s]$	$[Deg]$	$[Deg]$	$[Deg]$	$[Deg]$	$[Deg]$	$[Deg]$	$[Deg]$
0.01	5.41	3.08	2.60	2.22	1.62	2.54	3.09
0.05	7.09	6.91	5.82	4.97	3.63	5.68	6.90
0.10	7.96	9.79	8.25	7.04	5.14	8.05	9.76
0.20	8.94	13.91	11.70	9.99	7.28	11.42	13.80
0.30	9.57	17.13	14.39	12.26	8.93	14.04	16.90
0.40	10.05	19.88	16.67	14.20	10.32	16.27	19.51

Table 9.1: continued on next page

Table 9.1: continued from previous page

Tempo	Elastic	$\lambda = 0.1$	$\lambda = 10$	$\lambda = 20$	$\lambda = 50$	$\lambda = 11.4$	Frenkel
$[s]$	$[Deg]$	$[Deg]$	$[Deg]$	$[Deg]$	$[Deg]$	$[Deg]$	$[Deg]$
0.50	10.43	22.35	18.71	15.91	11.56	18.25	21.82
0.60	10.76	24.62	20.57	17.48	12.68	20.06	23.90
0.70	11.04	26.74	22.30	18.93	13.71	21.75	25.81
0.80	11.29	28.75	23.94	20.29	14.68	23.34	27.60
0.90	11.52	30.67	25.49	21.58	15.59	24.84	29.27
1.00	11.73	32.53	26.98	22.81	16.46	26.29	30.85
1.10	11.92	34.33	28.41	24.00	17.28	27.68	32.36
1.20	12.09	36.09	29.80	25.14	18.08	29.02	33.80
1.30	12.26	37.81	31.14	26.24	18.84	30.33	35.18
1.40	12.41	39.51	32.46	27.31	19.58	31.60	36.51
1.50	12.56	41.19	33.75	28.35	20.30	32.85	37.79
1.60	12.70	42.86	35.01	29.37	21.00	34.07	39.03
1.70	12.83	44.52	36.26	30.37	21.68	35.27	40.23
1.75	**12.84**	**45.35**	**36.88**	**30.86**	**22.01**	**35.87**	**40.82**

Table 9.1: Sintering angle comparison between all models.

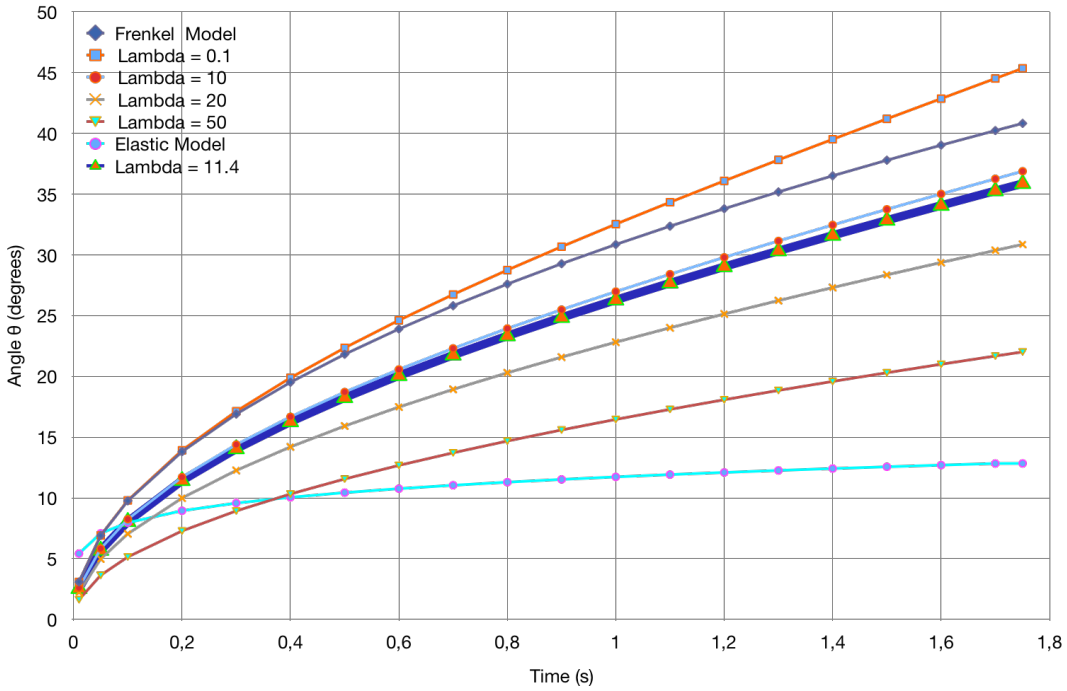

Figure 9.2: All models comparison: Frenkel - Maxwell - Elastic Models

As we expected, the elastic and frenkel models can be viewed as the lower and upper limits of the graph. In other words, viscoelastic material has a viscous component and a elastic component. The parameter that rules the material behaviour is the relaxation time.

In the next chapter, sintering angle obtained with different models will be used to have an idea of what will be the void density of printed speciment.

Part III

Moduli Calculation

Chapter 10

Lamination Analysis

As already mentioned in first chapters, the obtained solid is characterized by voids. It therefore tends to evaluate a characteristic volume (*representative volume*) and subsequently use the theories od homogeneization to merge the characteristic parameters of a compound heterogeneous in a single homogeneous compound equivalent. After the bonding process, the material is studied as a laminate.

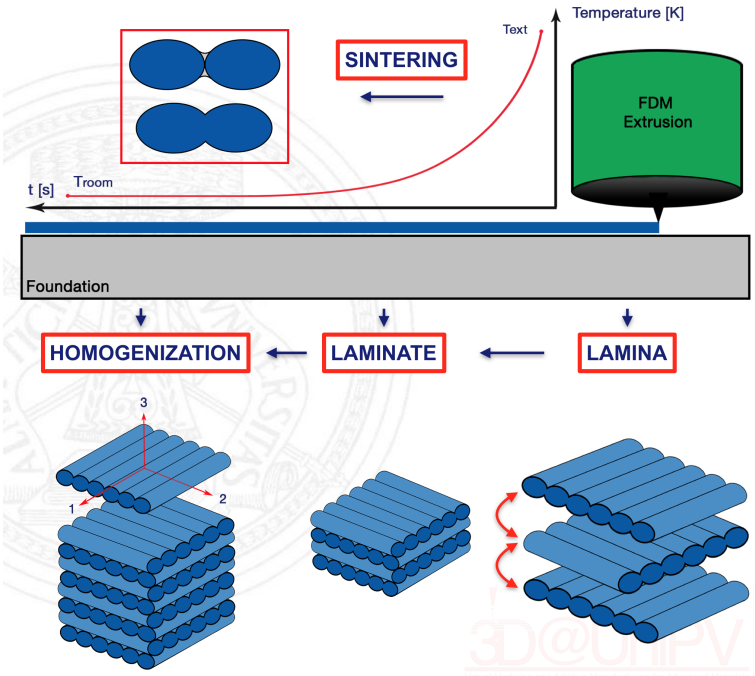

Figure 10.1: Void calculation

10.1 Lamination Theory

The equations describing the model are the classic solid mechanics's and Lamination Theory's equations.

The laminae composite are never used alone, but in the form of laminates, ie on the plates obtained by superimposing several layers, generally identical. The mechanical characteristics of rigidity and strength of the layers commonly used, make it impossible to use individual plates, and this mainly due to:

- a too strong anisotropy of the elastic response, at least for the laminae unidirectional reinforcement;
- a too small resistance in the transverse direction;
- a too small thickness, which makes the stiffness, especially that in bending, too small and a powerful danger of instability compression, in the two directions.

The plates are then used to create laminates, superimposing a sufficient number of layers, according to the project needs. This operation allows to create the plates whose mechanical characteristics, stiffness and strength, can be the subject of design. In fact, while for a plate in homogeneous material, the only design parameter is the thickness, once you have chosen the material, a laminate has finale mechanical characteristics that depend both from those of the layers that compose it, both by the number of these layers and especially on their relative orientation.

The use of a laminate therefore requires a planning stage, and verification. The design phase should include the normally design of strength and stiffness. You have to specify that this involves not only the determination of minimum requirements strength and stiffness, according to project needs, but also the type of elastic response (orthotropic, isotropic etc.). A laminate is ultimately a complex material completely by design. The classical theory of laminates responds to this; his objective is indeed to provide a mathematical model capable of synthesize the elastic response of a laminate as if this was simply constituted by a single equivalent layer. Ultimately, it is a process of homogenization of the mechanical characteristics of stiffness, on the thickness of the plate.

The results of the classical theory are condensed into a law, which formalizes the elastic response of the plate equivalent monolayer of the laminate, and having the same total

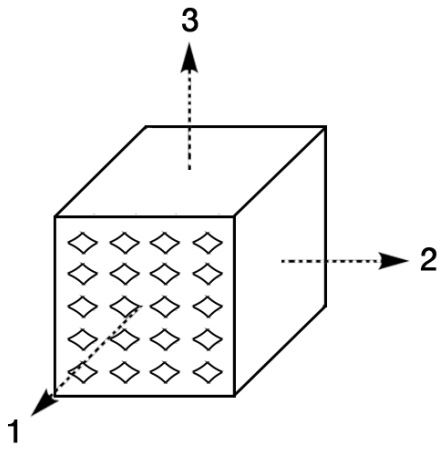

Figure 10.2: Void calculation

thickness. It should be stated from the outset that the classical theory of laminates is only a mathematical model, which is based on classical theory of plates under bending, and that as this is subject to the right critical, even more important in the case of laminates for many factors, as anysotrpy and especially heterogeneity (Overlay layers). Although the theory of lamination does not provide all the mechanical results of relief (especially the stress and deformation out of plane), it is useful in the design phase, and it is indispensable in the prediction of the global elastic characteristics of the laminate. It was said that the classical lamination theory finds its best application in the phase of the project. To date, the laminates design is still research argument, since it does not yet have a single method able to meet all project needs.

For further details, see [42], [44].

10.2 Modules Calculation

The plates will be treated as equivalet orthotropic material. It thus requires four constants for the bonding equations.

Referring to figure 10.3 the parameters to be determined are:

- the longitudinal Young's modulus: E_{11};
- the transverse modulus: E_{22};
- the in-plane shear modulus: G_{12};

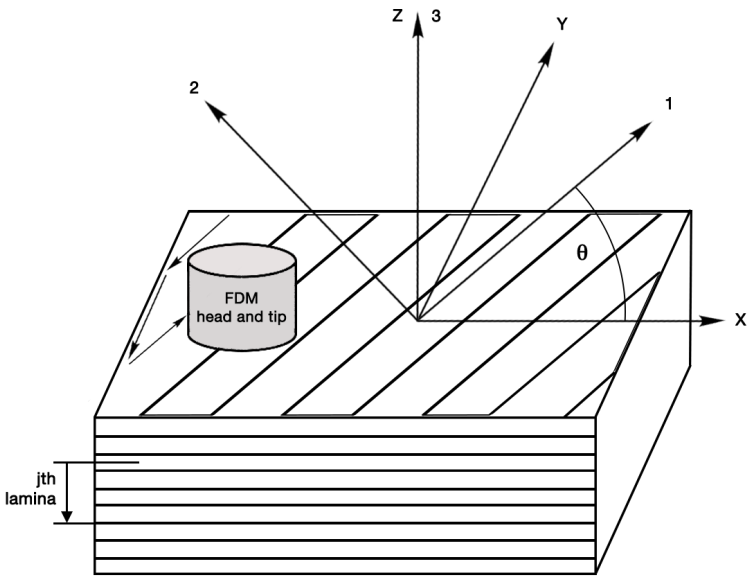

Figure 10.3: FDM - angle of deposition

- the in-plane Poisson ratio: ν_{12}

Since the material with voids can not be considerated as a fiber-renforced material because of the non-perfect bonding among filaments, the classical equation are not considered suitable for material with cavities. Researchers have dimostrated [38] that, the bonding, can never reach the perfect state in FDM state, therefore a new set of equations is proposed to calculate the elastic constant, which can be used to determine the constitutive properies of FDM parts.

The elastic moduli will be calculated as a portion of the total ones, that is [38]

- longitudinal Young's modulus:

$$E_{11} = (1 - \rho_1)E \tag{10.1}$$

  where E is the Young's modulus of polymer;

- transverse modulus:

$$E_{22} = (1 - \sqrt{\rho_1})E \tag{10.2}$$

- in-plane shear modulus:

$$G_{12} = (1 - \sqrt{\rho_1})G \tag{10.3}$$

- in-plane Poisson ratio:

$$\nu_{12} = (1 - \sqrt{\rho_1})\nu \tag{10.4}$$

where ν is the polymer Poisson ratio and ρ_1 is the void density.

For Further informations see B.4.

10.3 Analysis of Void Density

Several parameters affect the resistance of the final material. One of the most important is the void density. Referring to figure 10.2, theorical calculations of strength, modulus and other properties of a composite are based on the volume fraction of its continents.

The methodology employed in this work for parameters starts assuming the possibility of defining a representative volume element (RVE) for the material, represented in figure 10.4. In [62], RVE is defined as 'A material volume which is statistically representative of the infinitesimal material neighborhood of that material point.' Once the RVE is defined, a mathematical homogenization theory is used to transform the constitutive characteristics of a heterogeneous composite material to that of a homogeneous material with 'effective' properties that results in equivalent "average" macroscopic response.

Let recall sintering angle values shown in the previous part. By sintering models it's possible to know the rate of fusion of two polymer filaments, and consequently, by geometric consideration, RVE, void and void area are defined. Void index ρ_1 is calculated as:

$$\rho_1 = \frac{A_{RVE} - A_{filled}}{A_{RVE}} \tag{10.5}$$

In present work, two cases are studied:

1. Circular Shape: the voids are calculated hypothesizing two spheres inscribed in a rectangle;

2. Elliptical shape: the voids are calculate hypothesizing two ellipsis inscribed in a rectangle.

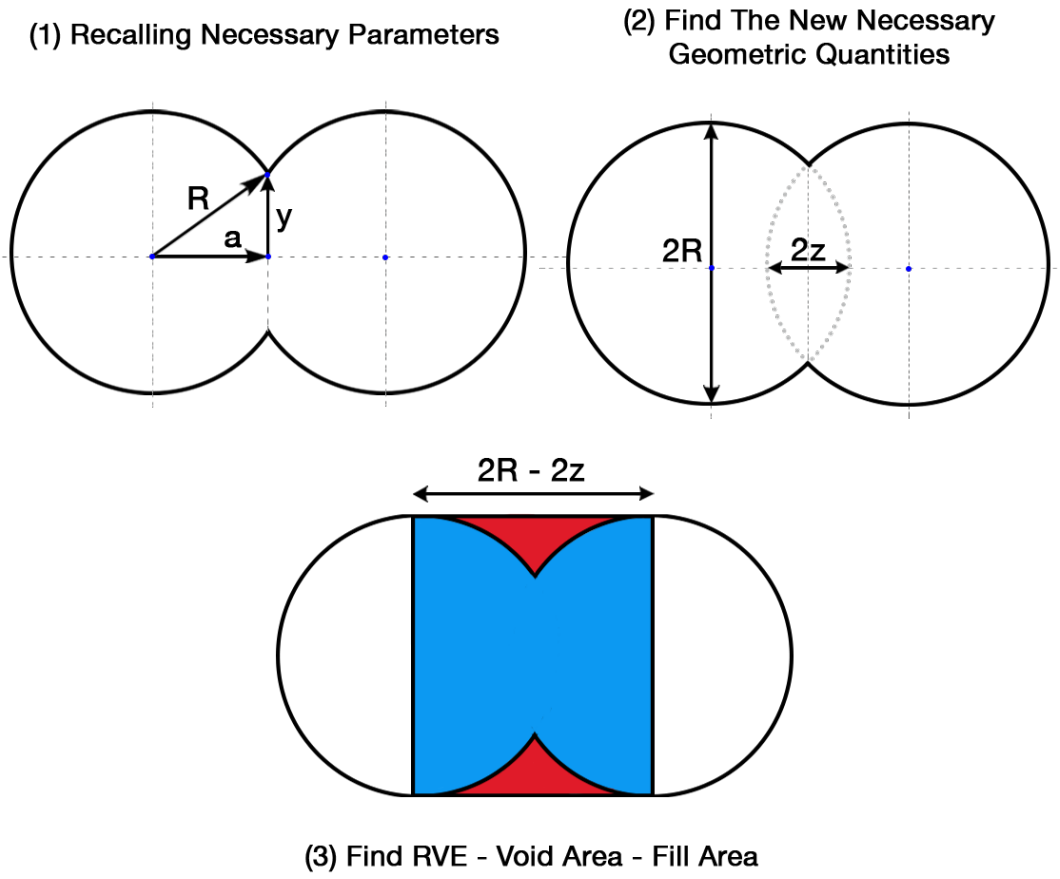

Figure 10.4: RVE calculation procedure

In the first case, using trigonometry and circle formulas, it can be possible to calcolate ρ. For the elliptical shape, it's more complicated to find the void area. Infact, in this case, since it can't be rely on trigonometry, it's necessary to refer to the dimensionless radius (a step before the angle calculation). To calculate the void area, it is needful to use the integral calculus.

The choice of the two models has a precise meaning. According to the authors, the circular pattern, at equal sintering angle achieved, better reflects the size of the voids present. While the elliptical model better reflects the actual shape of the filament. Despite the extruder is circular, during deposition, it is noted that, to reach layers height smaller of the extruder diameter, the filament is often crushed, thus achieving the elliptical shape. Doing experimental tests, it will be selected the model best approximates the real behaviour.

All values of parameters calculated are presented in the following tables:

Model	θ	A_f	RVE	A_e	ρ_1	E_{11}	E_{22}	G_{12}	ν_{12}
	$[Deg]$	$[mm^2]$	$[mm^2]$	$[mm^2]$	[%]	$[Mpa]$	$[Mpa]$	$[Mpa]$	[–]
Frenkel	40.82	0.0541	0.060	0.006	10.6	1967	1484	593	0.17
$\lambda = 0.1$	45.35	0.051	0.056	0.005	10	2002	1541	616	0.18
$\lambda = 10$	36.88	0.056	0.064	0.008	12	1935	1437	575	0.16
$\lambda = 20$	30.86	0.059	0.069	0.010	14.2	1887	1370	548	0.16
$\lambda = 50$	22.01	0.061	0.074	0.013	17.3	1820	1286	514	0.15
$\lambda = 11.4$	35.87	0.057	0.065	0.008	12.4	1927	1425	570	0.16
Elastic	12.84	0.063	0.078	0.016	19.8	1764	1220	488	0.14

Table 10.1: Elastic Moduli: sintering between two spheres (radius = 0.2 mm)

Model	X/a	A_f	RVE	A_e	ρ_1	E_{11}	E_{22}	G_{12}	ν_{12}
	$[Deg]$	$[mm^2]$	$[mm^2]$	$[mm^2]$	[%]	$[Mpa]$	$[Mpa]$	$[Mpa]$	[–]
Frenkel	0.65	0.012	0.013	0.001	7.7	2031	1591	636	0.18
$\lambda = 0.1$	0.71	0.013	0.014	0.001	9.2	1997	1532	613	0.17
$\lambda = 10$	0.60	0.011	0.012	0.001	6.4	2060	1644	658	0.19
$\lambda = 20$	0.51	0.010	0.010	0.000	4.6	2099	1729	692	0.20
$\lambda = 50$	0.37	0.007	0.007	0.000	2.4	2147	1860	744	0.21
$\lambda = 11.4$	0.59	0.010	0.012	0.002	5.0	1916	1410	564	0.16
Elastic	0.22	0.004	0.004	0.000	0.8	2182	2000	800	0.23

Table 10.2: Elastic Moduli: sintering between two Ellipsis (a = 0.2 mm, b = 0.1 mm)

10.4 Circular - Elliptical Comparison

As already mentioned, the circular pattern, at equal sintering angle achieved, better reflects the size of the voids present. While the elliptical model better reflects the actual shape of the filament. In this section, we present a comparison between moduli obtained with the hypothesis of circular shape and that with the elliptical shape. The aim is to study which shape better reflect the real behaviour of material in order to compare it with that obtained with sperimental tests. The following table shows the different (%) of all parameters.

Model	X/a	ρ_E	ρ_C	Err	E_{11_E}	E_{11_C}	Err
	$[Deg]$	[%]	[%]	[%]	$[Mpa]$	$[Mpa]$	[%]
Frenkel	0.65	7.7	10.6	27.68	2031	1967	3.28
$\lambda = 0.1$	0.71	9.2	9.0	2.76	1997	2002	0.27
$\lambda = 10$	0.60	6.4	12.0	47.03	2060	1935	6.44
$\lambda = 20$	0.51	4.6	14.2	67.83	2100	1887	11.25
$\lambda = 50$	0.37	2.4	17.3	86.14	2147	1820.	17.97
$\lambda = 16.8$	0.54	5.0	13.6	62.98	2089	1900	9.94
Elastic	0.22	0.8	19.8	95.82	2182	1764	23.70

Table 10.3: Circular(C) - elliptical(E) comparison (%) - ρ and ρ linearly dependent parameters

Model	X/a	E_{22_E}	E_{22_E}	G_{12_E}	G_{12_E}	ν_{12_E}	ν_{12_E}	Err
	$[Deg]$	$[Mpa]$	$[Mpa]$	$[Mpa]$	$[Mpa]$	[–]	[–]	[%]
Frenkel	0.65	1591	1484	636	593	0.18	0.17	7.22
$\lambda = 0.1$	0.71	1532	1541	613	616	0.17	0.18	0.59
$\lambda = 10$	0.60	1644	1437	658	575	0.19	0.16	14.46
$\lambda = 20$	0.51	1729	1370	692	548	0.20	0.16	26.22
$\lambda = 50$	0.37	1860	1286	744	514	0.21	0.15	44.62
$\lambda = 16.8$	0.54	1706	1388	682	555	0.19	0.16	22.92
Elastic	0.22	2000	1220	800	488	0.23	0.14	63.86

Table 10.4: Circular(C) - elliptical(E) comparison (%) - ρ square root dependent parameters

Chapter 11

Experimental Tests

In this section, numerical moduli obtained by lamination theory will be compared to experimental moduli obtained by traction tests. For experimental procedure we refer to ASTM *D* 3039/*D* 3039*M* standard: *'Standard Test Method for Tensile Properties of Polymer Matrix Composite Materials'* . Tensile tests aim is to evaluate the stress-strain curves and consequently to calculate, by procedure described in the ASTM standard, the elastic modulus of the specimens.

11.1 Test Procedure

We printed 15 specimens: 5 with filaments oriented to 90 degrees (in reference to the longitudinal axis), 5 with filaments to 45 degrees and 5 to 0 degrees. For simplicity, from now, 90 degrees oriented specimens will be call transversal specimens, and 0 degrees oriented will be call longitudinal specimens. Then, we did a total of 15 tensile tests.

Specimens used are represented in figure 11.2

The provine typology is described in the ASTM standard. In figure 11.1 is shown a 45 degrees specimen just printed.

Before proceeding, it was necessary to measure the printed specimens, in order to effectively evaluate the measurement uncertainties and, in case, print defects. We performed six measurements for each chosen section, respectively: width, thickness, distance between markers and the distance between tabs. In table 11.1 are summarized all measurements.

Testing machine and testing software are the same saw in section 8.1. Unlike the relaxation test, now, we used manual grips. We expected a test duration much lower, In fact, the average

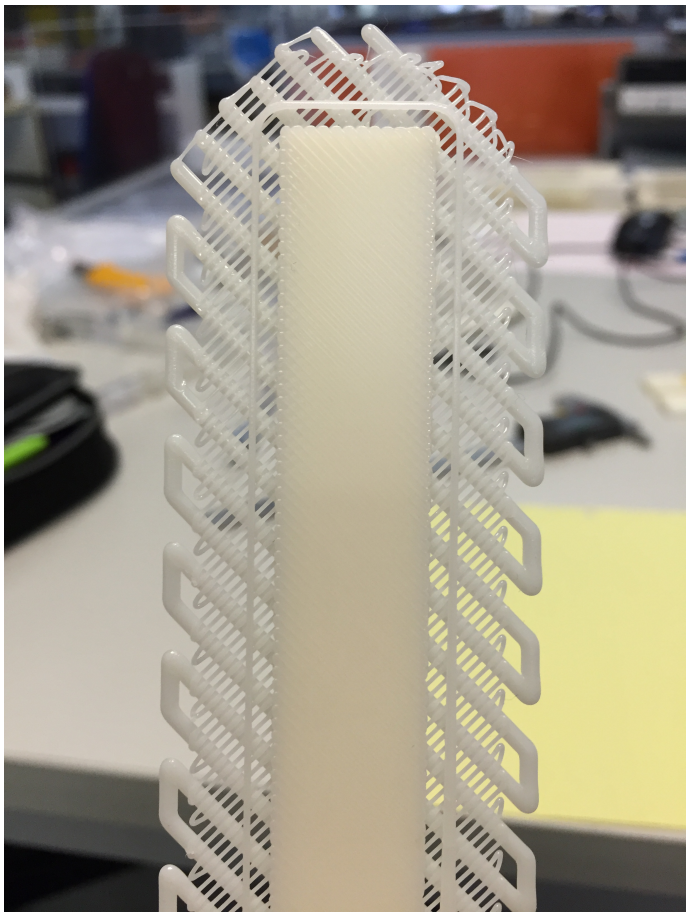

Figure 11.1: 45 Degrees fibers Specimens

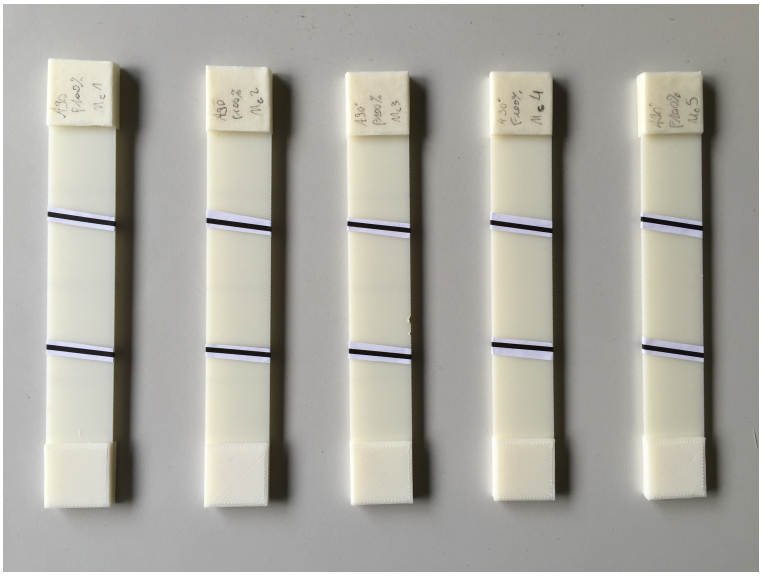

Figure 11.2: Transversal (90 Degrees) fibers Specimens

Specimen Type	Width	Thickness	Markers Distance	Tabs Distance
Transversal Specimens				
A0F100_1	15.28	1.73	29.95	137.01
A0F100_2	15.14	1.71	30.56	137.07
A0F100_3	15.13	1.72	29.94	137.85
A0F100_4	15.10	1.71	31.99	137.19
A0F100_5	15.17	1.72	29.91	137.21
45 Degrees Specimens				
A90F100_1	25.45	2.34	51.60	124.60
A90F100_2	25.42	2.27	51.10	123.84
A90F100_3	25.37	2.26	51.47	124.26
A90F100_4	25.41	2.28	49.42	124.19
A90F100_5	25.46	2.31	52.56	124.92
Longitudinal Specimens				
A45F100_1	15.48	2.29	29.80	137.45
A45F100_2	15.38	2.29	30.94	137.07
A45F100_3	15.48	2.27	31.09	137.13
A45F100_4	15.45	2.28	32.19	137.01
A45F100_5	15.46	2.27	29.61	137.17

Table 11.1: Tensile Test Specimens Measures [mm]

duration of test is about 15-20 minutes each (including time spent to setting machine and exporting data).

11.2 Results

In figures 11.3, 11.5 and 11.4 we can see how the specimens break. It's important to note that, by experimental evidence, that the tabs length influences the failure point along the specimen profile. Infact, in the case of transversal fibers, tabs length is shorter than the grips length, and the sample, breaks in a middle position between tabs. In the others two case, tabs length is greater than than of grips. Infact, the failure point is nearby the tabs starting point. Despite the length of tabs is recommended by the tensile test standard, it would be appropriate to reduce it, in order make it lower than the grips length.

Figure 11.3: Longitudinal Fibers Specimens Failure Point

Tests results are plotted in a txt file. We implemented the results in a MATLAB code. In this manner, we can plot the stress-strain curves. In figures 11.6, 11.7 and 11.8 are shown the obtained curves.

As we expected, the longitudinal specimens, have a pick resistence value higher than the others two. We also can see that, according to the orientation values of fibers, in addition to strength, also failure behaviour is different. In the 90 degrees case, we observe a fragile behaviour; once the maximum tolerable stress is reached, the specimen breaks. In the longitudinal case, after the pick values, probably, some materials fibers break and consequently,

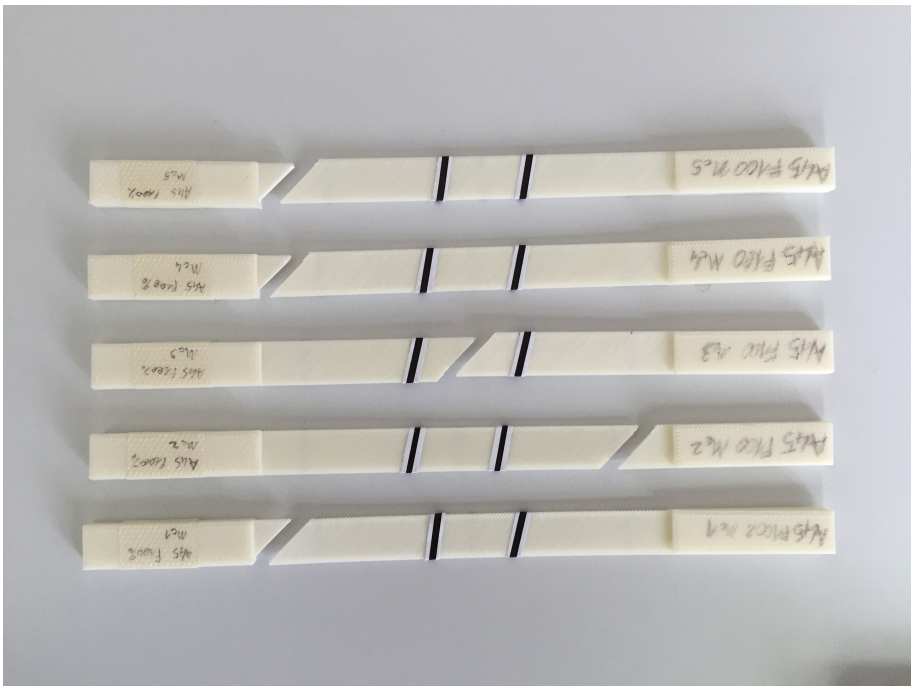

Figure 11.4: 45 Degrees Fibers Specimens Failure Point

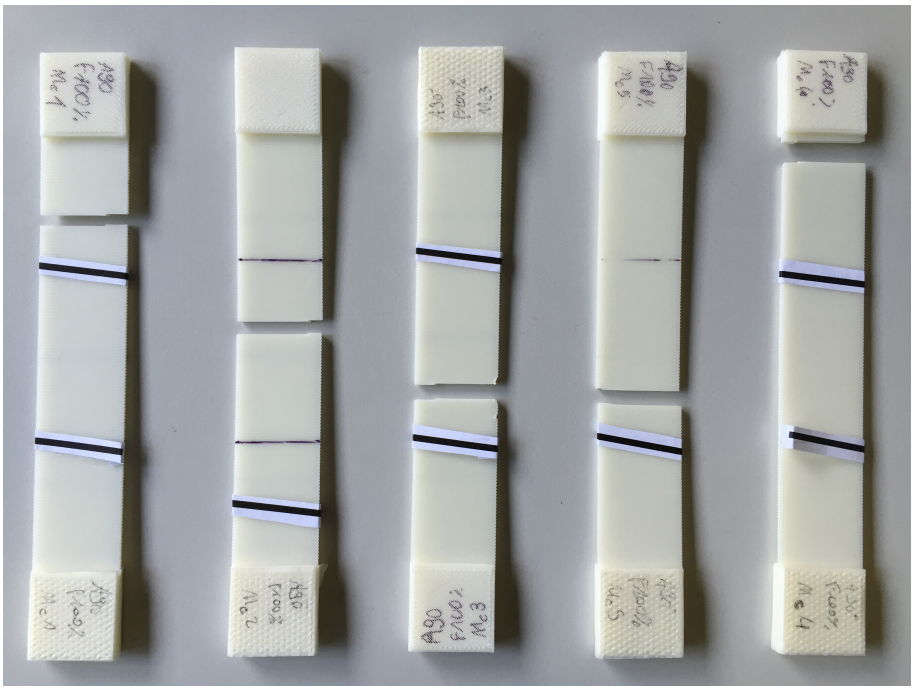

Figure 11.5: Transversal Specimens Failure Point

the stress deacreases in steps. In one case, we reached an elongation of about 1.5 cm. In the case of 45 degress fibers, 3d printed solid shows a perfect plastic behaviour.

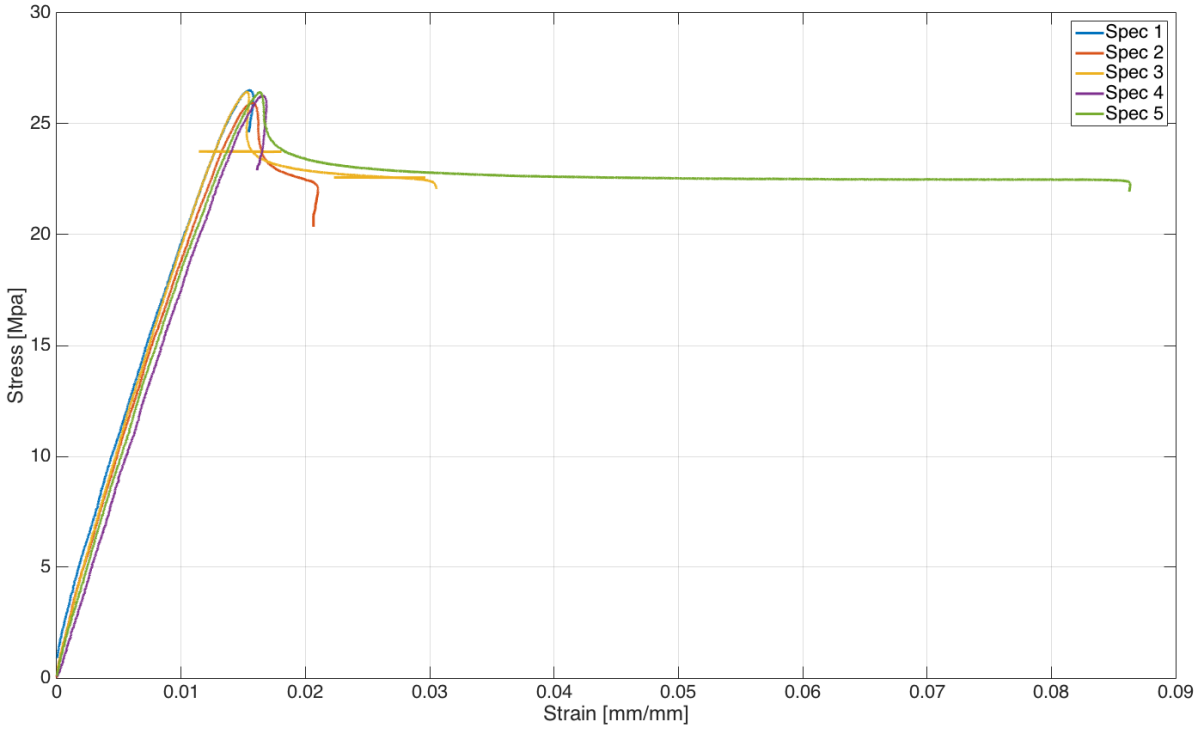

Figure 11.6: Longitudinal Fibers Specimens Stress-Strain Curve

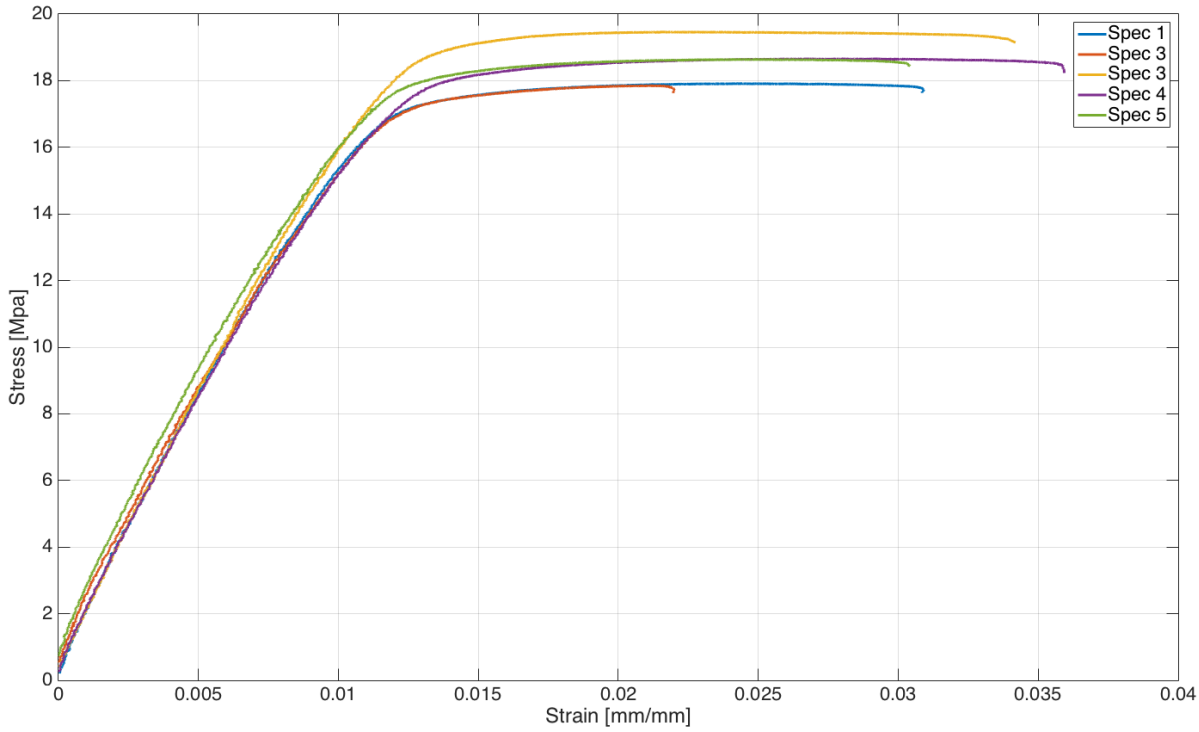

Figure 11.7: 45 Degrees Fibers Specimens Stress-Strain Curve

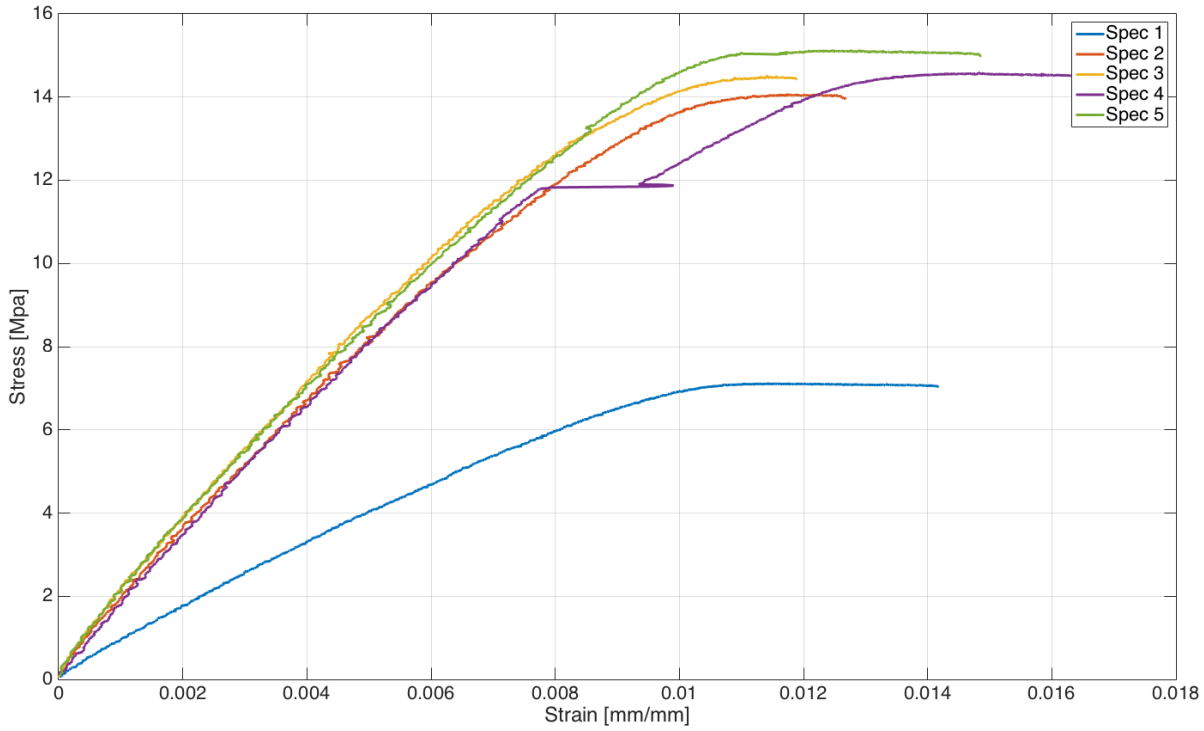

Figure 11.8: Transversal Specimens Stress-Strain Curve

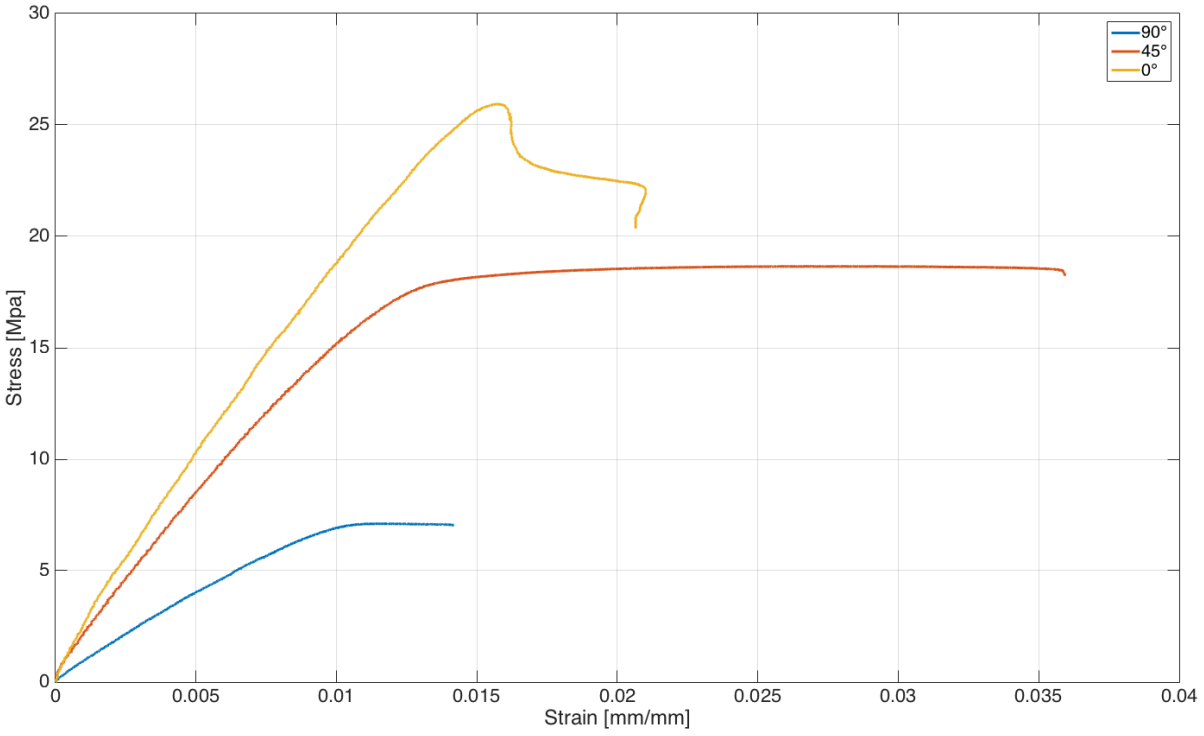

Figure 11.9: Comparison - Stress-Strain Curve

In figure 11.9, we can see the comparison between three different fibers-oriented specimens. It's immediately evident that, Young's modulus decreases with the increasing of fiber orientation, starting from 0 degrees, up to 90 degrees.

Now, we want to check if the 3D printed solids behave actually as an orthotropic transversely isotropic material. In figure 11.10 is shown the moduli values with their probability dispersion. Referring to theese results, and since the moduli values of 0 degrees specimens and 90 degrees specimens, don't overlap, we can say, with good probability that material is an orthotropic transversely isotropic material.

In this manner, we can enhance the lamination theory used for the moduli calculation.

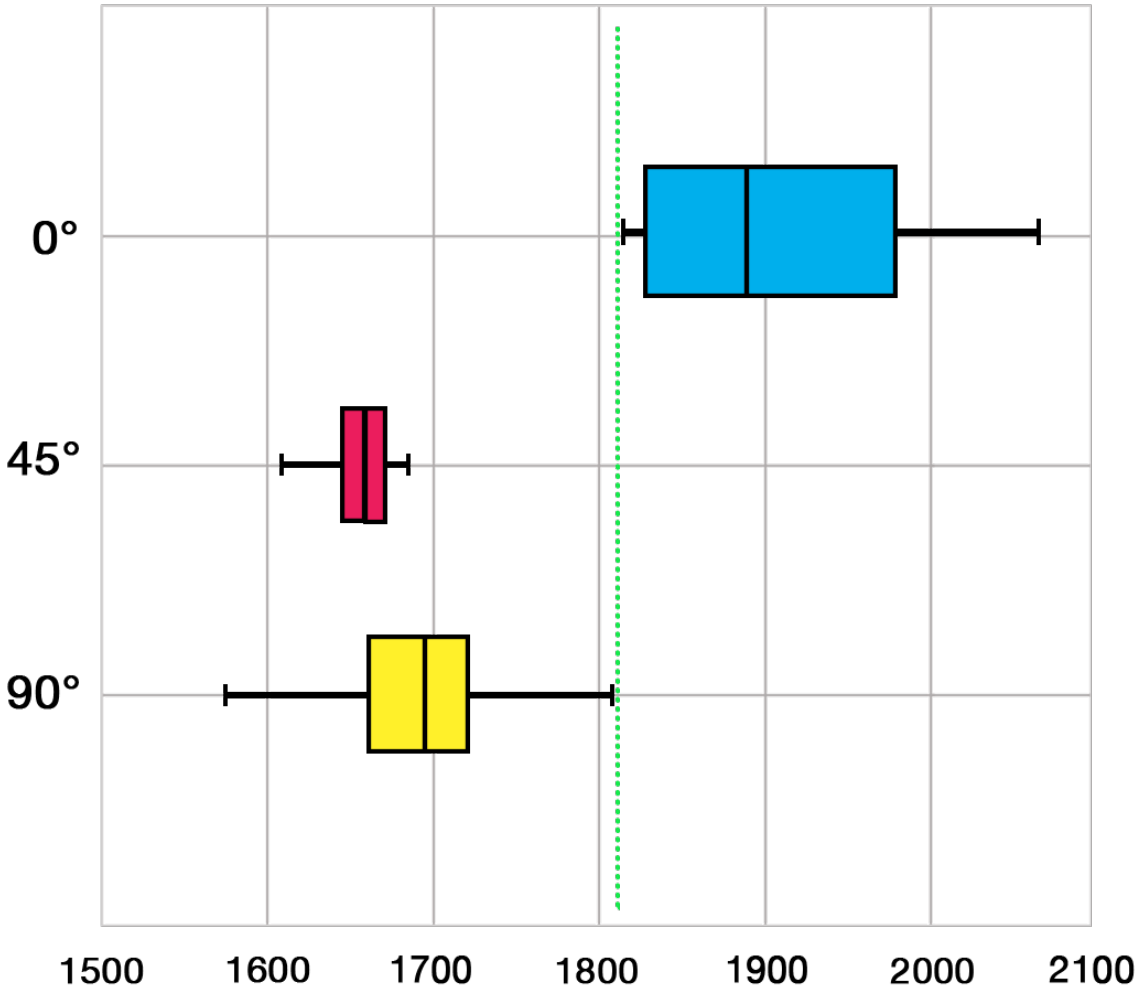

Figure 11.10: Moduli Values Dispersion

Chapter 12

Experimental - Numerical Moduli Comparison

By method shown in ASTM standard we can calculate Young's modulus.

In table 12.1, are shown the obtained moduli.

Specimen	**Young Modulus 90°**	**Young Modulus 45°**	**Young Modulus 0°**
Spec 1	1751	1687	1834
Spec 2	1681	1667	1818
Spec 3	1712	1657	2071
Spec 4	1606	1609	1956
Spec 5	818	1632	2006
Average	**1687**	**1650**	**1937**

Table 12.1: Young's Moduli Calculated by Tensile Tests [Mpa]

Since the tensile tests have been done in the longitudinale direction, only the longitudinal and transversal Young moduli will be compared. Furthermore, we see that the specimen 5 with fibers at 90 degrees, has localized weaknesses, in fact the test results, in terms of elastic modulus are much different from the others. For These Reasons, this test will be neglected in the moduli calculus.

In the table 12.2 we can see the matching of our data with the real data obtained with experimental tests.

Model	$E_{11_{EXP}}$	$E_{11_{ELL}}$	$E_{11_{CIRC}}$	**Error** $(E_{11_{ELL}})$	**Error** $(E_{11_{CIRC}})$
	$[Mpa]$	$[Mpa]$	$[Mpa]$	[%]	[%]
Frenkel - Eshelby	1937	2031	1967	4.6	1.5
Maxwell $\lambda = 11.4$	1937	1916	1927	1.1	0.5
Elastic	1937	2182	1764	11.2	9.8
Model	$E_{22_{EXP}}$	$E_{22_{ELL}}$	$E_{22_{CIRC}}$	**Error** $(E_{22_{ELL}})$	**Error** $(E_{22_{CIRC}})$
	$[Mpa]$	$[Mpa]$	$[Mpa]$	[%]	[%]
Frenkel - Eshelby	1687	1590.79	1483.62	6.1	13.7
Maxwell $\lambda = 11.4$	1687	1409.59	1424.99	19.7	18.4
Elastic	1687	1999.73	1436.62	15.6	17.4

Table 12.2: Young's Moduli Comparison

Firstly, we can say that the matching is very good, especially for the longitudinal Young modulus. The Model that better reflects the real material behaviour is the viscoelastic Model. The error is near 1%.

In the case of Transversal Modulus, the matching is slightly less good. The error is near 6% for the elliptical shape and near 14% for the circular shape. The important thing is that, for E_{22} the model that bettere reflects the material real behaviour is Frenkel Model, that is a pure Viscous Model.

Finally, we can say that, our model predict in a specific manner, the longitudinal modulus. Infact, in our work, we haven't taken into account other parameters that influence the solid obtained by 3D printing, particularly, the angle of deposition and the orientation of the fibers. Probably, introducing in our analytical model, a factor which evaluates the influence of the aforementioned parameters, it would be possible to correct results and get a better matching even in the case of transversal Modulus.

In figures 12.1, 12.2 are compared the different moduli values and in figures 12.4, **??** are compared the relative errors.

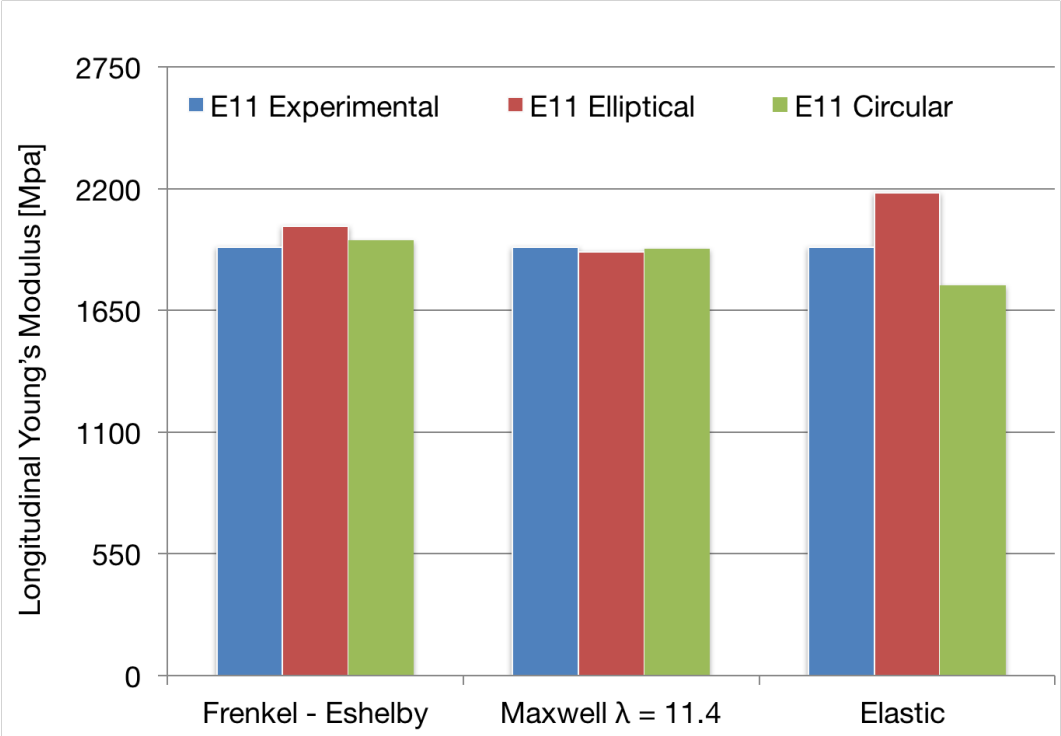

Figure 12.1: Longitudinal Young Modulus Comparison

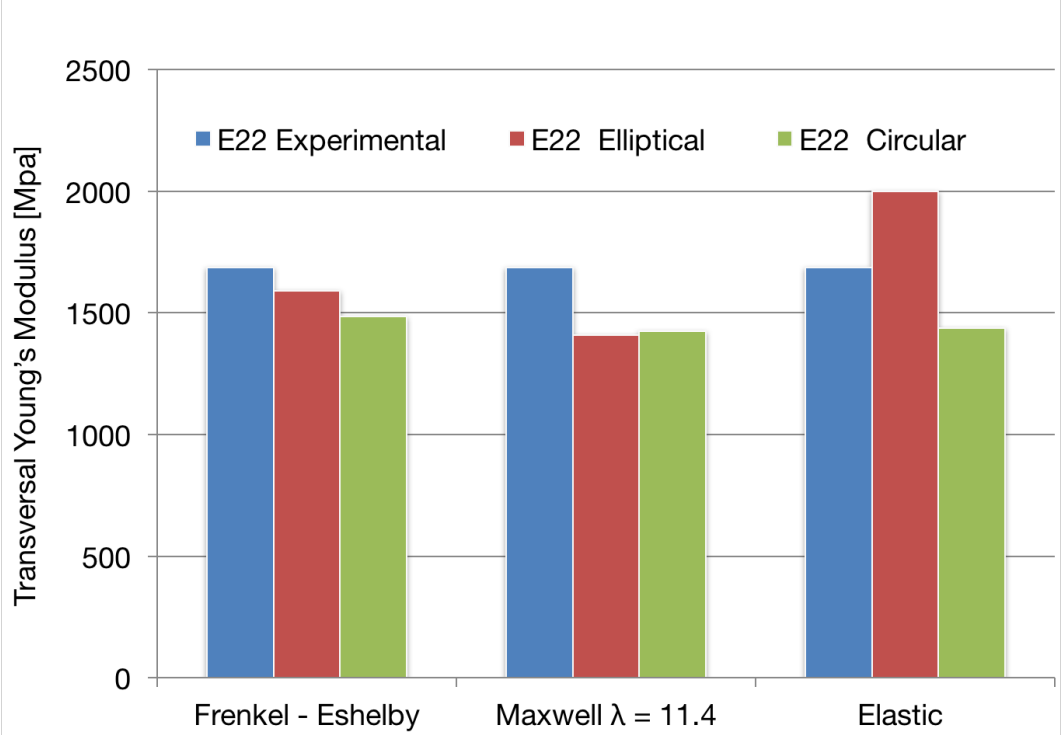

Figure 12.2: Transversal Young Modulus Comparison

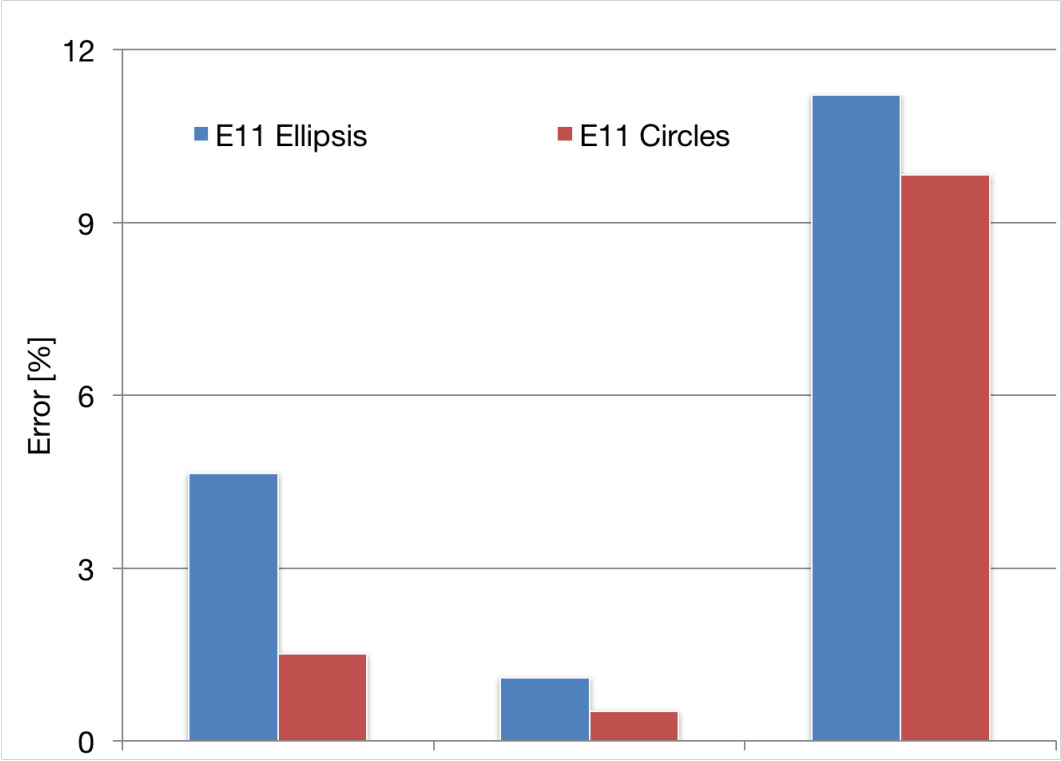

Figure 12.3: Longitudinal Young Modulus Error Comparison

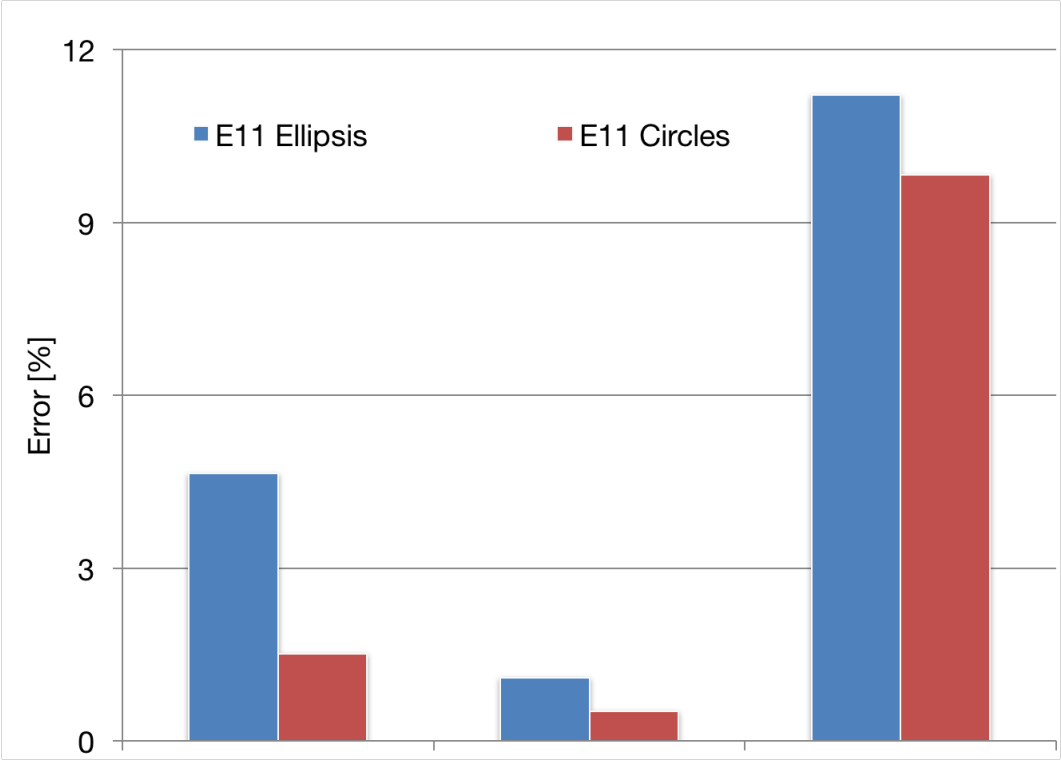

Figure 12.4: Longitudinal Young Modulus Error Comparison

Chapter 13

Conclusions and Future Developements

In this thesis, thermal process during the FDM extrusion was analyzed and the cooling temperature profile of the extruded filament was obtained. We can conclude that the filament will not be maintained above glass transition T_g long enough for perfect bonding to occur. Because of imperfect bonding, the existing methods of calculating the elastic constants of solid with voids are not adequate. We can also conclude that, the critical time in which bonding stops, can be modified changing filament dimensions or changing distance between deposited filaments. If we depose a filament with larger dimensions, closer to the previous, bonding phenomenon will probably totally occours.

Once found the temperature profile, we could go into details analysing how bonding really happens. Sintering is a very complex process involving several multiphysics phenomena. From a practical point of view there are many variables we have to control in order to obtain the desired properties of the final product. Because of these many variables and their interdependency, it's difficult to extract useful information from analytical data. Therefore numerical simulations represent a powerful tool that can provide meaningful information about this phenomena.

Considering the numerical tools available aiming at the simulation of the sintering process at the particle scale, a lack of a numerical approach able to handle the different diffusion mechanisms, complex geometries, and strong topological changes in 2D and even more drastically in 3D became evident.

In order to comprend how the made simplifications, lead to results that loose physical

meaning, In the present thesis, a simple numerical strategy, based on stabilized mixed finite elements, was developed for simulating sintering both by surface and volume diffusions. A characteristic of the proposed approach for volume diffusion, is to express the mass flux with respect to the gradient of pressure. Hence, contrary to the literature, where grains are considered as rigid bodies, grains were assumed to behave as elastic bodies. We can conclude that, modeling the fused polymer as a linear elastic simplified material, displacement, pressure and density obtained are not comparable to real displacements and real matarial properties.

We also present three analytical sintering models: viscous, viscoelastic and elastic. As we have already discussed, the real polymer behaviour depends on λ value, and thus, the material, can be modeled with good approximation. An experimental test has been done in order to evaluate λ and, with good approximation, we reached the sintering angle correct value.

Once obtined sintering angles, we proceded to evaluate the void density. We simulate the density obtained with sintering of two spheres and with sintering of two ellipsis. The elliptical shape hypothesis aims to simulate the deposited filament, with a dimension that is much greater than other two dimensions. In this manner, the filament is cutted and only studied in the two similar dimensions, i.e. the two radius.

The bonding is just one of many factors that influence the final product; different deposition densities, orientations and theis combinations can be employed in producing the required stiffness properties of manufactured parts. Considering different combinations of raster angles in succesive layers, it's obvious that a large variety of laminates may be crated. This work represent the first step to predict the final material behaviour.

Sperimental tests on different layered specimens show how material behaviour is affected by the deposition angle.

From data obtained by tensile tests, we can affirm, with good approximation that 3D printed material behave as an orthotropic transversely isotropic material.

In future, there are many possible developements. Referring to experimental tests, it could be considered in a more correct way the transverse Young modulus and perform other tests for calculation of Poisson Ratio and conseguently, the shear modulus. One other important step we can think to do is to develop a more accurate FEM simulation, in order to allows to cope with the severe topological changes and complex geometries that characterize the sintering process.

As regards the choice finite element (Quad-4), using a bilinear quadrilater finite element

with 9 nodes with quadratic shape functions, we can get a higher precision and definitely better numerical stability . In this way, it would be possible to give to the second derivatives of the shape functions, more physical meaning (it would remain constant in the quadratic case, while in QUAD-4 results 0 due the linear form); and the problem encountered in the two-field-mixed FEM formulation, will thus partly eliminated.

Furthermore, we can simulate the real material behaviour including non linear terms, but it's important to highlight that this kind of simulations are computationally very expensive, especially in 3D.

It's possible to extend present work to all other issues that affect the mechanical properties of the final solid, as raster angle, non-isothermal conditions, ... However, our results represent an optimal start point to future improvements in this research field.

Appendix A

Basic Equations

A.1 Fick's Law

Fick's laws of diffusion describe diffusion, it relates the diffusive flux to the concentration under the assumption of steady state. It postulate that the flux goes from region of high concentration to regions of low concetration with a magnitude that is proportional to the concentration gradient (spatial derivative), or in simplistic terms the concept that a solute will move from a region of high concentration to a region of low concentration across a concentration gradient. In one (spatial) dimension, the law is:

$$J = -D\nabla\phi \tag{A.1}$$

where J is the diffusion flux $\left[\frac{mol}{m^2 s}\right]$, D is the diffurion coefficent or diffusivity $\left[\frac{m^2}{s}\right]$, ϕ is the concentration $\left[\frac{mol}{m^3}\right]$.

The driving force for the one dimensional diffusion is the quantity $-\frac{\partial\phi}{\partial x}$ which for ideal mixtures is the concentration gradient. In chemical systems other than ideal solutions or mixtures, the driving force for diffusion of each species is the gradient of chemical potential of this species. Then Fick's first law (one-dimensional case) can be written as:

$$J_i = -\frac{Dc_i}{RT}\frac{\partial\mu_i}{\partial x}$$

where the index i denotes the ith species, c is the concentration (mol/m^3), R is the universal gas constant $(J/(Kmol))$, T is the absolute temperature (K), and μ is the chemical potential (J/mol).

A.2 Substantial derivate

The substantial derivate of a generic (scalar or vector) quantity Φ is defined as follow:

$$\frac{\mathbf{D}\Phi}{\mathbf{D}t} = \frac{\partial \Phi}{\partial t} + \boldsymbol{v}\frac{\partial \Phi}{\partial \boldsymbol{x}} \tag{A.2}$$

A.3 Time-derivative of volume integral in Euler formulation

Let us consider a scalar field $\boldsymbol{\phi}(\boldsymbol{y}, t)$ and a volume integral over the current deformed domain Ω:

$$I = \int_{\Omega} \boldsymbol{\phi}(\boldsymbol{y}, t) dV \tag{A.3}$$

Changes in $I(t)$ are due to two different phenomena:

1. change of $\Phi(..., t)$ inside of the fixed domain Ω over time dt:

$$dI_1 = \int_{\Omega} \frac{\partial \boldsymbol{\phi}(\boldsymbol{y}, t)}{\partial dt} dt dV = dt \int_{\Omega} \frac{\partial \boldsymbol{\phi}(\boldsymbol{y}, t)}{\partial dt} dy \tag{A.4}$$

2. Time flow (in-out flow) of continuum through $\partial\Omega$:

$$dI_2 = \int_{\partial\Omega} \Phi \boldsymbol{n} \cdot \boldsymbol{v} dt d\Gamma = dt \int_{\partial\Omega} \Phi n_i v^i d\Gamma \tag{A.5}$$

By the Divergence theorem:

$$dI_2 = \int_{\Omega} \frac{\partial}{\partial y^i}(\Phi v^i) dV \tag{A.6}$$

Then, by Eq. A.2, we obtain:

$$\begin{aligned} \frac{DI}{Dt} = \frac{d}{dt}(I_1 + I_2) = \int_{\Omega} \left[\frac{\partial \Phi}{\partial t} + \frac{\partial}{\partial y^i}(\Phi v^i) \right] dV = \\ = \int_{\Omega} \left[\frac{\partial \Phi}{\partial t} + v^i \frac{\partial}{\partial y^i}(\Phi) + \Phi \frac{\partial}{\partial y^i}(v^i) \right] dV = \int_{\Omega} \left[\frac{\mathbf{D}\Phi}{\mathbf{D}t} + \Phi \frac{\partial v^i}{\partial y^i} \right] dV \end{aligned} \tag{A.7}$$

A.4 Diffusion Coefficient

Diffusivity or diffusion coefficient is a proportionality constant between the molar flux due to molecular diffusion and the gradient in the concentration of the species (or the driving force for diffusion). Diffusivity is encountered in Fick's law and numerous other equations of physical chemistry.

The diffusivity is generally prescribed for a given pair of species and pairwise for a multi-species system. The higher the diffusivity (of one substance with respect to another), the faster they diffuse into each other. Typically, a compound's diffusion coefficient is $10,000$ times as great in air as in water.

Diffusivity has an SI unit of $[m^2/s]$ ($length^2/time$).

The diffusion coefficient in solids at different temperatures is generally found to be well predicted by the Arrhenius equation:

$$D = D_0 e^{-E_A/(kT)} \tag{A.8}$$

where:

- D is the diffusion coefficient (m^2/s);
- D_0 is the maximum diffusion coefficient (at infinite temperature, m^2/s);
- E_A is the activation energy for diffusion in dimensions of ($Jatom^{-1}$);
- T is the temperature (K);
- k is the Boltzmann constant.

Appendix B

Mechanics Recalls

Let us recall some important concepts of thermodynamic of continuum.

B.1 First Law of Thermodynamics: Conservation of Energy

Let us remark some basic state variable, which physical nature is linked to statistical mechanics beyond the scope of this lecture. We can consider them as certain averaged characteristics of the particle nature of the continuum:

- Temperature T: intensive quantity, ie. there is no 'specific temperature' or 'temperature per unit mass';
- Internal energy U and thermodynamical entropy S: extensive quantities, one defines specific internal energy ϵ and specific entropy η so that:

$$U = \int_\Omega \rho \epsilon dV \qquad S = \int_\Omega \rho \eta dV \tag{B.1}$$

The change of the kinetic and internal energy $\delta(K + U)$ of a body ω is equal to the work δW of mechanical forces and heat δQ, in formula:

$$\dot{K} + \dot{U} = \dot{W} + \dot{Q} \tag{B.2}$$

Now we have to apply the time derivate formula described in Eq. A.7, then:

- Time derivate of K:

$$K = \frac{1}{2}\int_\Omega \rho|v|^2 dV = \frac{1}{2}\int_\Omega \rho v^i v_i dV \tag{B.3}$$

$$\begin{aligned}\frac{DK}{Dt} &= \frac{1}{2}\int_\Omega \frac{\boldsymbol{D}(\rho \boldsymbol{v}^2)}{\boldsymbol{D}t} dV + \frac{1}{2}\int_\Omega \rho \boldsymbol{v}^2 \frac{\partial v^i}{\partial y_i} dV = \frac{1}{2}\int_\Omega \rho \frac{D(\boldsymbol{v}^2)}{Dt} dV + \\ &\frac{1}{2}\int_\Omega \boldsymbol{v}^2 \underbrace{\left(\frac{\boldsymbol{D}\rho}{\boldsymbol{D}t} + \rho \frac{\partial v^i}{\partial y_i}\right)}_{=0 \text{ by continuity eqsigma.}} dV = \frac{1}{2}\int_\Omega \rho \frac{D(\boldsymbol{v}^2)}{Dt} dV\end{aligned} \tag{B.4}$$

- Time derivate of U:

$$U = \int_\Omega \rho \epsilon dV \tag{B.5}$$

$$\frac{DU}{Dt} = \int_\Omega \rho \frac{D\epsilon}{Dt} dV \tag{B.6}$$

- Time derivate of heat Q:

$$\frac{DQ}{Dt} = -\int_\Omega \frac{\partial q^i}{\partial y^i} dV + \int_\Omega \rho h dV \tag{B.7}$$

  Here, q^i is the heat flux $[Jm^{-2}s^{-1}]$ and h is the specific heat source intensity $[Jkg^{-1}s^{-1}]$. The minus sign appears because n is the external normal.

- Time derivate of mechanical work W (power):

$$\frac{DW}{Dt} = -\int_\Omega \frac{\partial(\sigma^{ij} v_i)}{\partial y^j} dV + \int_\Omega \rho f^i v_i dV \tag{B.8}$$

Finally, for any $\omega \subset \Omega$, subdomain of continuum, the conservation of energy can be written as:

$$\int_\omega \left(\frac{\rho}{2}\frac{D(\boldsymbol{v}^2)}{Dt} + \rho \frac{D\epsilon}{Dt}\right) dV = \int_\omega \left(\rho h - \frac{\partial q^i}{\partial y^i} + \frac{\sigma^{ij} v_i}{\partial y^j} + \rho f^i v_i\right) dV \tag{B.9}$$

Hence:

$$\rho \frac{D\epsilon}{Dt} = \rho h + -\frac{\partial q^i}{\partial y^i} + \sigma^{ij} \frac{\partial v_i}{\partial y^j} + \underbrace{v_i \left(-\rho \frac{Dv^i}{Dt} + \frac{\partial \sigma^{ij}}{\partial y^j} + \rho f^i \right)}_{= 0 \text{ by force equilibrium.}} \tag{B.10}$$

And, we obtain the energy equation:

$$\rho \frac{D\epsilon}{Dt} = \rho h - \nabla_i q^j + \sigma^{ij} \cdot \nabla_j v_i \tag{B.11}$$

B.2 Second Law of Thermodynamics: Entropy

The change of total entropy in the body Ω over time is greater or equal to the sum of entropy flow over the boundary $\partial\Omega$ from the exterior and the entropy produced by internal heat sources on Ω.

Total entropy $[J/K]$, defined up to a constant by:

$$dS = \frac{dQ}{T} \tag{B.12}$$

B.3 Mathematical form of the 2nd law of thermodynamics - Clausius-Duhem inequality

$$\frac{DS}{Dt} \geq \int_\Omega \frac{\rho h}{T} dV - \int_{\partial\Omega} \frac{1}{T} \boldsymbol{q} \cdot \boldsymbol{n} d\Gamma \tag{B.13}$$

where, the sign '=' is for reversible processes, while the sign '>' is for irreversible ones.

Derivation

Using the specific entropy η:

$$\frac{D}{Dt} \left(\int_\Omega \rho \eta dV \right) \geq \int_\Omega \frac{\rho h}{T} dV - \int_{\partial\Omega} \frac{1}{T} \boldsymbol{q} \cdot \boldsymbol{n} d\Gamma \tag{B.14}$$

Time-derivative of an integral formula and the Divergence theorem:

$$\int_\Omega \rho \frac{D\eta}{Dt} dV + \underbrace{\int_\Omega \eta \frac{D\rho}{Dt} + \int_\Omega \rho \eta \frac{\partial v^i}{\partial y^i} dV}_{= 0 \text{ by continuity equation.}} - \int_\Omega \frac{\rho h}{T} dV + \int_\Omega \frac{\partial}{\partial y^i} \left(\frac{q^i}{T} \right) dV \geq 0 \tag{B.15}$$

and we obtain the Clausius-Duhem inequality in the integral form:

$$\int_\Omega \rho \frac{D\eta}{Dt} dV - \int_\Omega \frac{\rho h}{T} dV + \int_\Omega \frac{\partial}{\partial y^i}\left(\frac{q^i}{T}\right) dV \geq 0 \tag{B.16}$$

Local (pointwise) form of Clausius-Duhem inequality:

$$\rho\dot{\eta} - \frac{\rho h}{T} + \frac{\partial}{\partial y^i}\left(\frac{q^i}{T}\right) \geq 0 \qquad \text{or} \qquad \rho T\dot{\eta} - \rho h + \nabla_i q^i - \frac{q^i}{T}\nabla_i T \geq 0 \tag{B.17}$$

Clausius-Duhem inequality with Helmholz free-energy

By itself S does not have any meaning. However, dST is the increase of the portion of internal energy which cannot be used to do work.

We can define the Specific Helmholz free energy φ: the density of mechanically exploitable internal energy:

$$\varphi = \epsilon - T\eta \tag{B.18}$$

Deriving φ in time:

$$\dot{\varphi} = \dot{\epsilon} - \dot{T}\eta - T\dot{\eta} \tag{B.19}$$

and substitute into the Clausius-Duhem inequality. Express $\nabla_i q^i$ from the energy equation:

$$\nabla_i q^i = -\rho\dot{\epsilon} + \rho h + \sigma^{ij}\nabla_j v_i \tag{B.20}$$

And now, plug it into Clausius-Duhem inequality:

$$0 \geq \rho T\dot{\eta} + \rho h - \nabla_i q^i + \frac{q^i}{T}\nabla_i T =$$

$$-\rho T\dot{\eta} + \rho h - \rho\dot{\epsilon} - \rho h - \sigma^{ij}\nabla_j v_i + \frac{q^i}{T}\nabla_i T = \tag{B.21}$$

$$\rho\dot{\varphi} + \rho\dot{T}\eta - \sigma^{ij}\nabla_j v_i + \frac{q^i}{T}\nabla_i T$$

And we obtain the dissipation inequality:

$$\underbrace{\rho\dot{\varphi} + \rho\dot{T}\eta - \sigma^{ij}\nabla_j v_i}_{\equiv -\delta,\ \text{internal dissipation.}} + \frac{q^i}{T}\nabla_i T \geq 0 \tag{B.22}$$

Remarking that:

$$\dot{\epsilon}(t) = \frac{d\epsilon}{dt} = \frac{d}{dt}\left(\frac{L(t) - L_0}{L_0}\right) = \frac{1}{L_0}\frac{dL}{dt}(t) = \frac{v(t)}{L_0} \tag{B.23}$$

we can write the dissipation inequality as:

$$\rho\dot{\varphi} + \rho\dot{T}\eta - \sigma^{ij} : \dot{\epsilon}^{ij} + \frac{q^i}{T}\nabla_i T \geq 0 \tag{B.24}$$

B.4 Elastic Moduli Modeling. Mechanics of Materials Approach

In the following definitions, these assumption are made:

- Extruded ABS fibers are linear-elastic and isotropic;
- perfect bonding between fibers.

Referring on figure 10.2, the void area on a plane normal to the fibers, A_v, can be written as:

$$A_v^1 = \sum c l_i^2 \tag{B.25}$$

where l is a characteristic length, and c is a shape factor depending on void tipology [38]. Now, ones defined the RVE as seen in chapter 10, the areal void density in the plane normal to the fiber is given by:

$$A_v^1 = \rho_1 \bar{A} = \rho_1 L^2 \tag{B.26}$$

Equating eqts B.25 and B.26, we can write:

$$l = \sqrt{\frac{\rho_1}{c}} L \tag{B.27}$$

Now, as did before, we can also define the void area in orthogonal plane 2. In formula:

$$A_v^2 = \sqrt{\frac{\rho_1}{c}} \bar{A} = \sqrt{\frac{\rho_1}{c}} L^2 \tag{B.28}$$

Recalling that: $A_i = \bar{A} - A_v^i$, we obtain:

$$A_1 = (1 - \rho_1)A \qquad A_2 = (1 - \sqrt{\rho_1})A \tag{B.29}$$

To obtain the effective shear modulus in the two principal directions, identical bubes of actual and effective materials of side length dx are considered. Applying an uniform load F along principal direction 1 and 2, elongation along the direction of load F, for both materials, are given by

$$\delta^{het} = \frac{F dx}{A_i E} \qquad \delta^{hom} = \frac{F dx}{\bar{A}_i \bar{E}} \tag{B.30}$$

where E is Young's modulus of material, $\bar{A}$, is the cross sectional area of the RVE ($dx2$), and A_i is the material cross section in the heterogenous material.

Equating elungations, and by Eq. B.30, we obtain

$$\bar{E}_1 = (1 - \rho_1)E \qquad \bar{E}_2 = (1 - \sqrt{\rho_1})E \tag{B.31}$$

The effective shear moduli, G_{ij}, are determined by considering equal magnitude forces, F, applied to each face of the RVE, inducing a homogeneous shear strain γ in the material. The shear deformation in the heterogeneous and homogeneous material are:

$$e_{ij}^{het} = \frac{1}{2}\left(\frac{F/A_i}{G} + \frac{F/A_j}{G}\right) \qquad e_{ij}^{hom} = fracF/\bar{A}\bar{G} \tag{B.32}$$

where G is the effective material shear modulus. By Eq. B.29 and equating shear stresses defined above, we obtain:

$$\bar{G}_{12} = (1 - \sqrt{\rho_1})G \tag{B.33}$$

For the effective Poisson's ratio formulation, a constant stress s is applied along the $i-th$ direction, while keeping all others equal to zero. The elongations in the $j-th$ direction for the actual and effective material are given by:

$$\delta_j^{het} = \nu\frac{\sigma}{E} \qquad \delta_j^{hom} = \bar{\nu_{ij}}\frac{\sigma}{\bar{E}_i} \tag{B.34}$$

where ν is the effective material Poisson's ratio. As done before, results obtained are:

$$\bar{\nu}_{12} = (1 - \sqrt{\rho_1})\nu \tag{B.35}$$

Appendix C

Finite Element Formulation

C.1 Gauss - Legendre Quadrature

In numerical analysis, a quadrature rule is an approximation of the definite integral of a function, usually stated as a weighted sum of function values at specified points within the domain of integration.

Following figure, shows the integration points used in the Gaussian integration.

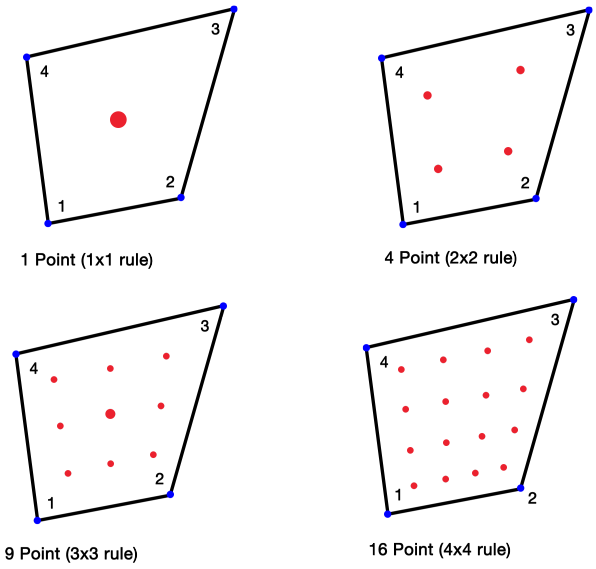

An n-point Gaussian quadrature rule, named after Carl Friedrich Gauss, is a quadrature rule constructed to yield an exact result for polynomials of degree $2n-1$ or less by a suitable choice of the points x_i and weights w_i for $i = 1, ..., n$. The domain of integration for such a

rule is conventionally taken as [−1, 1], so the rule is stated as

$$\int_{-1}^{1} f(x)\,dx = \sum_{i=1}^{n} w_i f(x_i). \tag{C.1}$$

Gaussian quadrature as above will only produce good results if the function $f(x)$ is well approximated by a polynomial function within the range $[-1, 1]$.

Some low-order rules for solving the integration problem are listed in table C.1.

Number of Points	Gauss Point	Gauss Weights
1	0	2
2	$\pm\sqrt{\frac{1}{3}}$	1
3	0	$\frac{8}{9}$
	$\pm\sqrt{\frac{3}{5}}$	$\frac{5}{9}$
4	$\pm\sqrt{\frac{3}{7} - \frac{2}{7}\sqrt{\frac{6}{5}}}$	$\frac{18+\sqrt{30}}{36}$
	$\pm\sqrt{\frac{3}{7} + \frac{2}{7}\sqrt{\frac{6}{5}}}$	$\frac{18-\sqrt{30}}{36}$
5	0	$\frac{128}{225}$
	$\pm\frac{1}{3}\sqrt{5 - 2\sqrt{\frac{10}{7}}}$	$\frac{322+13\sqrt{70}}{900}$
	$\pm\frac{1}{3}\sqrt{5 + 2\sqrt{\frac{10}{7}}}$	$\frac{322-13\sqrt{70}}{900}$

Table C.1: Gauss-Legendre Quadrature

Bibliography

[1] A. Bellini, Selcuk Guceri: Mechanical characterization of parts fabricated using fused deposition modeling. *Rapid Prototyping Journal.* **9-4**, 252-264, (2003).

[2] A. Bonito, M. Picasso, M. Laso: Numerical simulation of 3D viscoelastic flows with free surfaces. *Preprint submitted to Elsevier Science.* (7 November 2005).

[3] A. Costa, G. Macedonio: Viscous Heating in Fluids with Temperature-Dependent Viscosity: Implications for Magma Flows. *Nonlinear Processes in Geophysics* **10**, 543-555, (2003).

[4] A. Jagota, C. Argento, and S. Mazur: Growth of adhesive contacts for Maxwell viscoelastic spheres. *Journal of Applied Physics.* **83**, 250, (1998).

[5] A. N. Beris, A. J. Giacomin: Everythings Flows. *Applied Rheology.* **24-52918**, (2014).

[6] A. N. Brooks, T. J. R. Hughes: Streamline Upwind/Petrov - Galerkin Formulations for Convection Dominated Flows with Particular Emphasis on the Incompressible Navier-Stokes Equations. *Computers Methods in Apllied Mechanics and Engineering.* **32**, 199-259 (1982).

[7] A.Trigui, M. Karkri, C. Boudaya, Y. Candau, L. Ibos, M. Fois: Experimental investigation of a composite phase change material: Thermal-energy storage and release. *Journal of Composite Materials.* **48-1**, 49-62 (2014).

[8] B. Crawford, J. K. Watterson, P. L. Spedding, R. I. Gault, W. Herron, M. Proctor: Constitutive equations for modelling of polymeric materials and rubbers. *Asia-Pacific journal of Chemical Engineering.* **5**, 732-742 (2010).

[9] B. Huang, S. Singamneni: Raster angle mechanics in fused deposition modelling. *Journal of Composite Materials*, **1-21**, (2014).

[10] B. Julien, D. Pino: Finite Element Approach to the Sintering Process at the Grain Scale. (2014).

[11] B. N. Turner, R. Strong, S. A. Gold: A review of melt extrusion additive manufacturing processes: I. Process design and modeling. *Rapid Prototyping Journal.* **20-3**, 192–204, (2014).

[12] C.M. Oishia, F.P. Martinsa, M.F. Toméb, J.A. Cuminatob, S. McKeec: Numerical solution of the eXtended Pom-Pom model for viscoelastic free surface flows. *Journal of Non-Newtonian Fluid Mechanics.* **166**, 169-179 (2011).

[13] C. T. Bellehumeur, M. Kontopoulou, J. Vlachopoulos: The role of viscoelasticity in polymer sintering. *Rheologica Acta.* **37**, 270–278, (1998).

[14] C . T. Bellehumeur, M. K. Bisaria, J. Vlachopoulos: An Experimental Study and Model Assessment of Polymer Sintering. *Polymer Engineering and Science.* **35-17**, (1996).

[15] C. Verdier: Coalescence of polymer droplets: experiments on collision. *Laboratoire de Rhéologie* ., (2008).

[16] C. W. Macosko: Rheology Principles, Measurements and Applications. *WILEY-VCH.*, (1994).

[17] D. Lynn Johnson: New Method of Obtaining Volume, Grain Boundary, and Surface Diffusion COefficients from Sintering Data: An Experimental Study and Model Assessment of Polymer Sintering. *Journal of Applied Physics* **40-1**, (1-1969).

[18] D. H. P. Munoz: High Performance Computing of Sintering Process at Particle Scale. *Ecole Nationale Supérieure des Mines de Saint-Etienne - Dissertation.*, (10-2012).

[19] D. Defauchya, G. Regniera, P. Peyrea, I. Amrana, A. Ammarb:Direct manufacturing of thermoplastic parts by powder laser sintering: Comparison of coalescence simulations and Frenkel based physical model. *World Congress of the Polymer Processing Society.*, (10-2014).

[20] D.D. Joseph: Fluid Dynamics of visco-elastic liquids, Springer, New York, (1990).

[21] E. A. Olevsky: Theory of sintering: from discrete to continuum. *Materials Science and Engineering.*,**23**, 41–100, (1998).

[22] E. A. Olevsky, A. Molinari: Instability of sintering of porous bodies. *International Journal of Plasticity*, **16**, 1-37, (2000).

[23] E. Fried, M. E. Gurtin: A unified treatment of evolving interfaces accounting for small deformations and atomic transport: grain-boundaries, phase transitions, epitaxy.

[24] E. Mitsoulis: Three-dimensional non-Newtonian computations of extrudate swell with the finite element method. *Comput. Methods Appl. Mech. Engrg.* **180**, 333-344 (1999).

[25] E. Scribben, A. P. R. Eberle, D. G. Baird:Viscoelastic coalescence of thermotropic liquid crystalline polymers: The role of transient rheology. *Journal of Rheology.* **49**, 1159, (2005).

[26] F. Auricchio: Quick review on elasticity. Finite element method (FE). *Elementi di Meccanica Computazionale*, (2014).

[27] F. P. T. Baaijens: Mixed finite element methods for viscoelastic flow analysis: a review. *J. Non-Newtonian Fluid Mech.* **79**, 361-385 (1998) .

[28] F. Wakai, K.A. Brakke: Mechanics of sintering for coupled grain boundary and surface diffusion. *Acta Materialia.* **59**, 5379–5387, (2011).

[29] F. Parhami, R.M. McMeeking, A.C.F. Cocks, Z. Suo: A model for the sintering and coarsening of rows of spherical particles. *Mechanics of Materials.* **31**, 43–61, (1999).

[30] G. Alaimo: Travi Elastiche a Torsione e Teoria dei Sistemi Frazionari. *Master Thesis*, (2012)

[31] G. Van De Vorst: Modeling and Numerical Simulation of Viscous Sintering. (1994).

[32] G. C. Kuczynki: Self-diffusion in sintering of metallic particles. . *Transactions of the AIME.* **185**, 169–178, (1949).

[33] G. O. Aloku, Xue-Feng Yuan: Numerical simulation of polymer foaming process in extrusion flow. *Chemical Engineering Science.* **65**, 3749–3761 (2010) .

[34] H. E. Exner, E. Artz, Robert W., Cahn and P. Haasen: Sintering Processes. *Physical Metallurgy.* **59**, 2627–2662 (1996).

[35] H. Rezayat, W. Zhou, A. Siriruk, D. Penumadu, S. S. Babu: Structure–mechanical property relationship in fused deposition modelling. *Materials Science and Technology.* **31**, 192–204, (2015).

[36] J. F. Rodriguez, J. P. Thomas, J. E. Renaud: Characterization of the mesostructure of acrylonitrile butadiene styrene fused deposition materials modeling. *Rapid Prototyping Journal.* **6-3**, 175–185, (2000).

[37] J. F. Rodriguez, J. P. Thomas, J. E. Renaud: Design of Fused Deposition ABS COmponents for Stiffness and Strength. *Journal of Mechanical Design.* **125**, 545–551, (2003).

[38] J. F. Rodriguez, J. P. Thomas, J. E. Renaud: Mechanical behavior of acrylonitrile butadiene styrene fused deposition materials modeling. *Rapid Prototyping Journal.* **9-4**, 219–230, (2003).

[39] J. P. Thomas, J. F. Rodriguez: Modeling the Fracture Strength Between Fused-Deposition Extruded Roads. *Naval Research Laboratory*, (2003).

[40] J. Sun, M.D. Smith, R.C. Armstrong, R.A. Brown: Finite element method for viscoelastic flows based on the discrete adaptive viscoelastic stress splitting and the discontinuous Galerkin method: DAVSS-G/DG. *J. Non-Newtonian Fluid Mech.* **86**, 281-307, (1997).

[41] K. Katsura, Y. Shinoda, T.Akatsu, F.Wakai : Sintering force behind shape evolution by viscous flow. *Journal of the European Ceramic Society.* **35**, 1119–1122, (2015).

[42] L. Li, Q. Sun, C. Bellehumeur, P. Gu: Composite Modeling and Analysis of FDM Prototypes for Design and Fabrication of Functionally Graded Parts. *Dept. of Chemical Engineering, Dept. of Mechanical and Manufacturing Engineering* (2002).

[43] L. Li, Q. Sun, C. Bellehumeur, P. Gu: Modeling of Bond Formation Between Polymer Filaments in the Fused Deposition Modeling Process. *Journal of Manufacturing Processes* **6-2**, 170–178, (2004).

[44] L. Li, Q. Sun, C. Bellehumeur, P. Gu: Composite modeling and analysis for fabrication of FDM protorypes with locally controlled properties. *Journal of Manufacturing Processes.* **4-2** (2002).

[45] L. Li, Q. Sun, C. Bellehumeur, P. Gu: Investigation of Bond Formation in FDM Process. *Dept. of Chemical and Petroleum Engineering.* (2003).

[46] Q. Sun, G.M. Rizvi, C. Bellehumeur, P. Gu: Effect of Processing Conditions on the Bonding Quality of FDM Polymer Filaments. *Rapid Prototyping Journal.* **14-2**, 72–80, (2008).

[47] M. Boutaousa, P. Bourginb, M. Zineta: Thermally and flow induced crystallization of polymers at low shear rate. *Journal of Non-Newtonian Fluid Mechanics.* **165**, 227–237 (2010).

[48] M.M.Ristic, S.Dj.Milosevic: Frenkel's Theory of Sintering. *Science of Sintering.* **38**, 7-11 (2006).

[49] M. N. Rahaman: Ceramic processing and sintering. (1995).

[50] M. Nikzad, S.H. Masood, I. Sbarski: Thermo-mechanical properties of a highly filled polymeric composites for Fused Deposition Modeling. *Journal of Material and Design.*, **32**, 3448–3456, (2011).

[51] MTS Insight Electromechanical Testing Systems: Affordable and easy-to-use platforms for performing virtually any static test.

[52] M. Yardimci, Selcuk Guceri, S.C. Danforth: A Phenomenological Numerical Model for Fused Deposition Processing of Particle Filled Parts. (2000).

[53] O. Pokluda, C.T. Bellehumeur, J. Vlachopoulos: Modification of Frenkel's Model for Sintering. *AIChE Journal.* **43-11**, 3253–3256 (1997).

[54] O.C. Zienkiewicz, R.L. Taylor : The Finite Element Method. Volume 1: The Basis (2000).

[55] P.K. Mallick: Fiber-Reinforced Composites: Materials, Manufacturing, and Design. *Composite Materials.* 638 Pages, (2007).

[56] P.K. Mallick: Fiber-Reinforced-Composites Materials, Manufacturing, and Design. *Taylor & Francis Group.*, (2008).

[57] R. Cherizol1, M. Sain1, J. Tjong: Review of Non-Newtonian Mathematical Models for Rheological Characteristics of Viscoelastic Composites. *Journal of Non-Newtonian Fluid Mechanics.* **5**, 6-14 (28 January 2015).

[58] R. Hooper, Christopher W. Macosko, Je!rey J. Derby: Assessing a flow-based finite element model for the sintering of viscoelastic particles. *Chemical Engineering Science.*,**55**, 5733-5746, (2000).

[59] R. I. Tanner, S. Nasseri: Simple constitutive models for linear and branched polymers. *J. Non-Newtonian Fluid Mech.* **116**, 1-17 (2003).

[60] Sung. H. Ahn, M. Montero, D. Odell, S. Roundy, P.K. Wright: Anisotropic Material Properties of Fused Deposition Modeling ABS. *Rapid Prototyping Journal.* **8-4**, 248-257 (2002).

[61] S. L. Kang: Sintering: Densification,Grain Growth, and Microstructure. *Elsevier.*, (2005).

[62] S. Nemat-Nasser, M. Hori: Micromechanics: Overall Properties of Heterogeneous Materials. *Elsevier* (1993).

[63] S. Zhou, L. Hou: Decoupled algorithm for solving Phan-Thien–Tanner viscoelastic fluid by finite element method. *Journal Computers and Mathematics with Applications.* **69**, 423-437 (2015).

[64] Tim A. Osswald, Natalie Rudolph: Polymer Rheology: Fundamentals And Applications. Chap. 5. *Hanser Publishers.*, (2014).

[65] V. Ganvir, A. Lele, R. Thaokar, B.P. Gautham: Simulation of viscoelastic flows of polymer solutions in abrupt contractions using an arbitrary Lagrangian Eulerian (ALE) based finite element method. (2007).

[66] V. Ganvir, A. Lelec, R. Thaokarb, B.P. Gauthama: Prediction of extrudate swell in polymer melt extrusion using an Arbitrary Lagrangian Eulerian (ALE) based finite element method. *Journal of Non-Newtonian Fluid Mechanics.*, **156**, 21–28, (2009).

[67] V. Ganvira, B.P. Gauthama, H. Polc, M. S. Bhamlad, L. Sclesie, R. Thaokarb, A. Lelec, M. Mackleye: Extrudate swell of linear and branched polyethylenes: ALE simulations and comparison with experiments. *Journal of Non-Newtonian Fluid Mechanics.* **166**, 12-24 (2011).

[68] W. N. Findley, James S. Lai, Kasif Onaran: Creep and Relaxation of Nonlinear Viscoelastic Materials. *Dover Publications.*, (1989).

[69] W. D. Kingery:Densification during Sintering in the Presence of a Liquid Phase. I. Theory. *Journal of Applied Physics.* **30**, 301 (1959).

[70] W. R. Hwanga, M. A. Walkleyb, O. G. Harlen:A fast and efficient iterative scheme for viscoelastic flow simulations with the DEVSS finite element method. *Journal of Non-Newtonian Fluid Mechanics.* **166**, 354–362 (2011).

[71] W. Zhangh, J.H. Schneibel: The Sintering of Two Particles by Surface and Grain Boundary Diffusion - a Two-Dimensional Numerical Study . *Acta Metallurgica.* **43.12**, 4377-4386 (1995).

[72] X. Xingming, Z. Guoqun, Q. Shengxue, W. Wei: Numerical Simulation of Viscoelastic Extrudate Swell Through Elliptical Ring Die. *Fluid Flow and Transport Phenomena.* **19-1**, 10-17 (2011).

[73] Y. Li, J. Zheng, C. Xia, W. Zhou : A Finite Piece Method for Simulating Polymer Melt Flows in Extrusion Sheet Dies. *Journal of Applied Polymer Science.* **123**, 3189–3198 (2012).

[74] Y. Y. Lin, C.Y. Hui, A. Jagota: The Role of Viscoelastic Adhesive Contact in the Sintering of Polymeric Particles. *Journa of Colloid and Interface Science.* **237**, 267-282 (2001).

[75] Y. Mu, G. Zhaoa, A. Chenb, X. Wu: Numerical investigation of the thermally and flow induced crystallization behavior of semi-crystalline polymers by using finite element–finite difference method. *JournalComputers and Chemical Engineering.* **46**, 190-204, (2012).

[76] Y. Mu, G. Zhao, X. Wu, J. Zhai: Modeling and simulation of three-dimensional planar contraction flow of viscoelastic fluids with PTT, Giesekus and FENE-P constitutive models. *Journal of Applied Mathematics and Computation.* **218**, 8429-8443 (2012).

[77] Y. Mu: Finite-Element Simulation of Polymer Flow and Extrudate Swell through Hollow Profile Extrusion Die with the Multimode Differential Viscoelastic Model. *Advances in Polymer Technology.* **32-S1**, E1–E19 (2013).

[78] Y. Mu, G. Zhao, X. Wu, L. Hang, H. Chu: Continuous modeling and simulation of flow-swell-crystallization behaviors of viscoelastic polymer melts in the hollow profile extrusion process. *Advances in Polymer Technology.* **39**, 1352-1368 (2015).

[79] Y. Mu, G. Zhaoa, A. Chenb, G. Donga, S. Lia: Numerical investigation of the crystallization and orientation behavior in polymer processing with a two-phase model. *Computers and Chemical Engineering.* **63**, 91-107 (2014).

[80] Z.Tadmor, C. G. Gogos: Principles of Polymer Processing (Second Edition). *A John Wiley & Sons Inc.*, (2005).

Ringraziamenti

Nonostante la gioia di raggiungere un traguardo così importante come la laurea, personalmente, provo un po' di amarezza, sapendo di dover abbandonare i colleghi conosciuti negli anni di studio.

É impossibile elencare in qualche riga tutte le persone che hanno contribuito a formare la persona che sono oggi e sono quasi certo che anche loro lo sanno. Purtroppo il tempo é volato e il lavoro condotto per questa tesi é necessariamente non completo, o meglio, sono molte le cose che mi sarebbe piaciuto affinare, ampliare e sviluppare. Nonostante questo spero di essere stato all' altezza del compito che mi é stato dato.

Vorrei, prima di tutto, ringraziare il mio relatore, il prof. Ferdinando Auricchio, conosciuto nel corso di Meccanica Computazionale. Grazie alla sua "nonchalance" nel parlare di elementi finiti é riuscito a farmi appassionare. Senza i suoi pazienti insegnamenti e la sua disponibilità, la mia tesi non avrebbe prodotto risultati.

Un grazie speciale a Gianluca Alaimo (DOC), per tutto il sapere che ha condiviso con me, esprimibile non tanto in nozioni, quanto nel trasmettere la forma mentis con la quale affronta le situazioni. Grazie anche per tutte le critiche e per avermi sempre fornito un punto di vista sulle cose molto diverso dal mio, aiutandomi a migliorare il mio lavoro.

Grazie ai ragazzi del laboratorio 3D@UniPv. Grazie a Stefania, Valeria, Luca.

Ai miei coinquilini: Alberto, Filippo, Gianluca e Federico. Casa Marchesi rimarrà sempre nel mio cuore. E soprattutto, grazie per avermi sopportato.

A tutti i miei compagni. Citarli tutti sarebbe impossibile, quindi, grazie per i momenti di gioia e di tristezza. Potrei stare ore a scrivere quanto tenga a voi, ma qualsiasi parola sarebbe superflua. Mi mancherete.

Un grazie speciale a Giulio Sineri (alfa), con cui ho condiviso l'esperienza di tesi.

Infine vorrei ringraziare le persone a me più vicine, Claudia, per avermi sostenuto. La mia

famiglia, per avermi sopportato e sponsorizzato. Mia madre Delia, mio padre Giuseppe e il mio fratellino Michele. Grazie a te, nonna. Purtroppo, non posso condividere questo momento con te, ma sappi che non smetterò mai di pensarti.